Chapter 3.
FIELD QUALITY IMPROVEMENTS THROUGH YOKE DESIGN

The research work described in this chapter is partly based on the following papers :

- R.C. Gupta, G.H. Morgan, *A Design for a High Field Combined Function Superferric Magnet*, Proceedings of the 1985 Particle Accelerator Conference, Vancouver; IEEE Transaction on Nuclear Science, Volume NS-32, Oct 1985, pp. 3687-3688 (1985).
- R.C. Gupta, G.H. Morgan, P.A. Thompson, *A Single Layer Coil Superconducting Magnet for SSC*, Proceedings of the 1987 Particle Accelerator Conference, Washington DC, pp. 1413-1415(1987).
- R.C. Gupta, G.H. Morgan, P.J. Wanderer, *A Comparison of Calculations and Measurements of the Iron Saturation Characteristic of the SSC Design D Dipole Magnet*, Proceedings of the 1987 Particle Accelerator Conference, Washington DC, pp. 1405-1407 (1987).
- R.C. Gupta, G.H. Morgan, *Collarless, Close-in, Shaped Iron Aperture Designs for the SSC Dipole*, Proceedings of the 1989 Particle Accelerator Conference, Chicago, pp. 500-502 (1989).
- R.C. Gupta, S.A. Kahn and G.H. Morgan, *Coil and Iron Design for SSC 50 mm Magnet*, Proceedings of the 1990 American Society of Mechanical Engineers (ASME) Winter Annual Meeting in Dallas (1990).
- R.C. Gupta, S.A. Kahn and G.H. Morgan, *A Comparison of Calculations and Measurements of the Field Harmonics as a Function of Current in the SSC Dipole Magnets*, Proceedings of the 1991 IEEE Particle Accelerator Conference, San Francisco, pp. 42-44 (1991).
- R.C. Gupta, et al., *RHIC Insertion Magnets*, Proceedings of the 1991 IEEE Particle Accelerator Conference, San Francisco, pp. 2239-2241 (1991).
- R.C. Gupta, S.A. Kahn and G.H. Morgan, *SSC 50 mm Dipole Cross section*, Proceedings of the International Industrial Symposium on Super Collider (IISSC), Atlanta, pp. 587-600 (1991).
- R.C. Gupta, *Correcting Field Harmonics after Design in Superconducting Magnets*, Proceedings of the 4^{th} International Industrial Symposium on Super Collider (IISSC), New Orleans, pp. 773-780 (1992).
- R. Gupta, et al., *Large Aperture Quadrupoles for RHIC Interaction Regions*, Proceedings of the 1993 Particle Accelerator Conference, Washington, D.C., pp. 2745-2747 (1993).
- R.C. Gupta, A.K. Jain, *Variation in a_1 saturation in SSC Collider Dipoles*, Proceedings of the 1993 Particle Accelerator Conference, Washington, D.C., pp. 2778-2780 (1993).
- R. Gupta, et al., *Field Quality Improvements in Superconducting Magnets for RHIC*, Proceedings of the 1994 European Particle Accelerator Conference, London, UK, pp. 2928-2930 (1994).
- R. Gupta, et al., *Field Quality Control Through the Production Phase of RHIC Arc Dipoles*, Proceedings of the 1995 International Particle Accelerator Conference, Dallas, Texas (1995).
- A. Jain, R. Gupta, et al., *Skew Quadrupole in RHIC Dipole Magnets at High Fields*, Proceedings of the Fourteenth International Conference on Magnet Technology (MT-14), Tampere, Finland, June 11-16 (1995).
- R. Gupta, *Field Quality in the Superconducting Magnets for Large Particle Accelerators*, Proceedings of the 1996 European Particle Accelerator Conference at Sitges, Spain (1996).

3.1. Introduction

An iron yoke plays an important role in superconducting magnets. The superconducting coils are placed in a cylindrical yoke having one or more cavities for the coils. The yoke reduces the fringe field outside the magnet structure by several orders of magnitude and more importantly it shields the field in the aperture of the magnet from the surroundings, which may contain some magnetic material. Moreover, the yoke iron is magnetized by the magnetic field produced by the coil and this magnetized iron, in turn, contributes to the field at the center of the magnet. This enhancement of the field will be computed later for a constant μ in the iron.

In accelerator magnets, the central field is changed during the accelerating cycle by changing the current in the coil. Whereas, the contribution to the central field from the coil is proportional (linear) to the current in the coil, the contribution from the iron becomes non-linear when the iron magnetization (M) approaches the saturation magnetization (M_s), which is around 2.1 Tesla for the most common type of iron used in accelerator magnets. This phenomena is shown in Fig. 3.1.1 and Table 3.1.1, where B is the magnetic induction or flux density and H is the magnetic field intensity. It may be recalled that $\vec{B}/\mu_o = \vec{H} + \vec{M}$ and H is proportional to the current in the coil. It may be noted that there is a non-linearity in the curve at low field also but here the discussion will be limited to the high field case where the non-linearity is commonly referred to as iron saturation, since the magnetization in the iron reaches a maximum saturated value that can not be exceeded.

The saturation magnetization (M_s) is primarily determined [100] by the impurities (such as nitrogen, sulphur, aluminium, etc.) in the iron. The relative contribution of the field from the iron is further reduced at high field by the presence of small gaps between the laminations. The packing factor (or filling factor by which the iron laminations are packed in the given space) in RHIC and SSC magnets was about 97.5%.

This non-linearity in the iron properties complicates the design and performance of the magnet since the azimuthal distribution of the magnetization in the iron yoke changes with the field. This in turn changes the azimuthal distribution of the field in the aperture of the magnet as represented by circular harmonic components. The magnet must be designed in such a way that this change in field harmonics as a function of current is minimized.

The contribution of the iron shell with yoke inner radius R_f and yoke outer radius R_a to the field produced by a $cos(m\theta)$ current sheet at radius a is computed for constant μ iron. For easy reference the expressions for the field in the coil aperture (r<a) in the presence of

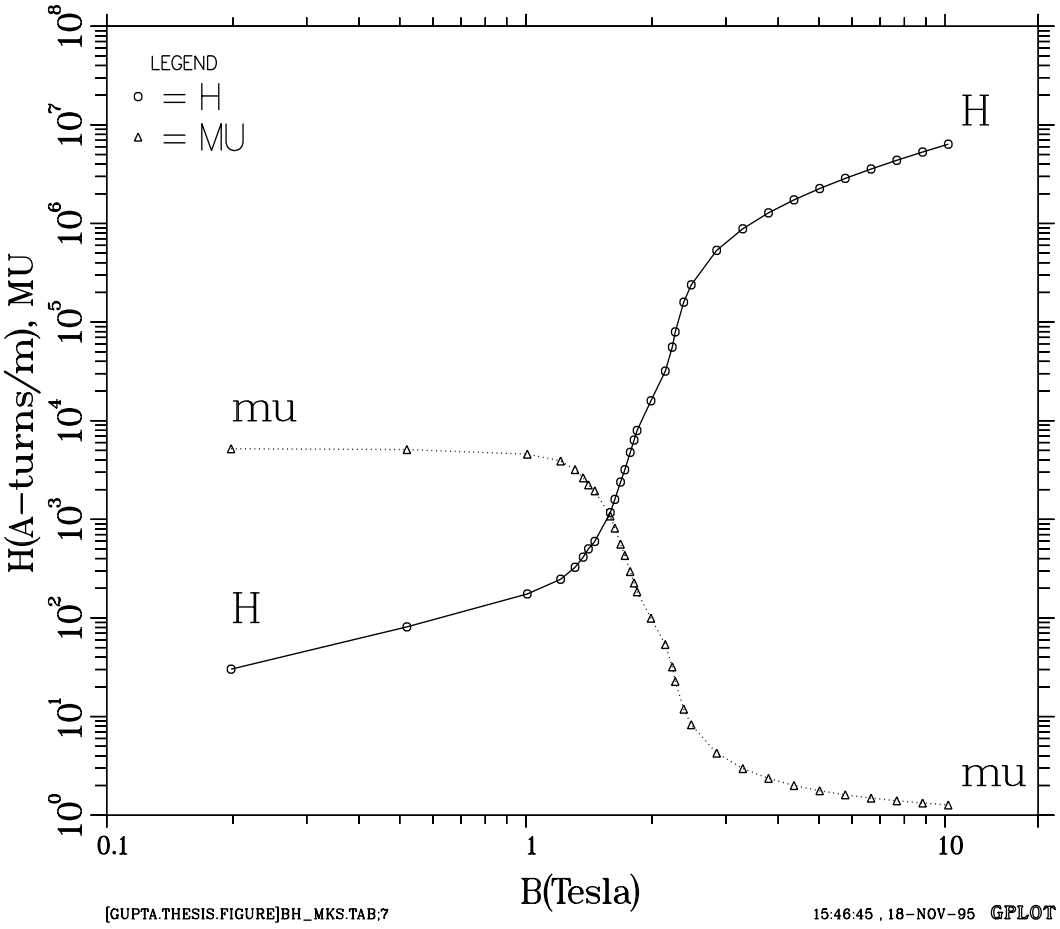

Figure 3.1.1: B-H table used in the calculations carried out with the computer code POISSON. One can note the non-linear relationship between the magnetic induction (B) and magnetic field (H). The relative permeability μ (mu) is also plotted.

the yoke (which were obtained before in Eqs. (1.5.112)) are given here again. However, first a saturation parameter is defined as follows :

$$S_\mu = \frac{\mu - 1}{\mu + 1} \frac{\left[1 - \left(\frac{R_f}{R_a}\right)^{2m}\right]}{\left[1 - \left(\frac{\mu-1}{\mu+1}\right)^2 \left(\frac{R_f}{R_a}\right)^{2m}\right]}. \tag{3.1.1}$$

The value of this saturation parameter is 1.0 when μ is large. A value of one indicates no saturation. A reduction in the value of saturation parameter from 1.0 indicates the onset of

Table 3.1.1: The following B-H table is used in the calculations carried out with the computer code POISSON. Here, B is the magnetic induction, H is the magnetic field, μ is the relative permeability and $\gamma = \frac{1}{\mu} = \frac{\mu_0 H}{B}$.

N	B(Tesla)	H(A-turns/m)	μ (MU)	γ (GAMMA)
1	0.000521	0.00	5210.00	1.920E-04
2	0.198	3.024E+01	5194.12	1.930E-04
3	0.52	8.117E+01	5098.04	1.960E-04
4	1.008	1.751E+02	4581.82	2.180E-04
5	1.21	2.467E+02	3903.23	2.560E-04
6	1.31	3.263E+02	3195.12	3.130E-04
7	1.37	4.138E+02	2634.62	3.800E-04
8	1.41	5.014E+02	2238.1	4.470E-04
9	1.46	5.968E+02	1946.67	5.140E-04
10	1.59	1.170E+03	1081.63	9.250E-04
11	1.63	1.592E+03	815	1.227E-03
12	1.682	2.387E+03	560.67	1.784E-03
13	1.722	3.183E+03	430.5	2.323E-03
14	1.774	4.775E+03	295.67	3.382E-03
15	1.812	6.366E+03	226.5	4.415E-03
16	1.842	7.958E+03	184.2	5.429E-03
17	1.988	1.592E+04	99.4	1.006E-02
20	2.272	7.958E+04	22.72	4.401E-02
21	2.38	1.592E+05	11.9	8.403E-02
22	2.481	2.387E+05	8.27	1.209E-01
23	2.852	5.332E+05	4.26	2.349E-01
24	3.292	8.833E+05	2.97	3.372E-01
25	3.792	1.281E+06	2.36	4.246E-01
26	4.362	1.735E+06	2	4.998E-01
27	5.022	2.260E+06	1.77	5.655E-01
28	5.782	2.865E+06	1.61	6.226E-01
29	6.662	3.565E+06	1.49	6.725E-01
30	7.672	4.371E+06	1.4	7.159E-01
31	8.842	5.302E+06	1.33	7.534E-01
32	10.182	6.366E+06	1.27	7.857E-01

iron saturation and a value of 0.0 indicates complete saturation. Complete saturation takes place when the field in the yoke iron is so high that μ approaches 1 (which is the value of μ in air). A reduction in R_a also causes a reduction in the saturation parameter and in the limiting case when R_a approaches R_f, the saturation parameter approaches zero.

The use of the saturation parameter in Eqs. (1.5.112)) gives :

$$A_z(r,\theta) = \frac{\mu_o I_o}{2m}\ cos(m\theta)\left(\frac{r}{a}\right)^m\left[1+S_\mu\left(\frac{a}{R_f}\right)^{2m}\right], \tag{3.1.2a}$$

$$B_\theta(r,\theta) = -\frac{\mu_o I_o}{2a}\ cos(m\theta)\left(\frac{r}{a}\right)^{m-1}\left[1+S_\mu\left(\frac{a}{R_f}\right)^{2m}\right], \tag{3.1.2b}$$

$$B_r(r,\theta) = -\frac{\mu_o I_o}{2a}\ sin(m\theta)\left(\frac{r}{a}\right)^{m-1}\left[1+S_\mu\left(\frac{a}{R_f}\right)^{2m}\right]. \tag{3.1.2c}$$

For the m^{th} order multipole (m=1 for dipole), the ratio of the field provided by the iron yoke to the field provided by the current sheet is given by :

$$\frac{B_{fe}}{B_c} = S_\mu\left(\frac{a}{R_f}\right)^{2m}. \tag{3.1.3}$$

The theoretical maximum value of the above is 1.0 at low field (large μ) when $R_f = a$. In RHIC arc dipole magnets this ratio is $\sim$0.55 (55%) at low field and $\sim$0.50 (50%) at high field.

The field enhancement factor B_{enhc} due to the iron is defined as the field provided by the iron to the total field and is given by :

$$B_{enhc} = \frac{S_\mu\left(\frac{a}{R_f}\right)^{2m}}{\left[1+S_\mu\left(\frac{a}{R_f}\right)^{2m}\right]}. \tag{3.1.4}$$

The enhancement in the field due to the iron yoke is in the range of 20% to 40% in the magnets examined in this thesis.

The vector potential and the field components at the inside surface of the iron in air at $r = R_f$ are obtained from Eqs. (1.5.115) as :

$$A_z(R_f,\theta) = \frac{\mu_o I_o}{2m}\ cos(m\theta)\left(\frac{a}{R_f}\right)^m[1+S_\mu], \tag{3.1.5a}$$

$$B_\theta(R_f,\theta) = \frac{\mu_o I_o}{2a}\ cos(m\theta)\left(\frac{a}{R_f}\right)^{m+1}[1-S_\mu], \tag{3.1.5b}$$

$$B_r(R_f,\theta) = -\frac{\mu_o I_o}{2a}\ sin(m\theta)\left(\frac{a}{R_f}\right)^{m+1}[1+S_\mu]. \tag{3.1.5c}$$

For large μ (low field), S_μ is $\simeq$ 1; therefore the magnetic field at $r = R_f$ would have only a radial component (field perpendicular condition) with its magnitude doubled over its value in the absence of the yoke. The magnitude of field for any μ is obtained as $|B| = \sqrt{(B_r^2 + B_\theta^2)}$. Therefore,

$$|B(R_f, \theta)| = \frac{\mu_o I_o}{2a}\left(\frac{a}{R_f}\right)^{m+1}\sqrt{1 + S_\mu^2 - 2S_\mu \ cos(2m\theta)}. \tag{3.1.6}$$

In a magnet, the normal poles are at $\theta = (2n-1)\frac{\pi}{2m}$, with n=1,2,...,2m (m is 1 for dipoles and 2 for quadrupoles, etc.) and the coil midplanes are at $\theta = (n-1)\frac{\pi}{m}$. At the poles Eq. (3.1.6) reduces to

$$|B(R_f, \text{poles})| = \frac{\mu_o I_o}{2a}\left(\frac{a}{R_f}\right)^{m+1}(1 + S_\mu), \tag{3.1.7}$$

and at the midplanes to

$$|B(R_f, \text{midplanes})| = \frac{\mu_o I_o}{2a}\left(\frac{a}{R_f}\right)^{m+1}(1 - S_\mu). \tag{3.1.8}$$

Since S_μ is nearly one at low fields and nearly 0 at high fields, the ratio B/I_o at the yoke inner surface decreases at the poles and increases at the midplanes as the field increases from low to high.

To study a relative change in the azimuthal field distribution, two limiting cases are examined. First for the case when the iron saturation is negligible (low field and hence large μ in iron) and the saturation parameter (S_μ) is one. In this case the expression given in Eq. (3.1.6) reduces to :

$$|B(R_f, \theta)| = \frac{\mu_o I_o}{a} \ |sin(m\theta)| \ \left(\frac{a}{R_f}\right)^{m+1}, \tag{3.1.9}$$

and then the case when the saturation parameter (S_μ) is zero (the maximum saturation case with $\mu \simeq 1$), the expression given in Eq. (3.1.6) reduces to

$$|B(R_f, \theta)| = \frac{\mu_o I_o}{a}\left(\frac{a}{R_f}\right)^{m+1}. \tag{3.1.10}$$

A comparison of Eq. (3.1.9) and Eq. (3.1.10) shows that there is a change in the azimuthal distribution of the field at the yoke inner surface in the two cases. Whereas, at low fields, the magnitude of the field at the yoke inner radius changes as sin(mθ), it is completely independent of the angle at high fields. Therefore, yoke saturation causes a change in the azimuthal field distribution which in turn would cause a change in field harmonics.

The actual situation is much more complex than the expressions derived here under the assumption of constant μ in the iron everywhere. In a realistic case μ is not constant in the iron and varies as the field varies as a function of radius and angle. A local change in field, therefore, also causes a local change in μ which is not accounted in the above expressions. That situation is too complex to be solved analytically. However, most qualitative conclusions reached under the constant μ assumptions remain valid and are useful to develop strategies to minimize the dependence of field harmonics on iron saturation.

At low and medium field, the magnetization in the iron is such that it is maximum at the poles (90° and 270° in dipoles and 45°, etc. in quadrupoles) and minimum at the midplane (0° and 180° in dipoles and 0°, 90°, etc. in quadrupoles). However, most of the flux from the aperture returns through the iron yoke at the midplane and at high field this changes the distribution of flux lines such that the iron may be more magnetized at the midplane depending on the yoke thickness. This is the basis of the statement given earlier that the azimuthal distribution of the magnetization in the iron is a function of the central field. The harmonics in the aperture of the magnet change with central field if the iron magnetization approaches the saturation magnetization and if there is a significant variation in the azimuthal distribution of this iron magnetization, particularly near the yoke inner surface. During the course of this work, the yoke inner surface (opening) will be referred as the yoke aperture also.

In a simple magnet design where no steps are taken to force an early saturation elsewhere, the poles will saturate first with increasing excitation. This saturation effectively reduces the field at the poles of the magnet giving a positive contribution to b_2 in dipoles, b_5 in quadrupoles and b_8 in sextupoles. The pole saturation also gives a negative contribution to the next allowed harmonic which is b_4 in dipoles, b_9 in quadrupoles and b_{14} in sextupoles. At sufficiently high field, because of the limited yoke thickness, the iron at the midplane will saturate and this effectively reduces the field at the midplane. The midplane saturation gives a negative contribution to all allowed harmonics.

In an improved design the harmonics induced due to iron saturation can be minimized by controlling the iron saturation across the azimuth from midplane to pole. In the simplest of such schemes the return flux can be manipulated such that the midplane saturates sooner than it otherwise would and the change in the first allowed harmonic is minimized balancing the negative midplane saturation against the positive pole saturation. This, however increases the saturation in the next allowed harmonic (b_4 in dipoles and b_9 in quadrupoles) for

which the contribution from the midplane and pole saturation have the same sign. The drop in transfer function (field/current) is determined by the change in the relative permeability μ in the iron, or more precisely by $\frac{\mu-1}{\mu+1}$ (see Eqs. (3.1.3)).

In a still more sophisticated design the field lines are controlled such that the iron saturates uniformly along the yoke aperture. The goal is to minimize the variation in $\frac{\mu-1}{\mu+1}$ as a function of angle at different levels of excitation. This azimuthal minimization in variation is more important in the iron near the yoke inner radius since that contributes to the central field much more than the iron near the yoke outer radius. A minimization in the variation of $\frac{\mu-1}{\mu+1}$ minimizes the relative change in the azimuthal distribution of field, which by definition minimizes the change in field harmonics. (This argument will be visited again at the conclusion of this chapter, using the RHIC arc dipole magnet as an example). A further benefit of controlling the saturation induced harmonics is that the iron can be brought closer to the coil. This increases the field in the aperture of the magnet for a given amount of superconductor, which is much more expensive than the iron. Moreover, a reduction in saturation induced harmonics reduces the need for multipole corrector magnets, which increase the cost and complexity of the accelerator.

For reference, the field lines in the present design of the 80 mm aperture RHIC arc dipoles are shown in Fig. 3.1.2 at 1000 A (0.7 Tesla central field) and in Fig. 3.1.3 at 7000 A (4.5 Tesla central field). The influence of holes, notch and cutout can be clearly seen.

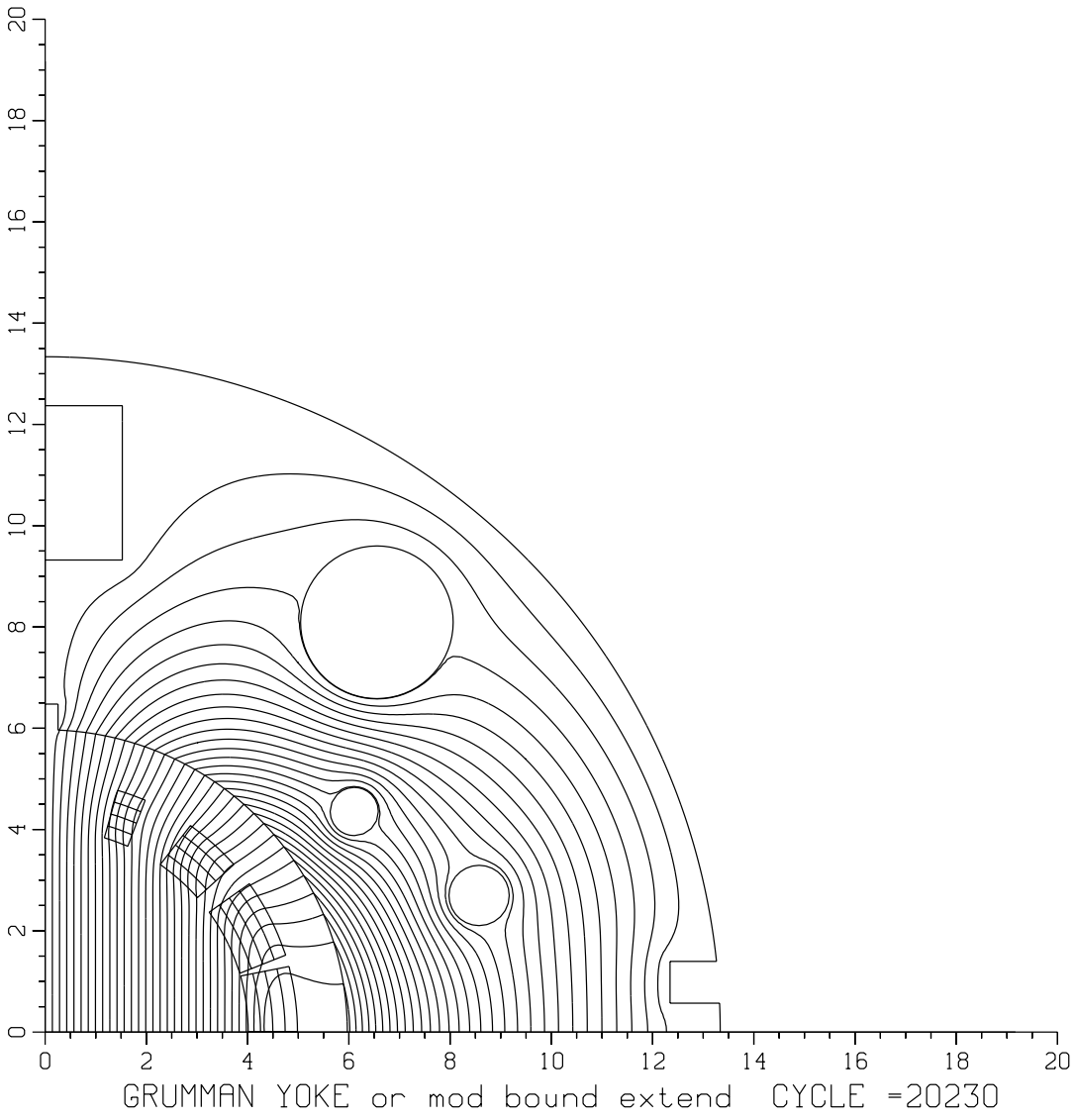

Figure 3.1.2: The field lines at 1000 A (~0.7 Tesla central field) in the present design of the 80 mm aperture RHIC arc dipoles.

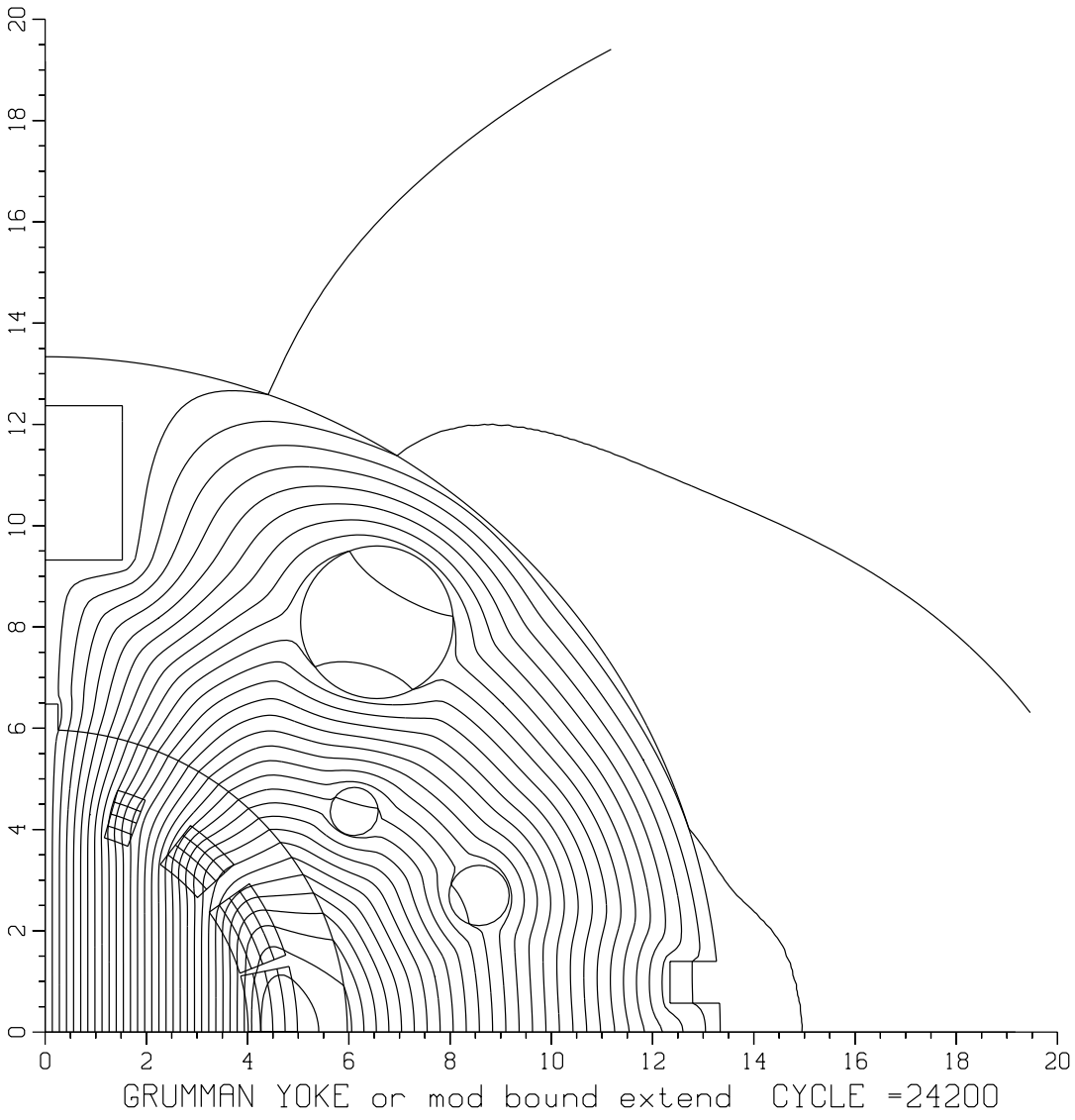

Figure 3.1.3: The field lines at 7000 A (~4.5 Tesla central field) in the present design of the 80 mm aperture RHIC arc dipoles.

3.2. Reduction in Saturation Induced Allowed Harmonics

A number of schemes are examined here for reducing the saturation induced harmonics in superconducting magnets. In many cases, similar work has been done by other authors [21,30,118,119,157]. The methods described here are built upon theirs and developed further to achieve optimum results in RHIC and SSC magnets. The saturation induced harmonics are defined as the difference between the low field and high field values of harmonics due to the non-linear properties of the iron yoke. The effectiveness of an individual method depends on the type of magnet (dipole, quadrupole, etc.), on the size of the magnet and on the field in the aperture of the magnet. The methods to be described have been examined [67,71,72] in the magnets for RHIC and SSC. A computer model for the cross section of a quadrant of the cold mass (i.e. coil and iron) of the 80 mm aperture RHIC arc dipole is shown in Fig. 3.2.1 and of the 50 mm aperture SSC main collider dipole magnet in Fig. 3.2.2. For dipoles, one needs to make a computer model only for a quadrant of the magnet since the rest is symmetric. In these two cases, the cold mass itself is off-center inside a circular cryostat (vacuum tank), which breaks the four fold symmetry of the model. This has a small influence on the non-allowed harmonics which will be discussed in the next section. For the purpose of studying the allowed harmonics only, this small effect is neglected here.

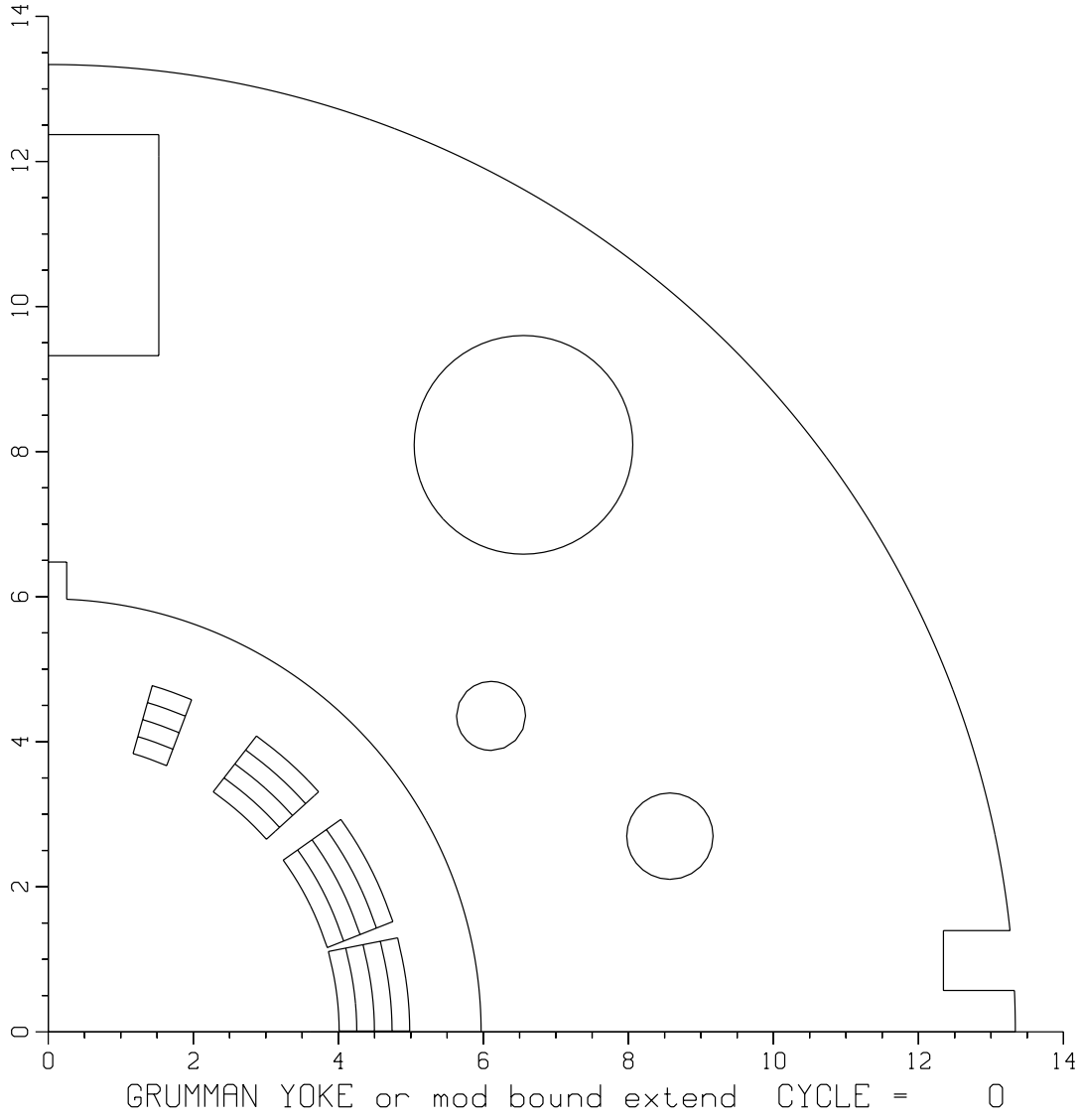

Figure 3.2.1: A computer model of the cross section of the cold mass of the 80 mm aperture RHIC arc dipole.

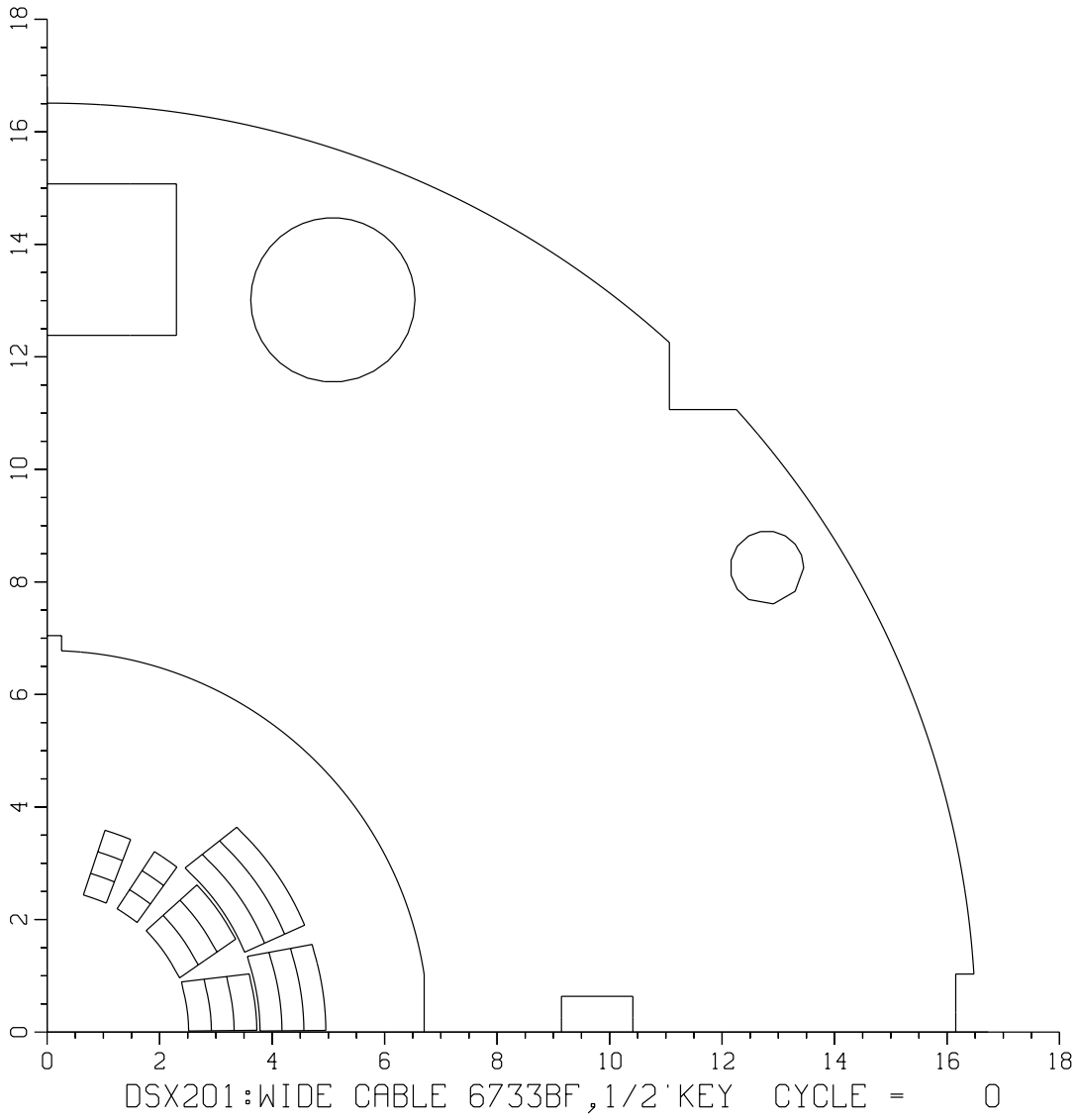

Figure 3.2.2: A computer model of the cross section of a quadrant of the 50 mm aperture SSC main collider dipole.

3.2.1. Varying the yoke inner radius

The yoke inner radius has a large influence [21] on the iron saturation, particularly when the gap between the coil and iron is small. The magnetic field for the m^{th}-pole outside the coil is proportional to $(\frac{1}{r})^{m+1}$), where m is 1 for dipole, 2 for quadrupole, etc. Thus the magnetic field falls rapidly as a function of radius and a larger yoke inner radius would therefore mean a lower field in the yoke. This in turn means a lower effect of the saturating iron on the field at the center of the magnet. However, a larger yoke inner radius implies that the yoke is further away from the coil, which reduces the iron contribution to the magnetic field at the center of the magnet (see Eqs. (3.1.4)). For these reasons, one would like to make the yoke inner radius as small as possible as long as the saturation induced harmonics are acceptable.

In Fig. 3.2.3 the transfer function (field divided by current) computed using code POISSON, at 1 kA and at 5 kA is plotted as a function of the yoke inner radius in the RHIC arc dipole magnet. The design yoke inner radius is 59.69 mm and the above variations are made in the present yoke design with all holes and cutouts preserved. The maximum operating current for the RHIC arc dipole is 5 kA. The yoke outer radius is kept constant at its nominal value of 133.35 mm. The values of the transfer function at 1 kA and 5 kA as a function of radius are given in Table 3.2.1. In Fig. 3.2.4 the computed saturation induced sextupole, decapole and 14-pole harmonics (b_2, b_4, b_6) are plotted as a function of yoke inner radius at 5 kA, and the values are given in Table 3.2.2. Recall that in dipoles, the b_i are $10^4 \frac{B_i}{B_o}$, where B_i is the magnitude of field due to the i^{th} harmonic at the reference radius and B_o is the central field. In the RHIC arc dipoles, the reference radius is 25 mm.

In Fig. 3.2.5 the transfer function computed using code POISSON, at 1 kA and at 6.6 kA is plotted as a function of the yoke inner radius in the SSC 50 mm aperture collider dipole magnet. The design yoke inner radius is 67.8 mm and the above variations are made in the present yoke design with all holes and cutouts preserved. The maximum operating current for this magnet is 6.6 kA. The yoke outer radius is kept constant at its nominal value of 165.1 mm. In Fig. 3.2.6 the computed saturation induced sextupole and decapole harmonics are plotted as a function of yoke inner radius at 6.6 kA. The reference radius is 10 mm.

Fig. 3.2.3 and Fig. 3.2.5 show that the transfer function is increased as the yoke inner radius is reduced, or in other words as the yoke is brought closer to the coil by reducing the coil to iron gap. However, Fig. 3.2.4 and Fig. 3.2.6 show that this increases the saturation

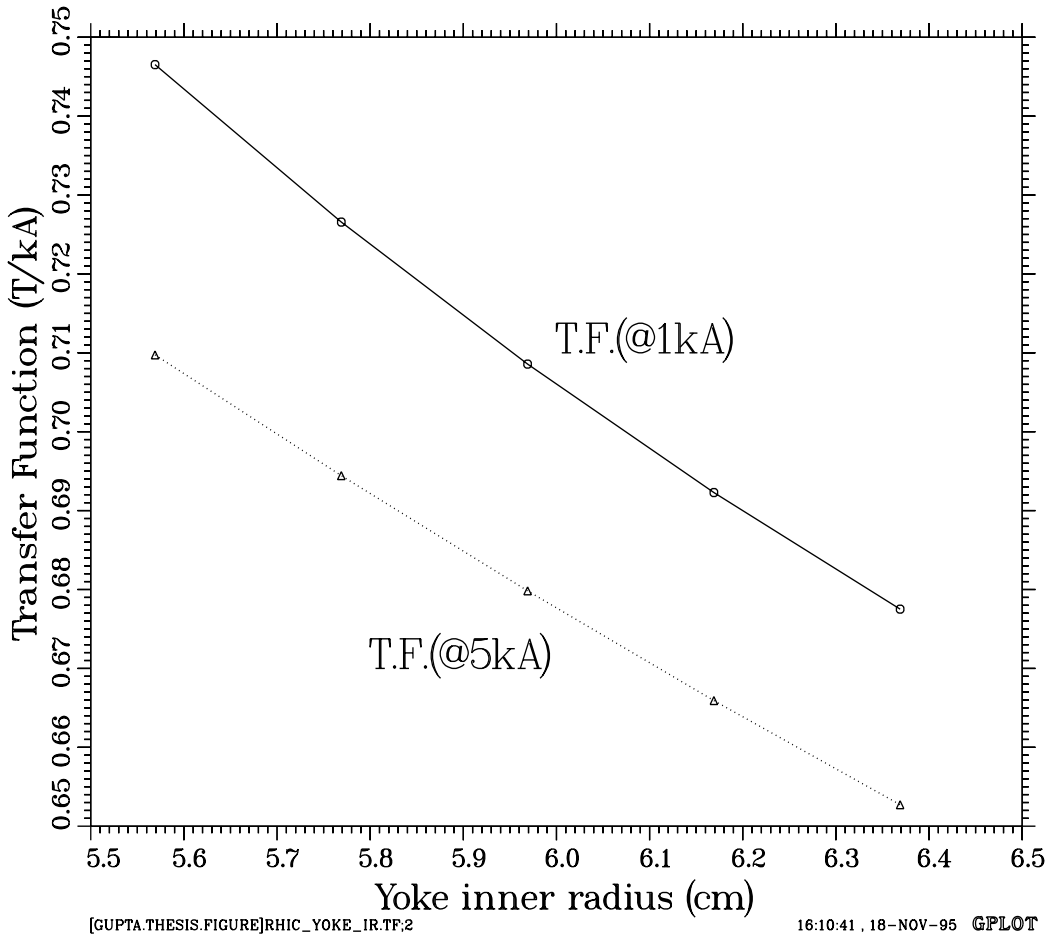

Figure 3.2.3: The computed transfer function (using POISSON) as a function of yoke inner radius at the operating current of 1 kA and 5 kA in the RHIC arc dipole magnet. The design yoke inner radius is 59.69 mm. The yoke outer radius is kept constant at a value of 133.35 mm.

induced harmonics. Therefore, in designing superconducting magnets the yoke inner radius is determined by a compromise between the transfer function and the saturation induced harmonics. It may be pointed out that the coil to iron gap is also influenced by mechanical design considerations. Generally, in magnets that use stainless steel or aluminum collars to provide compression on the coils (such as SSC and HERA magnets), the gap is determined by the collar thickness needed to satisfy the given mechanical requirements. In magnets

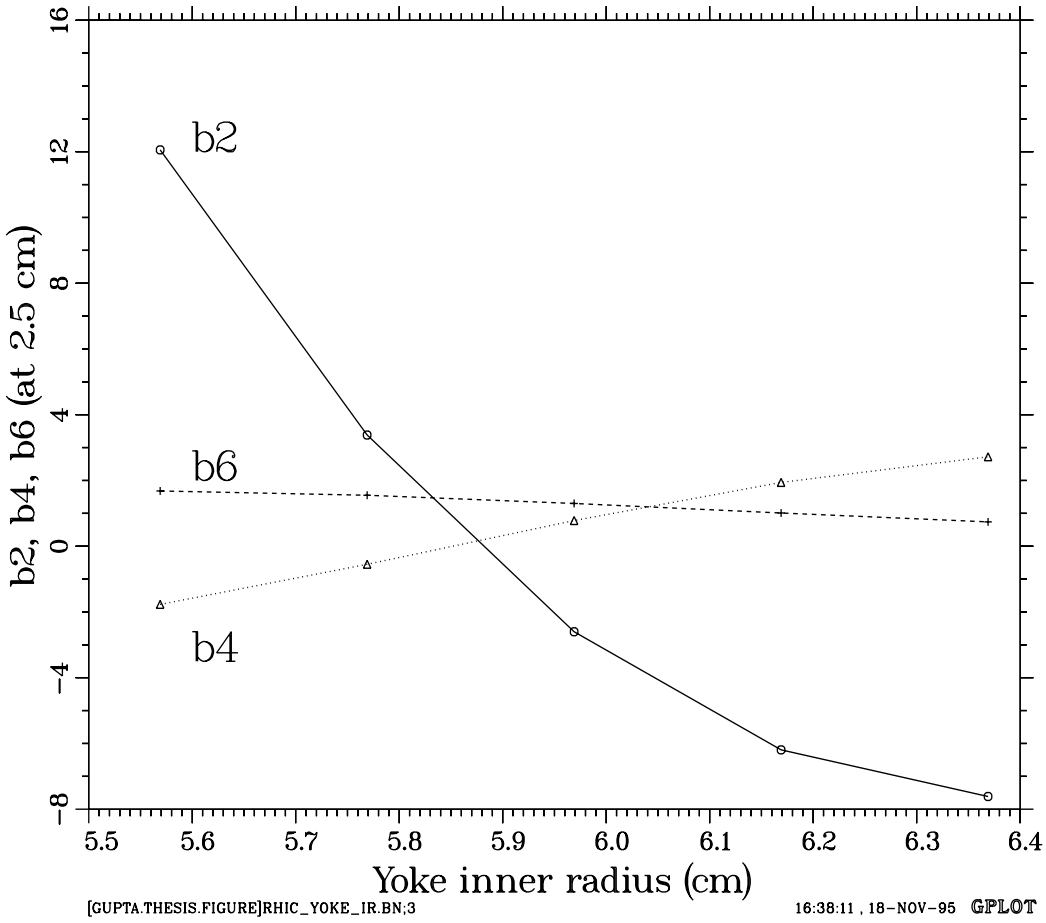

Figure 3.2.4: The computed saturation induced harmonics, b_2, b_4 and b_6 (using POISSON) as a function of yoke inner radius at a maximum design operating current of 5 kA in the RHIC arc dipole magnet. The design yoke inner radius is 59.69 mm and the reference radius is 25 mm. The saturation induced harmonics are defined as the difference between the low field and high field values of harmonics due to the non-linear properties of the iron yoke. The yoke outer radius is kept constant at a value of 133.35 mm.

where the yoke also acts as the collar (such as RHIC), the coil to iron gap can be significantly reduced. This gives a higher transfer function and also higher saturation induced harmonics. These saturation induced harmonics can be reduced by using methods described in the subsequent sections.

Table 3.2.1: The computed transfer function (TF) as a function of yoke inner radius at the operating currents of 1 kA and 5 kA in the RHIC arc dipole magnet. δTF (%) is the computed percentage change (loss) in transfer function at 5 kA from its low field value at 1 kA. The yoke outer radius is kept constant at a value of 133.35 mm in this analysis.

Inner Radius(mm)	TF(@1kA)	TF(@5kA)	δTF (%)
55.69	0.746528	0.709736	4.928
57.69	0.72657	0.69443	4.423
59.69	0.70857	0.67983	4.056
61.69	0.69229	0.66592	3.809
63.69	0.67751	0.65272	3.660

Table 3.2.2: The computed saturation induced harmonics, b_2, b_4 and b_6 as a function of yoke inner radius at a maximum design operating current of 5 kA in the RHIC arc dipole magnet. The yoke outer radius is kept constant at a value of 133.35 mm.

Inner Radius(mm)	b_2	b_4	b_6
55.69	12.056	-1.77	1.68
57.69	3.382	-0.55	1.55
59.69	-2.602	0.78	1.30
61.69	-6.195	1.94	1.01
63.69	-7.614	2.72	0.74

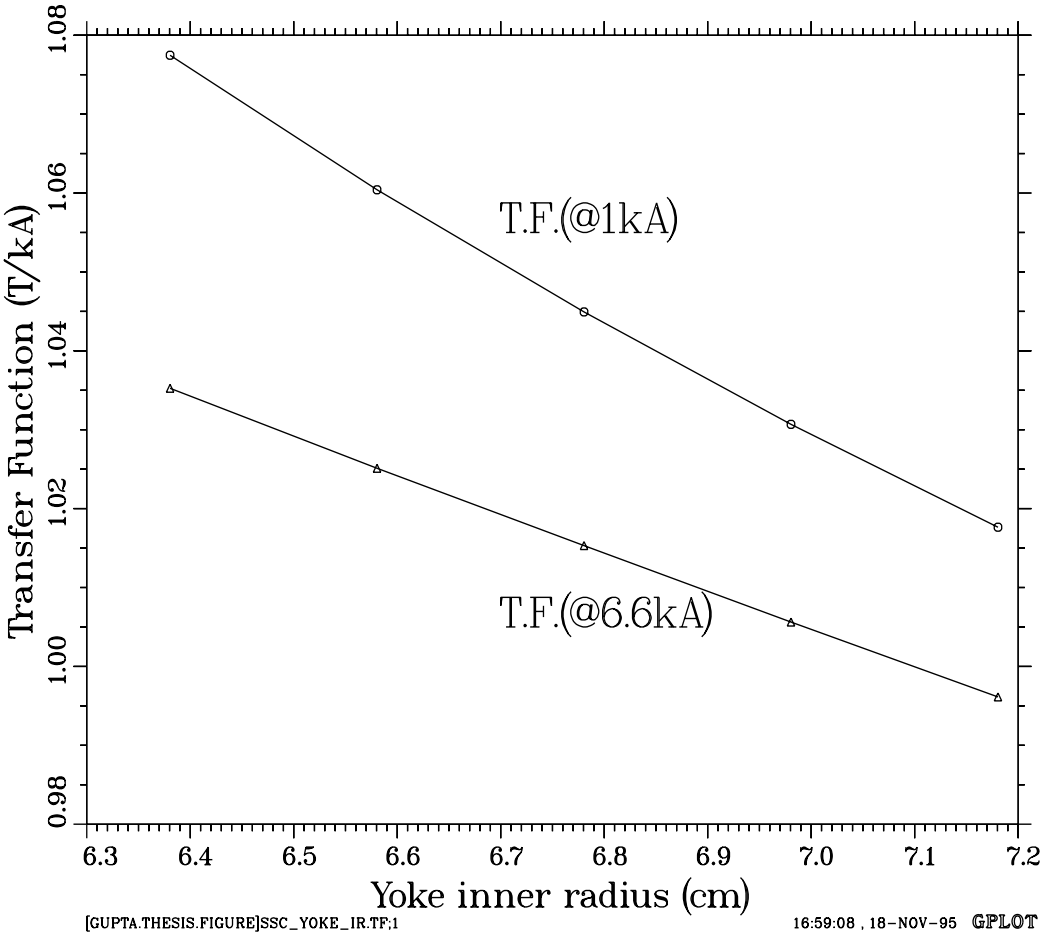

Figure 3.2.5: The computed transfer function as a function of yoke inner radius at the operating currents of 1 kA and 6.6 kA in the SSC 50 mm aperture collider dipole magnet. The design yoke inner radius is 67.8 mm. The yoke outer radius is kept constant at a value of 165.1 mm.

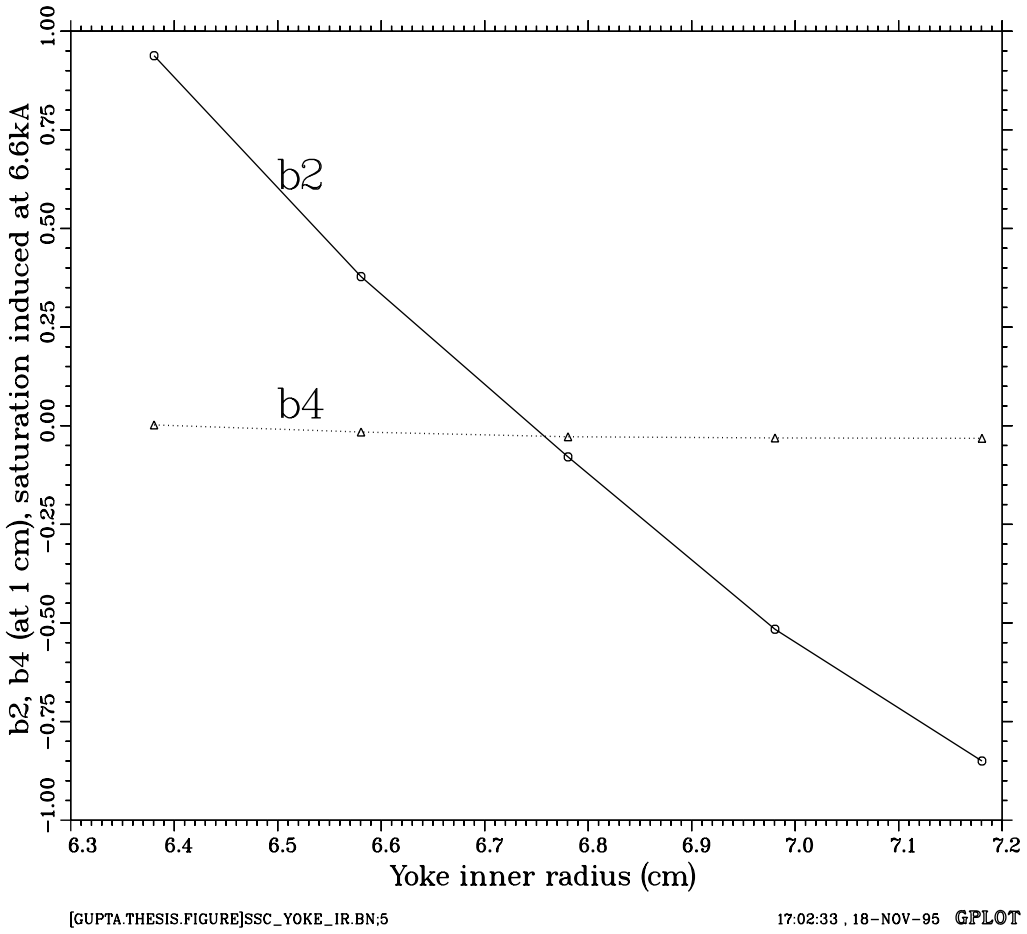

Figure 3.2.6: The computed saturation induced harmonics, b_2 and b_4 as a function of yoke inner radius at a maximum design operating current of 6.6 kA in the SSC 50 mm aperture collider dipole magnet. The saturation induced harmonics are defined as the difference between the low field and high field values of harmonics due to the non-linear properties of the iron yoke. The design yoke inner radius is 67.8 mm and the reference radius is 10 mm. The yoke outer radius is kept constant at a value of 165.1 mm.

3.2.2. Varying the yoke outer radius

The outer yoke radius affects the field only at high current and has little effect at low current. At high field, in addition to changing the transfer function and the saturation induced harmonics, a change in outer yoke radius may also have a significant effect on the fringe field, i.e., the field outside the magnet. Changing the outer yoke radius reduces the yoke thickness which provides a return path for the magnetic field lines or magnetic flux. If the yoke thickness is not enough, the iron at the midplane will saturate. As mentioned earlier, the midplane saturation gives a negative contribution to all allowed harmonics. However, in dipole magnets, the pole saturation gives a positive contribution to the sextupole, a negative decapole, etc. Therefore, the iron saturation, particularly in the first allowed harmonic after fundamental, which is the sextupole in dipole magnets, can be significantly controlled by optimizing the midplane thickness of the yoke. This could be done either by making the yoke outer surface elliptical or by changing the iron outer radius. For simplicity and construction reasons, the yoke outer surface is kept circular while the optimization of the yoke outer radius is examined.

In Fig. 3.2.7, the variation in the saturation induced sextupole and decapole harmonics and the percentage drop in transfer function (from the low field value of transfer function) of the SSC 50 mm dipole magnet are plotted as a function of yoke outer radius at the design current of 6.6 kA. The inner radius of the yoke is kept constant at 67.81 mm and the computer model contains all the holes and cutouts of the optimized design [66]. The values are given in Table 3.2.3.

Table 3.2.3: Saturation induced harmonics and the percentage drop in Transfer Function (δTF) at 6.6 kA as a function of yoke outer radius in the SSC 50 m aperture collider dipole magnets.

Outer Radius (mm)	b_2	b_4	δTF(%)
145.1	-3.303	-0.032	5.579
155.1	-1.768	-0.042	3.886
165.1	-0.073	-0.028	2.819
175.1	1.291	-0.008	2.114
185.1	2.1854	0.008	1.699

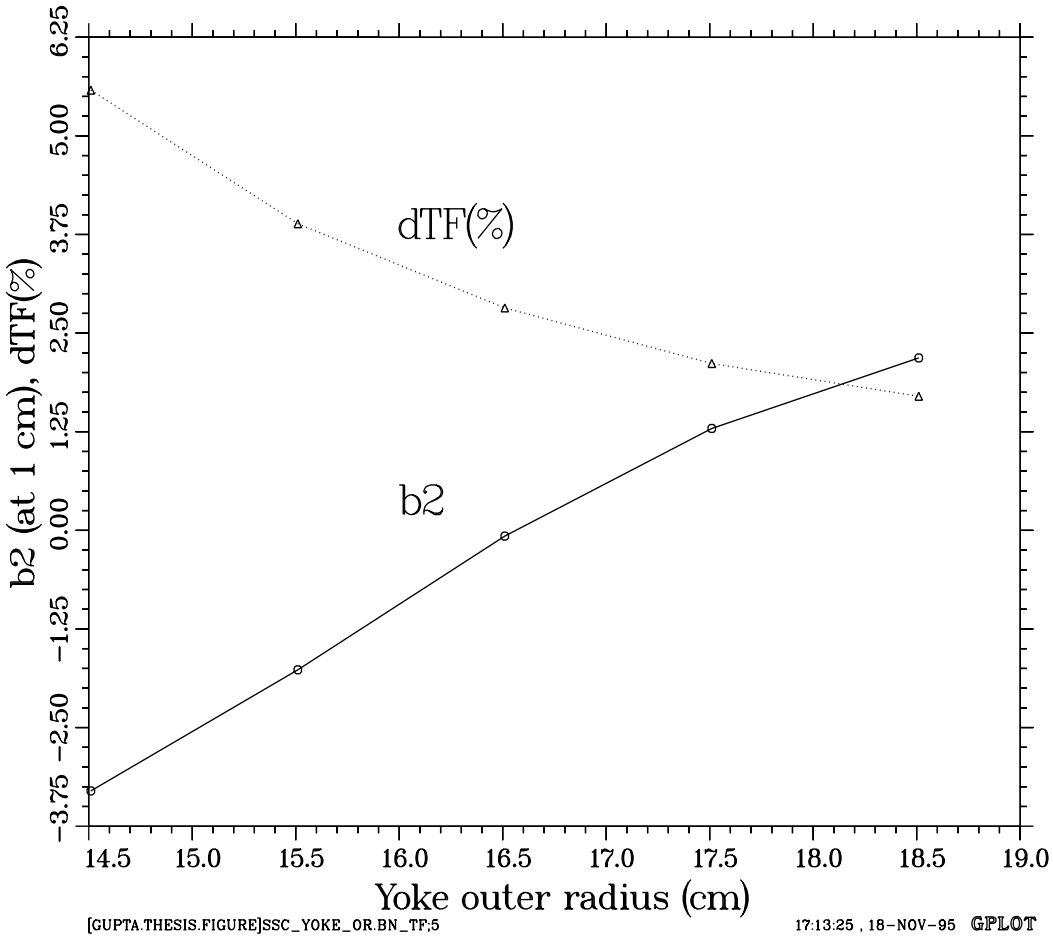

Figure 3.2.7: The effects of varying the outer yoke radius in the SSC 50 mm collider dipole magnet. The nominal value in the design is 165.1 mm. These are the saturation induced harmonics at 6.6 kA, the maximum operating current. dTF(%) is the percentage drop in transfer function at 6.6 kA as compared to its low field value.

The values of the fringe field (the field outside the yoke) on the horizontal plane are given in Table 3.2.4 for an outer radius of 165.1 mm at the maximum operating current of 6.6 kA. In Fig. 3.2.8, the fringe field of the SSC 50 mm dipole outside the yoke on the midplane and in Fig. 3.2.9 on the vertical plane is plotted as a function of distance from the magnet center at a current of 6.6 kA when the yoke outer radius is respectively 14.51,

Table 3.2.4: Fringe field at 6.5 ka on the X-axis in the SSC 50 mm aperture collider dipole magnet at the maximum design current of 6.6 kA. The distance is measured from the magnet center. The yoke outer radius is 165.1 mm.

X (mm)	B_y(Gauss)	$\frac{\partial B_y}{\partial x}(\frac{Gauss}{cm})$
170	1526.160	-4.7933E+02
180	1030.736	-4.2402E+02
190	723.291	-2.1871E+02
200	557.745	-1.2484E+02
210	456.130	-8.2494E+01
220	386.219	-5.9519E+01
230	334.205	-4.5438E+01
240	293.840	-3.5949E+01
250	261.480	-2.9184E+01
260	234.872	-2.4258E+01
270	212.594	-2.0477E+01
280	193.659	-1.7528E+01
290	177.367	-1.5135E+01
300	163.236	-1.3251E+01
310	150.831	-1.1625E+01
320	139.879	-1.0328E+01
330	130.137	-9.1954E+00
340	121.439	-8.2198E+00
350	113.653	-7.4616E+00
360	106.702	-6.7260E+00
370	100.562	-5.7218E+00
380	94.340	-6.6750E+00
390	89.080	-3.5703E+00
400	85.332	-4.0159E+00

16.51 (nominal) and 185.1 mm. In both cases, the fringe field outside the iron falls as $\frac{1}{r^2}$ as expected for a dipole magnet. By comparing the last two figures, one can note that the leakage (fringe) field is much more on the horizontal plane (X-axis) than on the vertical plane (Y-axis). It is clear from these plots, that though the outer radius is a useful parameter to minimize the saturation induced sextupole harmonic, care must be taken so that the yoke outer radius is not made so small as to increase the fringe field above a tolerable limit. In the above calculations, the influence of the cryostat, which is made of magnetic steel, is not included. It can contain a part of the flux outside the yoke.

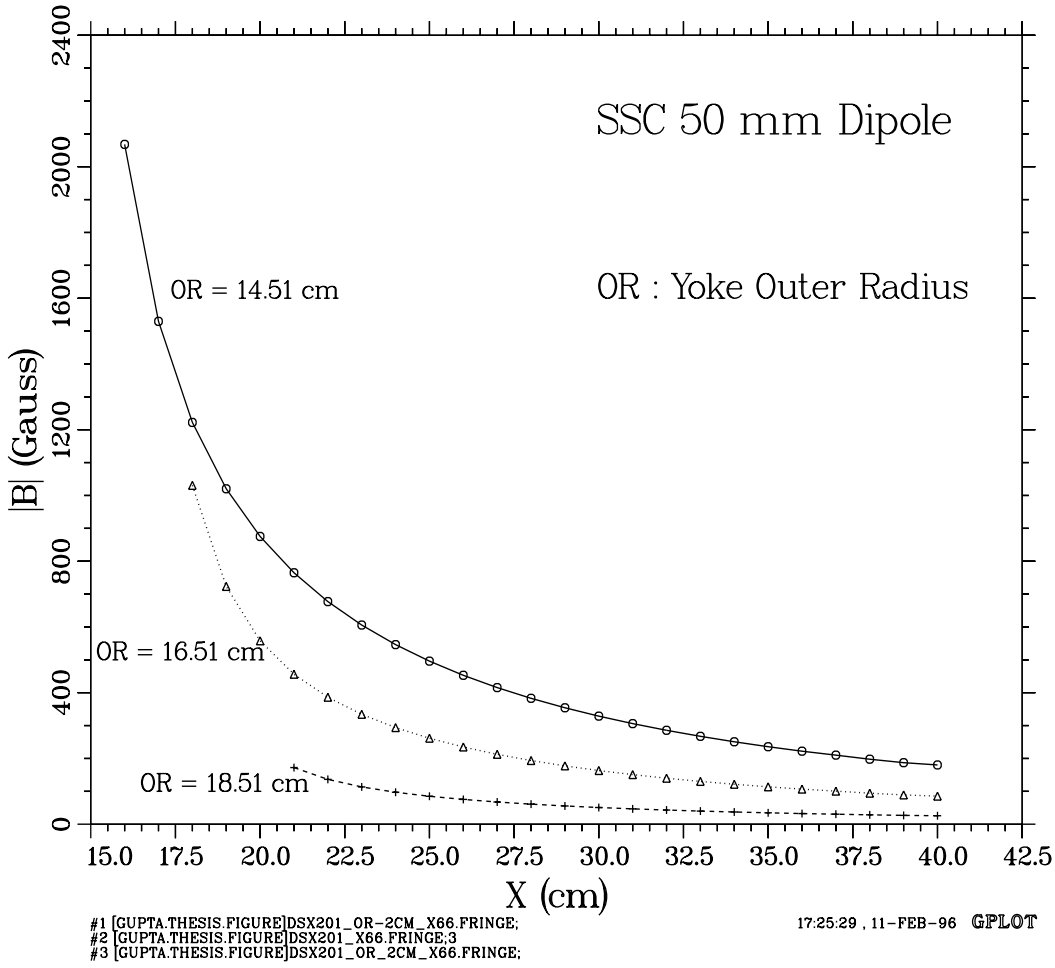

Figure 3.2.8: The effects of varying the outer yoke radius in the SSC 50 mm collider dipole magnet on the fringe field on the horizontal plane (X-axis). The nominal value of the yoke outer radius in the design is 165.1 mm. The cryostat is not present in these model calculations.

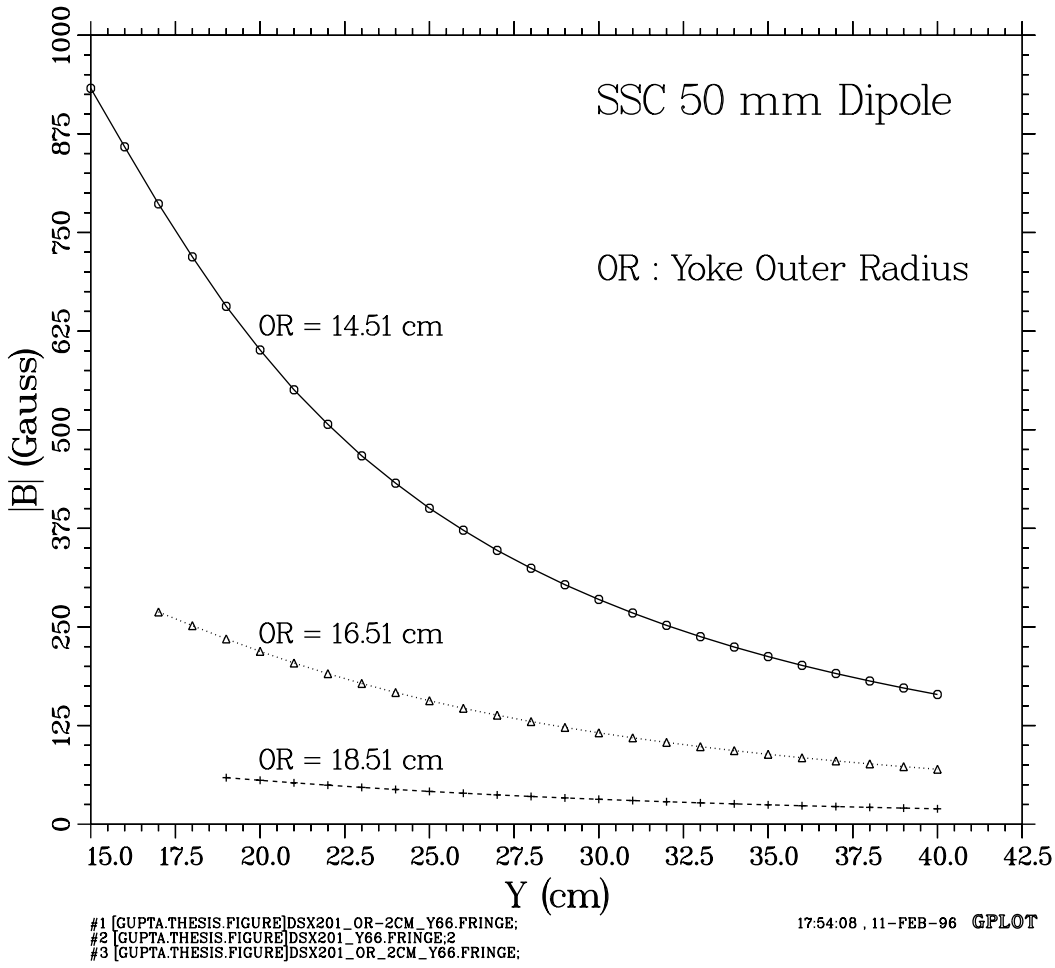

Figure 3.2.9: The influence of varying the outer yoke radius in the SSC 50 mm collider dipole magnet on the fringe field on the vertical plane (Y-axis). The nominal value of the yoke outer radius in the design is 165.1 mm. The cryostat is not present in these model calculations.

3.2.3. Varying the location of the helium bypass hole in the yoke

In superconducting accelerator magnets, the helium coolant must be transported through spaces in the coil and its vicinity and also through several holes in the yoke. The cross section and size of these holes are computed from the cooling requirements. In the RHIC and SSC magnets these holes, which are known as helium bypass holes, have a significantly large cross section. Because of their large size, their effect on the iron saturation can be sizable. In earlier designs they were placed at passive locations (at the poles where the flux density is low) such that their presence would not cause any additional saturation in the yoke. However, it is shown here that by placing them at a proper active location (so that their presence changes the saturation characteristic of the yoke), one can effectively reduce or cancel a few saturation induced harmonics. This method does not have the drawback of significantly increasing the fringe field or of reducing the transfer function.

In the RHIC arc dipole magnets, the location of these holes has been optimized to reduce saturation induced b_2 and b_4 harmonics. There are four holes of equal size and they are placed in the four quadrant of the yoke so that they maintain the basic dipole symmetry. If the hole in the first quadrant is located at a radius R and at an angle θ, the other three must be located at the same radius but at the angles of $(\pi - \theta)$, $(\pi + \theta)$ and $(-\theta)$, respectively. However, in a computer model of the dipoles, only one quarter of the problem needs to be defined. The rest of the geometry is implicitly included by the boundary conditions. Therefore, in the subsequent discussion, the location of only one hole in the first quadrant will be given — the other three holes in other quadrants are implicit as explained above.

In Fig. 3.2.10, the saturation induced b_2 and b_4 harmonics are plotted as a function of the angular position of the helium bypass hole in the RHIC arc dipole at 5 kA current. The values are given in Table 3.2.5. The variation in hole location is performed on a computer model which retained the other holes and cutouts of the present design. The radius of the helium bypass hole is 15.075 mm. Though the radial location of the hole has a significant impact on the saturation induced harmonics, in this figure it is always kept at a radius of 104.1 mm and only the angular position is varied. The final optimized location of the helium bypass hole in the RHIC arc dipole magnet is $R = 104.1$ mm and $\theta = 51°$. The three other holes required by dipole symmetry are placed at the angles of 129°, 231° and 309°, respectively.

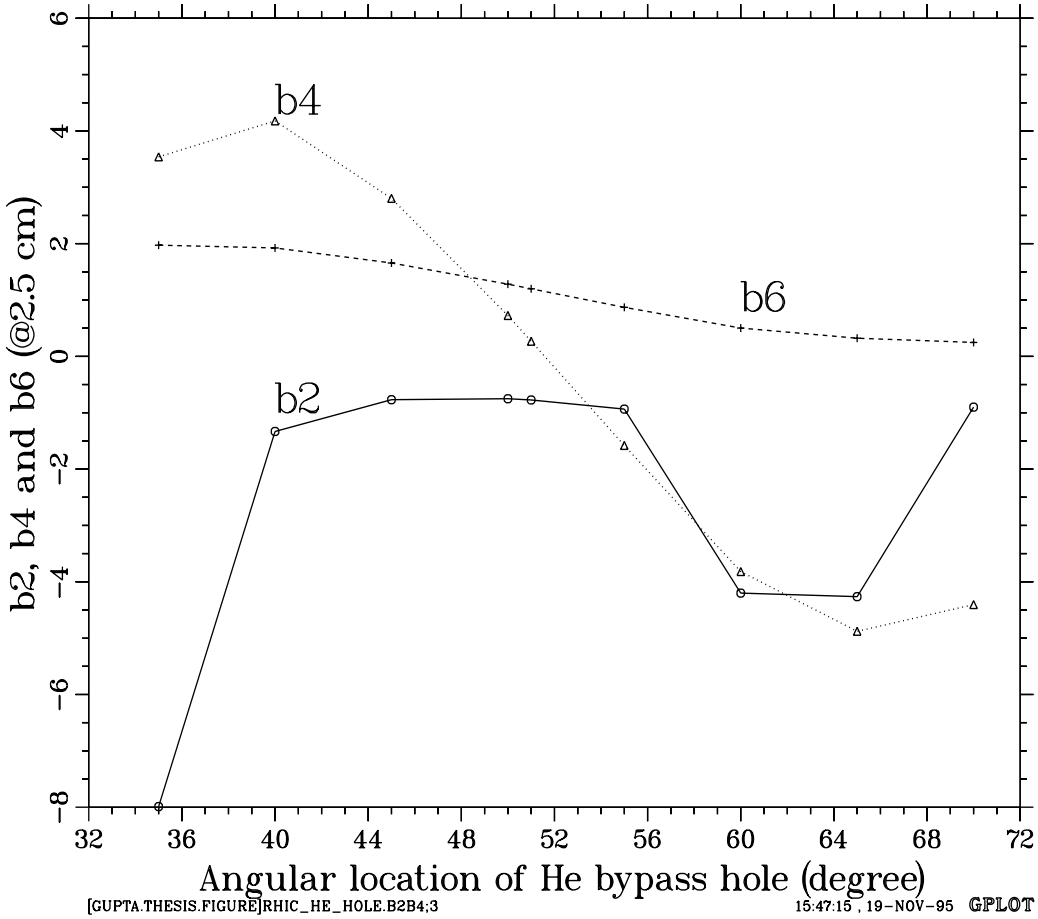

Figure 3.2.10: The influence of the angular location of the helium bypass hole on the saturation induced sextupole (b_2), decapole (b_4) and 14-pole (b_6) harmonics at 5 kA in the RHIC arc dipole magnet. The radial position of this hole is kept at 104.13 mm. There are four such holes in the magnet; their location is determined by the dipole symmetry.

The radial location of the helium hole was optimized in the 100 mm aperture RHIC insertion dipole magnet *D0*. A model for the cross section of a quadrant of this magnet is shown in Fig. 3.2.11. In Fig. 3.2.12, the saturation induced b_2 harmonic is plotted and in Fig. 3.2.13 the saturation induced b_4 and b_6 harmonics are plotted at 4.5 kA (near the nominal maximum operating current) as a function of the angular location of the helium

Table 3.2.5: The influence of the variation in the angular location of the helium bypass hole on the saturation induced harmonics at 5.0 kA in the RHIC arc dipole magnet. The radial position of this hole is kept at 104.13 mm.

Location	Bo(T)	δTF(%)	δb_2	δb_4	δb_6	δb_8	δb_{10}	δb_{12}
35°	3.36241	-5.09321	-7.989	3.540	1.973	0.040	-0.047	-0.016
40°	3.37448	-4.75252	-1.333	4.178	1.924	0.004	-0.052	-0.016
45°	3.38795	-4.37232	-0.769	2.803	1.657	-0.008	-0.046	-0.015
50°	3.40612	-3.85946	-0.752	0.725	1.281	-0.019	-0.035	-0.012
51°	3.41005	-3.74853	-0.774	0.268	1.199	-0.020	-0.033	-0.012
55°	3.42589	-3.30144	-0.936	-1.581	0.870	-0.027	-0.024	-0.010
60°	3.43560	-3.02736	-4.201	-3.819	0.502	-0.032	-0.014	-0.007
65°	3.44521	-2.75612	-4.264	-4.879	0.322	-0.035	-0.008	-0.006
70°	3.44024	-2.89639	-0.901	-4.405	0.247	-0.044	-0.007	-0.006

bypass hole for three radial locations, namely 100 mm, 110 mm and 120 mm. The helium bypass hole itself has a radius of 15.075 mm. The reference radius for the *D0* dipole is 31 mm. During these variations, the two smaller holes shown in Fig. 3.2.11 were not present. The results of the calculations are also shown in Table 3.2.6. In the final design the bypass hole is located at R=106 mm and θ=46°.

The differences in the variation of the harmonics as a function of the angular position of helium bypass hole between 80 mm aperture RHIC arc dipoles (see Fig. 3.2.10) and 100 mm aperture RHIC insertion dipoles *D0* (see Fig. 3.2.12 and Fig. 3.2.13) is attributed to the following factors : *(a)* in the case of the arc dipole magnet model used in this study, all other holes and cutouts beside the helium bypass hole were retained whereas in the *D0* magnet model they were not and *(b)* the relative yoke thickness (i.e. yoke outer radius minus yoke inner radius divided by the coil aperture) is larger in the arc dipoles than in the *D0* dipoles. The maximum operating field is about the same (~3.5 tesla) in the two magnets.

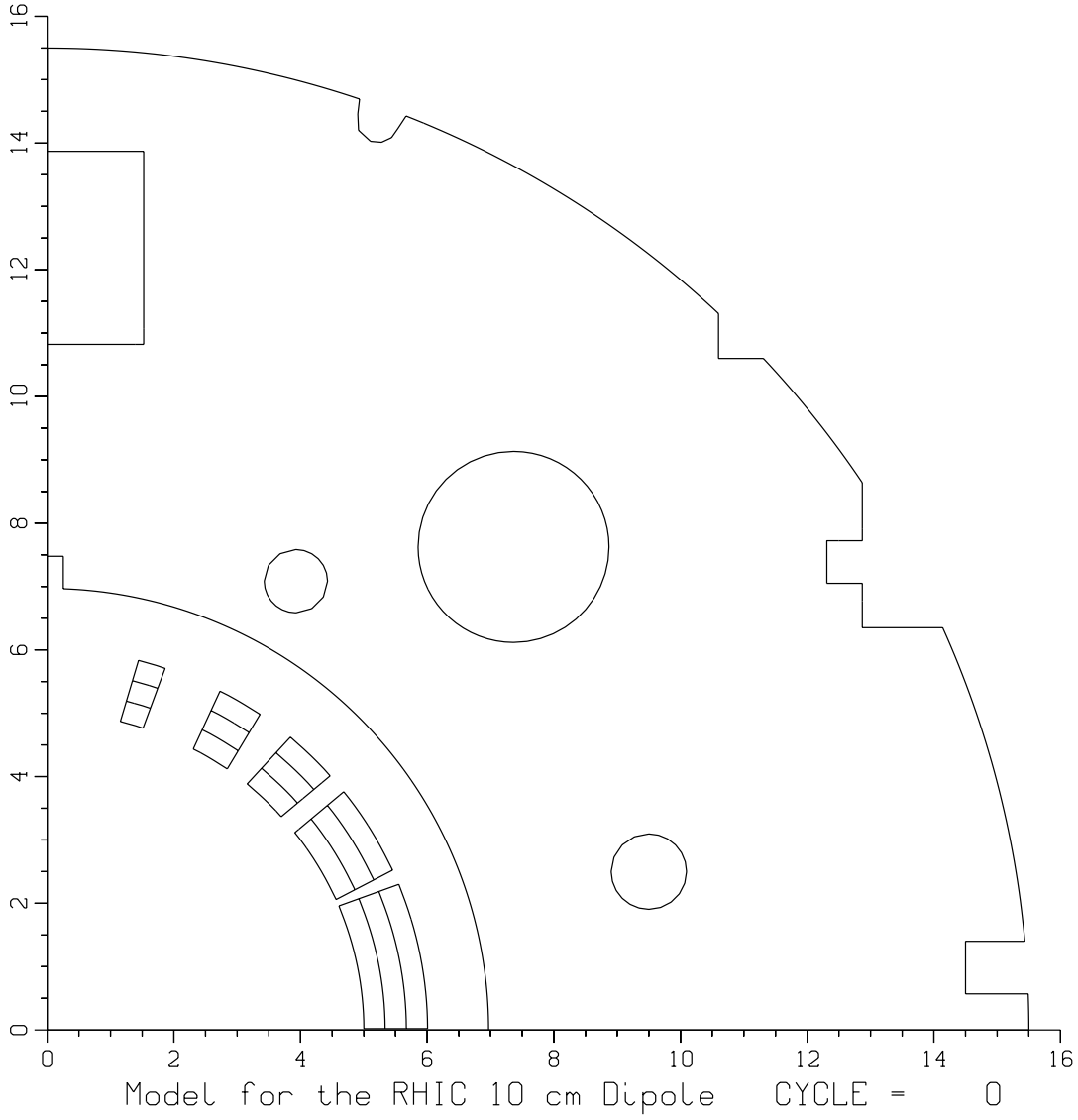

Figure 3.2.11: A computer model of the cold mass of a quadrant of the 100 mm aperture RHIC insertion dipole *D0*. Two cold masses will be put inside a common cryostat (not shown here).

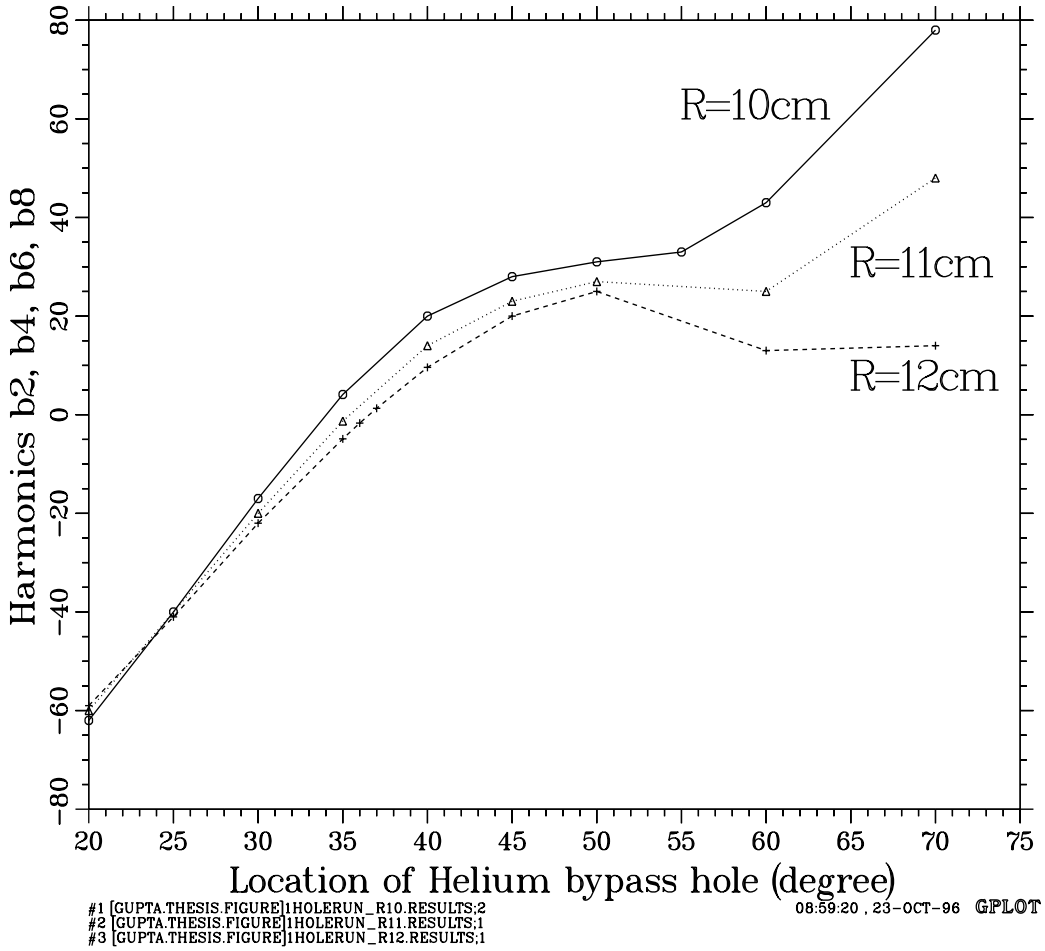

Figure 3.2.12: The influence of the angular location of the helium bypass hole on the saturation induced sextupole harmonic at 4.5 kA in the 100 mm aperture RHIC insertion dipole *D0*. The influence is examined at three radial positions of this hole, namely 100 mm, 110 mm and 120 mm. There are four such holes in the magnet; the location of the three others is determined by dipole symmetry.

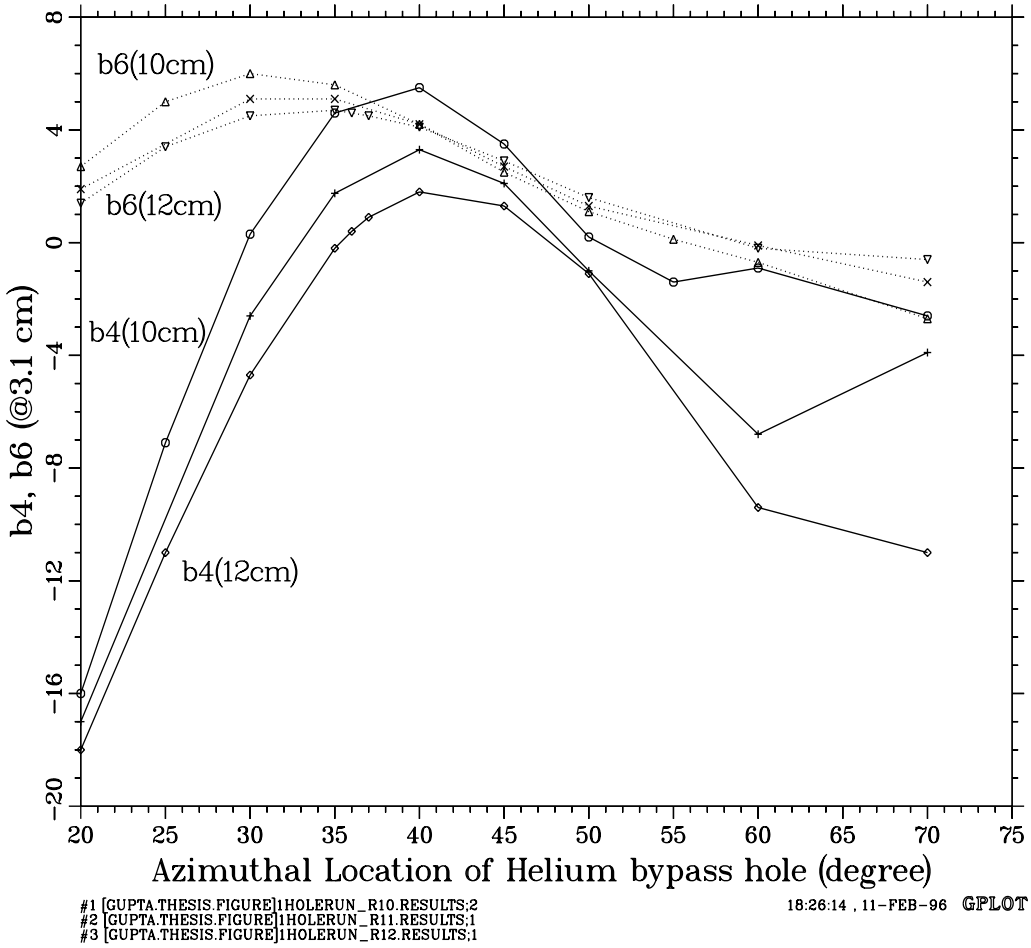

Figure 3.2.13: The influence of the angular location of the helium bypass hole on the saturation induced b_4 and b_6 harmonics at 4.5 kA in the 100 mm aperture RHIC insertion dipole *D0*. The influence is examined at three radial positions of this hole, namely 100 mm, 110 mm and 120 mm. There are four such holes in the magnet; the location of the three others is determined by the dipole symmetry.

Table 3.2.6: Saturation induced harmonics at 4.5 kA in the 100 mm aperture RHIC insertion dipole D0 for various locations of the Helium Bypass Hole. The reference radius for computing field harmonics in is 31 mm. R and θ in the table below indicates the location of the hole.

R mm	θ degrees	δTF %	b_2 Units	b_4 Units	b_6 Units	b_8 Units
100	20	6.68	-62	-16	2.7	1.1
100	25	6.37	-40	-7.1	5.0	1.4
100	30	5.97	-17	0.3	6.0	1.1
100	35	5.50	4.1	4.6	5.6	0.6
100	40	5.00	20	5.5	4.2	0.02
100	45	4.52	28	3.5	2.5	-0.4
100	50	4.13	31	0.2	1.1	-0.5
100	55	4.04	33	-1.4	0.12	-0.6
100	60	4.23	43	-0.9	-0.7	-0.7
100	70	4.81	78	-2.6	-2.7	-0.4
110	20	6.50	-60	-17	1.9	0.8
110	30	5.87	-20	-2.6	5.1	1.0
110	35	5.46	-1.3	1.75	5.1	0.7
110	40	5.00	14	3.3	4.2	0.2
110	45	4.53	23	2.1	2.7	-0.2
110	50	4.07	27	-1.0	1.3	-0.4
110	60	3.53	25	-6.8	-0.1	-0.4
110	70	4.16	48	-3.9	-1.4	-0.5
120	20	6.38	-59	-18	1.4	0.7
120	25	6.14	-41	-11	3.4	1.0
120	30	5.81	-22	-4.7	4.5	1.0
120	35	5.42	-4.9	-0.2	4.7	0.8
120	36	5.34	-1.7	0.4	4.6	0.6
120	37	5.26	1.3	0.9	4.5	0.5
120	40	5.00	9.6	1.8	4.1	0.3
120	45	4.56	20	1.3	2.9	-0.1
120	50	4.12	25	-1.1	1.6	-0.3
120	60	3.78	13	-9.4	-0.2	-0.3
120	70	3.66	14	-11.	-0.6	-0.3

3.2.4. Additional Saturation suppressor holes in the iron yoke

In the last section, the location of the helium bypass holes was adjusted to alter the saturation characteristics of the yoke. In this section, the use of additional holes is investigated for controlling several saturation induced harmonics. In principle, a sufficient number of holes could reduce all required saturation induced harmonics. However, in practice, they can not be placed in any arbitrary position and the location and size of them may be restricted by structural (mechanical) considerations. In the magnet designs examined during the course of this work, an optimized solution was always found such that the mechanical integrity of the magnet was not compromised. These holes do not change the transfer function at low field and their effect is minimal at high field unless they are very large in size.

The calculated predictions were compared with the results of measurements in a RHIC short model of the arc dipole magnet. This magnet, DRS006, was re-built adding one saturation suppressor hole per quadrant. The angular location of this saturation suppressor hole in the first quadrant was $\theta = 33°$ at a radial location of $R = 75$ mm with a size of 4.76 mm. For reference, the location of the helium bypass hole discussed here and in the other cases throughout the rest of this section, is fixed at R =104.1 mm and $\theta = 51°$. The diameter of the helium bypass hole is 30.15 mm. The measurements on DRS006 with saturation suppressor holes were compared with those of another short model magnet DRS008 which did not have these holes but was otherwise built with the same design. These results are shown in Fig. 3.2.14 where the saturation induced harmonics are plotted as a function of current. A significant reduction in the variation in sextupole (b_2) and decapole (b_4) harmonics can be seen. In this particular case, there is an increase in (b_6), however, this is of no significant consequence to machine performance.

In Table 3.2.7, the change in harmonics in the DRS008 design due to the additional saturation suppressor hole is given as a function of its size and location at the maximum design operating current of 5 kA in the RHIC arc dipoles. In Fig. 3.2.15, the computed change in the saturation induced b_2, b_4 and b_6 harmonics due to a circular hole are plotted as a function of its angular location at 5 kA in the RHIC arc dipoles. The radius of this hole is 5 mm and it is always located at a radius of 75 mm. The change in the field harmonics is computed by taking the difference in the saturation induced harmonics between a magnet with and without saturation suppressor holes. The inner radius of the yoke is 59.69 mm. In Fig. 3.2.16, the angular location of the hole is kept at $\theta = 35°$ but the radial location

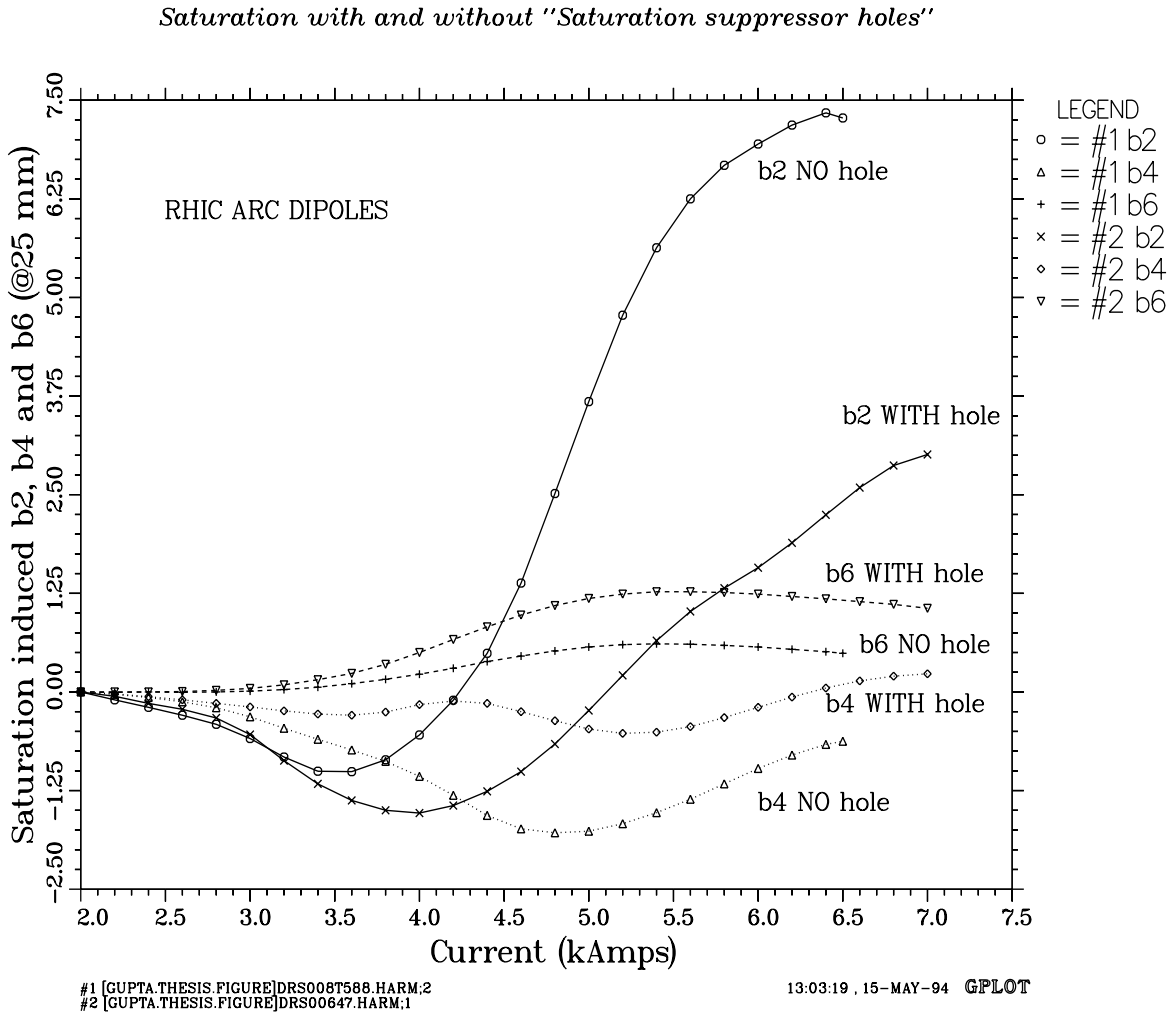

Figure 3.2.14: Saturation induced b_2, b_4 and b_6 harmonics as a function of current in model magnets for RHIC arc dipoles with and without the saturation suppressor holes. Magnet DRS006 was built with these holes and had much smaller saturation as compared to magnet DRS008, which did not have these holes. The harmonics are the average of the measured up and down ramp and they are shifted to start from zero at 2 kA for easy comparison.

is varied. The radius of the hole is still 5 mm. In Fig. 3.2.17, the size of the hole is changed by changing its radius but the location is fixed at $R = 75$ mm and $\theta = 35°$. These plots show that the angular location of the hole determines how much each harmonic will change and the radial location and size of the hole determines the magnitude of this change.

Table 3.2.7: Change in the saturation induced harmonics due to variations in the location of the saturation suppressor holes in an 80 mm aperture RHIC arc dipole at the maximum design operating current of 5 kA. In this table the effect of changing the radial size (R), the radial location (R_0) and the angular location (θ_0) of the saturation suppressor holes is respectively examined.

$R(mm)$	$R_0(mm)$	θ_0	δB_o	$\%\delta$(TF)	δb_2	δb_4	δb_6	δb_8
5	75	10°	-0.02540	-0.71693	-17.34	-3.238	-0.491	-0.056
5	75	15°	-0.03044	-0.85919	-17.10	-2.083	-0.057	0.053
5	75	20°	-0.02441	-0.68899	-9.695	0.128	0.418	0.125
5	75	25°	-0.01431	-0.40390	-4.419	0.867	0.483	0.108
5	75	30°	-0.01758	-0.49620	-7.500	0.667	0.577	0.119
5	75	35°	-0.02311	-0.65229	-4.622	2.161	0.719	0.076
5	75	40°	-0.02756	-0.77790	2.914	3.868	0.544	-0.030
5	75	45°	-0.02590	-0.73104	11.132	4.247	0.054	-0.115
5	75	50°	-0.01717	-0.48463	14.543	2.794	-0.407	-0.110
5	75	55°	-0.00708	-0.19983	9.621	0.889	-0.394	-0.040
5	75	60°	-0.00286	-0.08072	2.191	0.293	-0.085	-0.006
5	75	65°	-0.00383	-0.10811	2.775	0.301	-0.102	-0.001
5	75	70°	-0.00448	-0.12645	3.828	0.172	-0.127	0.007
5	70	35°	-0.02705	-0.76350	-2.180	3.255	0.796	0.042
5	75	35°	-0.02311	-0.65229	-4.622	2.161	0.719	0.076
5	80	35°	-0.01877	-0.52979	-5.461	1.336	0.592	0.085
5	85	35°	-0.01419	-0.40052	-4.864	0.794	0.438	0.073
5	90	35°	-0.00983	-0.27746	-3.141	0.543	0.284	0.050
5	95	35°	-0.00745	-0.21028	-1.148	0.609	0.185	0.025
5	100	35°	-0.00766	-0.21621	-1.111	0.601	0.173	0.024
3	75	35°	-0.00886	-0.25008	-2.737	0.699	0.318	0.043
4	75	35°	-0.01508	-0.42564	-3.896	1.298	0.509	0.063
5	75	35°	-0.02311	-0.65229	-4.622	2.161	0.719	0.076
6	75	35°	-0.03272	-0.92354	-4.898	3.264	0.940	0.085
7	75	35°	-0.04354	-1.22895	-4.899	4.529	1.171	0.090
8	75	35°	-0.05549	-1.56624	-4.771	5.924	1.413	0.095

In the 80 mm aperture RHIC arc dipoles, this method has been used in the final design for optimizing the yoke. By putting a small additional saturation suppressor hole having a radius of 4.76 mm at $R = 75$ mm and $\theta = 35.5°$ in addition to the other holes and cutout

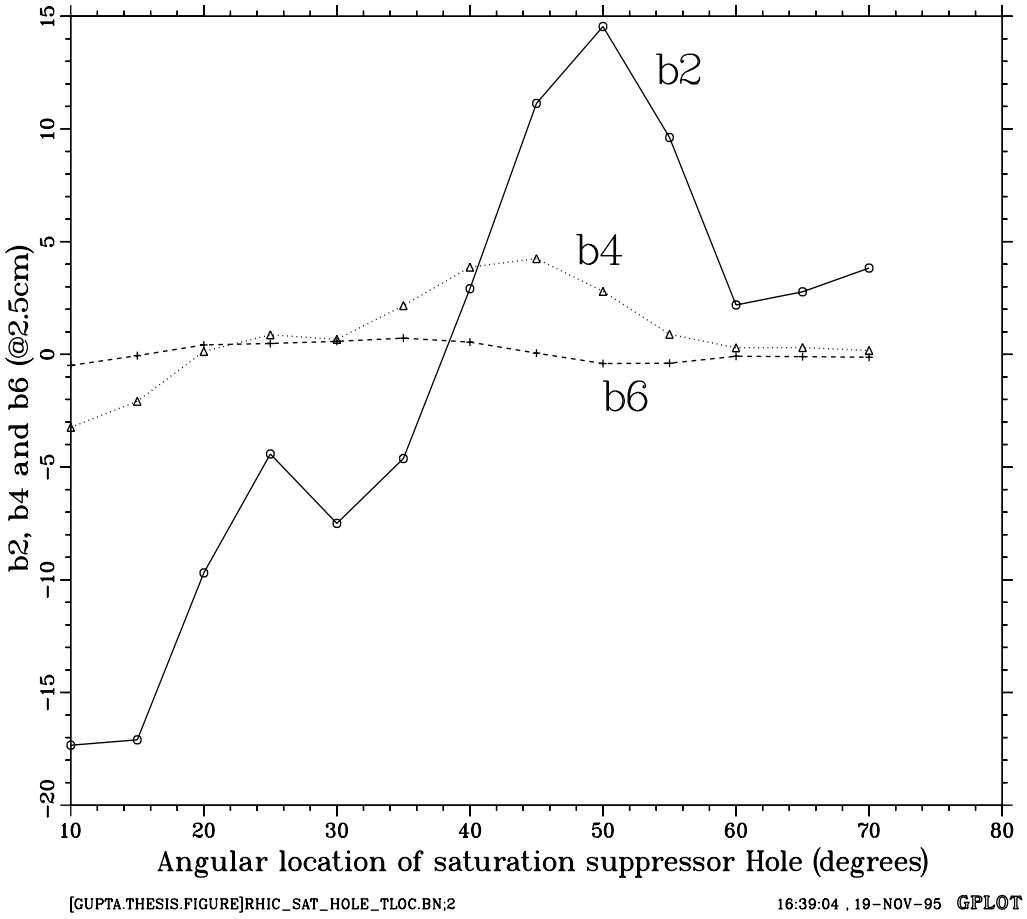

Figure 3.2.15: Saturation induced b_2, b_4 and b_6 harmonics generated at 5 kA by a 10 mm diameter saturation suppressor hole as a function of its angular location in the first quadrant. The radial location of this hole was kept at 75 mm. The location of three other holes is determined by the basic dipole symmetry. These are the changes in the harmonics which are computed by taking the difference in the saturation induced harmonics when (a) these holes were present and (b) were not present in the computer model.

required for various purpose (see Fig. 3.2.1), the b_2 saturation is kept below 3 unit and b_4 saturation below 0.6 unit in the entire range of operation.

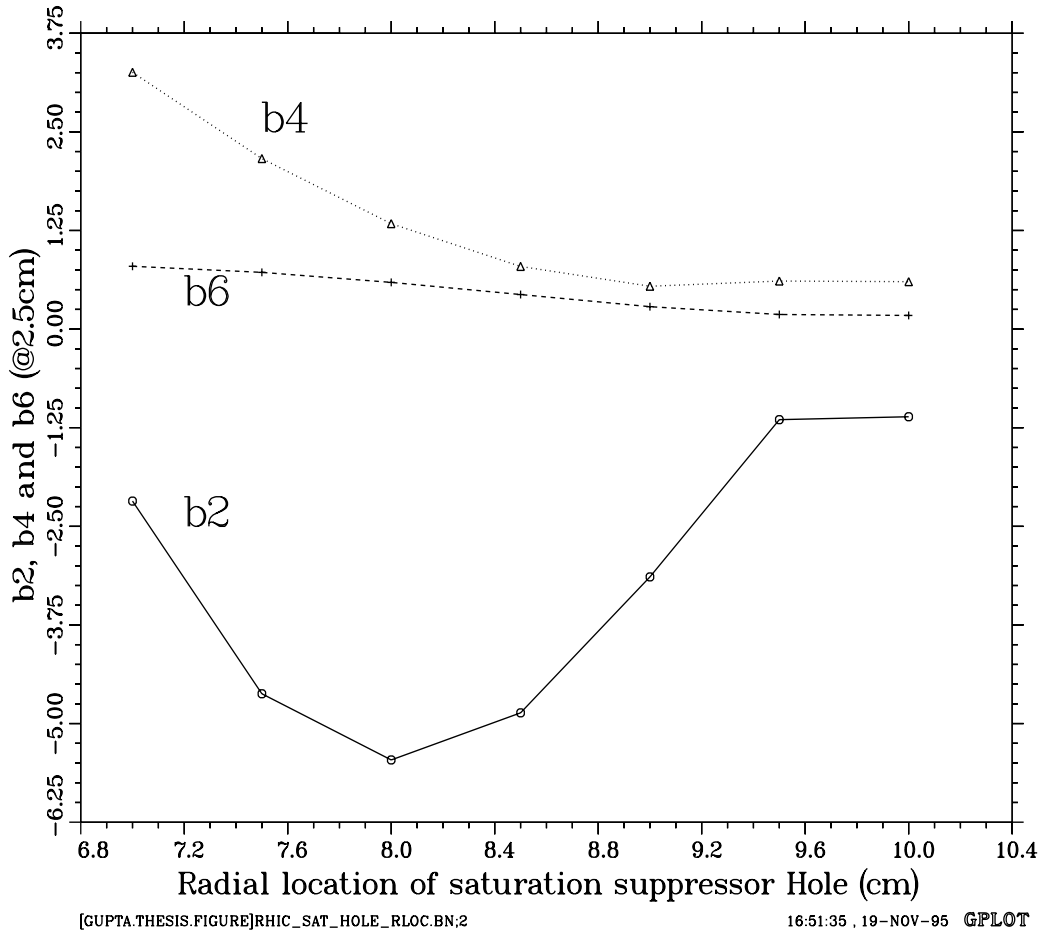

Figure 3.2.16: Saturation induced b_2, b_4 and b_6 harmonics generated at 5 kA by a 10 mm diameter saturation suppressor hole as a function of its radial location. The angular location of this hole was kept at 35°. These are the changes in the harmonics which are computed by taking the difference in the saturation induced harmonics when (a) these holes were present and (b) were not present in the computer model.

In the 100 mm aperture RHIC insertion *D0* dipoles, a similar hole (having a radius of 10 mm) has been placed at $R = 81$ mm and $\theta = 61°$. This, in addition to properly positioning the helium bypass hole, has reduced b_2, b_4 and b_6 saturation to less then 3, 1, 0.5 unit respectively. The saturation in higher order harmonics is less than 0.2 unit.

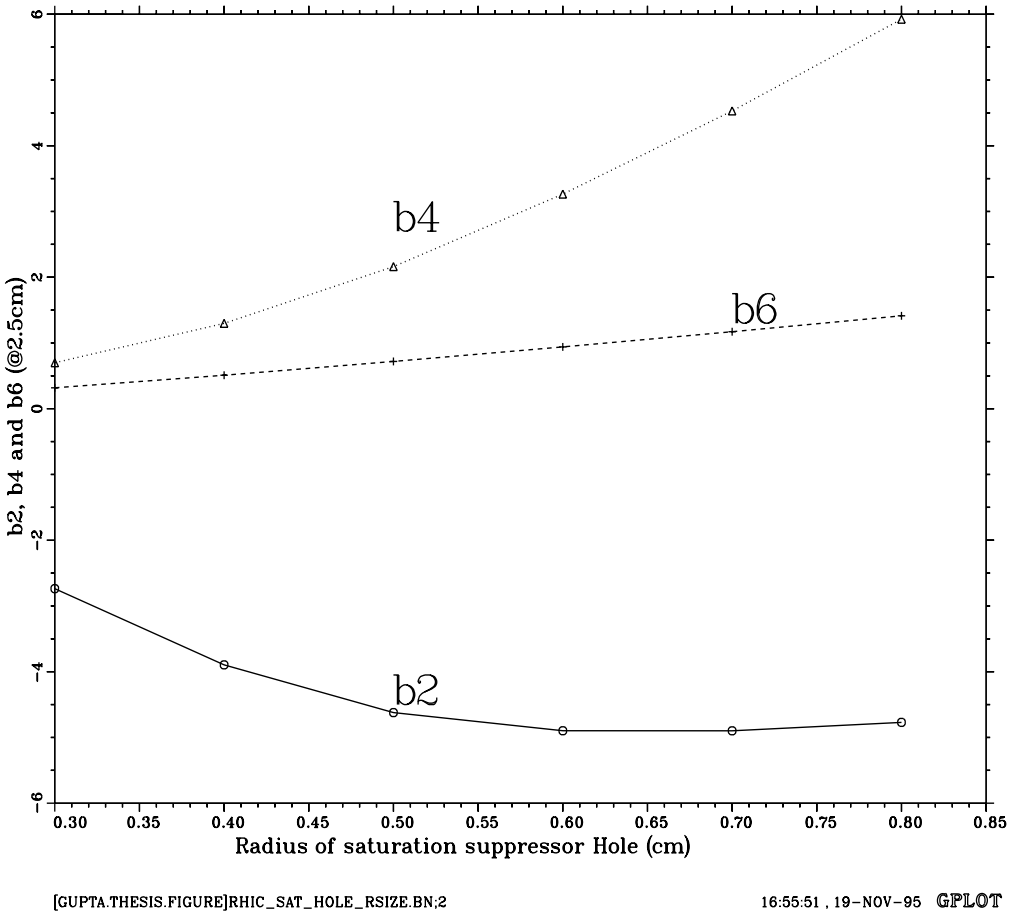

Figure 3.2.17: Saturation induced b_2, b_4 and b_6 harmonics generated at 5 kA by a saturation suppressor hole as a function of its size (radius). The center of this hole was kept at a radius 75 mm and at an angle of 35°. These are the changes in the harmonics which are computed by taking the difference in the saturation induced harmonics when (a) these holes were present and (b) were not present in the computer model.

3.2.5. Yoke-yoke alignment keys

The SSC magnets built at BNL were based on a horizontally split yoke design. In such designs the top and bottom yoke halves of the magnet are aligned with the help of two keys at the midplane, the slot for one of which is shown in Fig. 3.2.2 . At high field, the saturation induced harmonics depend on the type of material used in the keys. These keys are usually made of low carbon magnetic steel to provide the maximum magnetic material in the return path for the flux at the yoke midplane. However, the structural requirement is satisfied by keys made of either low carbon magnetic steel or non-magnetic stainless steel. When the keys are made of non-magnetic stainless steel, the return flux density on the midplane is greater. This makes the midplane saturate more and at a relatively lower field than otherwise it would have. Since the midplane saturation gives a negative b_2, which is opposite to the sign of b_2 given by the pole saturation, one can optimize the size and/or location of the stainless steel keys to minimize this harmonic. A similar saturation control can be achieved by adjusting the yoke outer diameter, with an undesirable increase in the fringe field if the diameter is decreased.

In SSC magnets, a stainless steel key of 12.7 mm$\times$ 12.7 mm cross section was placed at x = 91.44 mm to keep b_2 saturation under 0.4 unit over the entire range of operation. As shown in Fig. 3.2.18, the b_2 saturation is first positive and then negative but the magnitude is always under 0.4 unit. In the Fermilab-built SSC magnets, the yoke is vertically split and therefore the yoke-yoke alignment key is located on the vertical axis. To obtain the BNL-type saturation control in the Fermilab design, a square cutout was placed at the yoke midplane.

In Fig. 3.2.18, the saturation induced sextupole and decapole harmonics are plotted as a function of current in the SSC 50 mm aperture dipole magnets when these keys were made of either magnetic or non-magnetic material. The values are given in Table 3.2.8 in the case of non-magnetic keys and in Table 3.2.9 in the case of magnetic keys. Though in the nominal design, the material of the keys was non-magnetic stainless steel, a magnet was built at KEK in which the keys were made of low carbon magnetic steel. Good agreement was found between the calculations and measurements in these two cases.

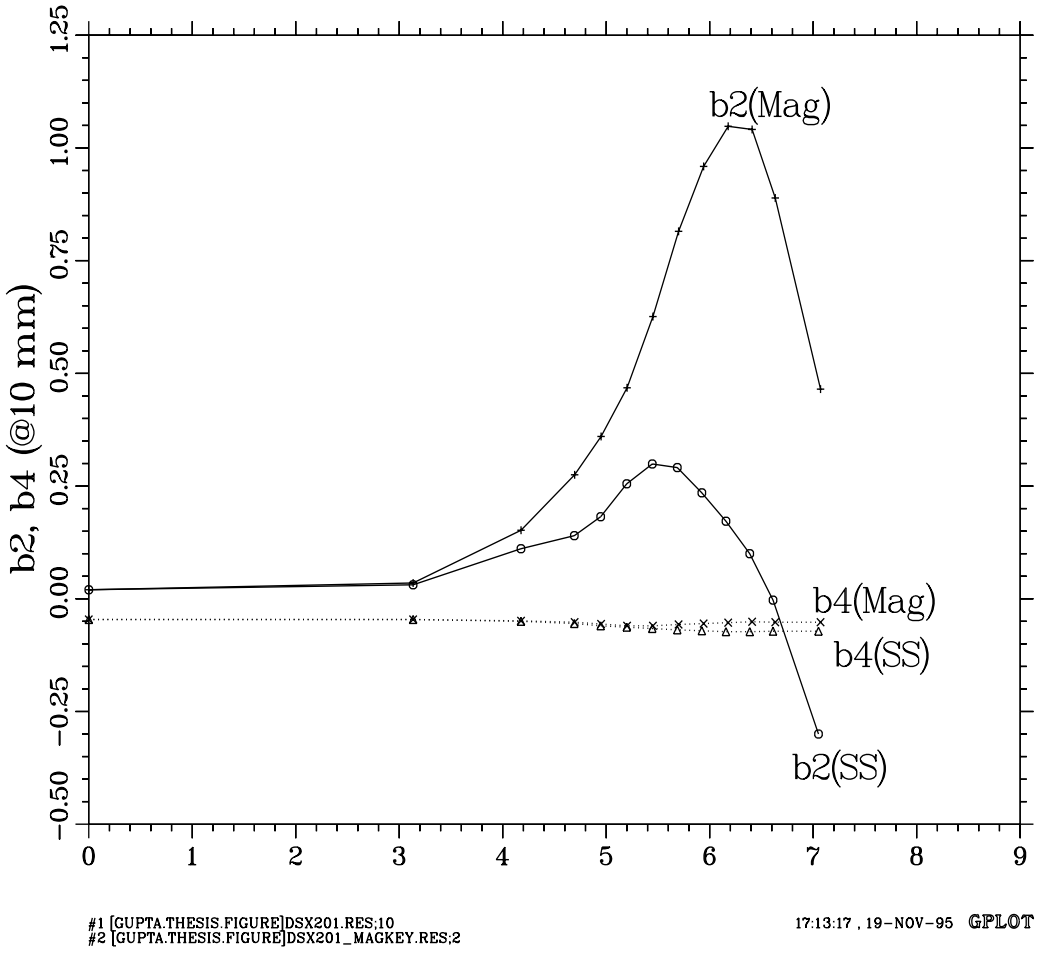

Figure 3.2.18: The computed saturation induced harmonics as a function of current in the Brookhaven design of the SSC collider arc dipole magnets when the material of the yoke-yoke alignment keys is (a) stainless steel (non-magnetic) or (b) low carbon steel (magnetic). The material of the key has been used as the primary method of reducing the saturation induced harmonics in the SSC 40 mm aperture and SSC 50mm dipole magnets. In the Fermilab vertically split yoke design, a cutout was introduced in the midplane of the yoke since the yoke-yoke alignment key is on the vertical plane.

Table 3.2.8: The computed harmonics as a function of current in the BNL-built SSC 50 mm aperture dipoles in the case when the yoke-yoke alignment keys are made of *non-magnetic stainless steel (ss).*

I(kA)	B_o(T)	TF(T/kA)	$(b_2)_{ss}$	$(b_4)_{ss}$	$(b_6)_{ss}$	$(b_8)_{ss}$
0.00	0.00	1.04493	0.020	-0.046	0.000	0.047
3.00	3.13413	1.04471	0.031	-0.046	0.001	0.047
4.00	4.17625	1.04406	0.111	-0.050	0.001	0.047
4.50	4.69208	1.04268	0.140	-0.055	0.001	0.047
4.75	4.94641	1.04135	0.182	-0.060	0.001	0.047
5.00	5.19846	1.03969	0.255	-0.063	0.001	0.047
5.25	5.44536	1.03721	0.299	-0.066	0.001	0.047
5.50	5.68711	1.03402	0.291	-0.069	0.001	0.048
5.75	5.92405	1.03027	0.235	-0.071	0.001	0.048
6.00	6.15729	1.02621	0.172	-0.073	0.000	0.048
6.25	6.38679	1.02189	0.100	-0.073	0.000	0.048
6.50	6.61214	1.01725	-0.003	-0.072	0.000	0.048
7.00	7.05133	1.00733	-0.300	-0.072	0.000	0.049

Table 3.2.9: The computed harmonics as a function of current in the BNL-built SSC 50 mm aperture dipoles in the case when the yoke-yoke alignment keys are made of *magnetic low carbon steel (mag).*

I(kA)	B_o(T)	TF(T/kA)	$(b_2)_{mag}$	$(b_4)_{mag}$	$(b_6)_{mag}$	$(b_8)_{mag}$
0.00	0.00	1.04493	0.020	-0.046	0.000	0.047
3.00	3.13418	1.04473	0.035	-0.046	0.001	0.047
4.00	4.17703	1.04426	0.152	-0.049	0.001	0.047
4.50	4.69495	1.04332	0.275	-0.052	0.001	0.047
4.75	4.95052	1.04221	0.360	-0.056	0.001	0.047
5.00	5.20167	1.04033	0.468	-0.060	0.001	0.047
5.25	5.45140	1.03836	0.626	-0.060	0.001	0.047
5.50	5.69941	1.03626	0.815	-0.057	0.001	0.048
5.75	5.94138	1.03328	0.959	-0.055	0.001	0.048
6.00	6.17865	1.02978	1.048	-0.053	0.001	0.048
6.25	6.41005	1.02561	1.041	-0.051	0.001	0.048
6.50	6.63365	1.02056	0.889	-0.052	0.000	0.048
7.00	7.07118	1.01017	0.465	-0.052	0.001	0.049

3.2.6. Yoke collaring keys

All RHIC magnets are based on a horizontally split yoke design. Moreover, in most of these magnets, the yoke also acts as the collar providing pre-compression on the coils. Yoke collaring keys are inserted on the outer periphery near the midplane to hold the applied compression on the coil. The present RHIC design uses a total of four keys in the complete 360° cross section; the slot for one of which is shown in Fig. 3.2.1. These collaring keys can be made of either low carbon magnetic steel or non-magnetic stainless steel. As in the case of yoke-yoke alignment keys, the saturation induced harmonics depends on the type of material used in the keys. However, in this case there is less flexibility in choosing their size and location. Nonetheless, it is a useful tool.

In Fig. 3.2.19, the saturation induced sextupole and decapole harmonics are plotted as a function of current in the RHIC magnets when these keys were made of magnetic or non-magnetic material. The values are given in Table 3.2.10 in the case of non-magnetic keys and in Table 3.2.11 in the case of magnetic keys. The final design of the RHIC arc dipole magnets uses the stainless steel keys.

Table 3.2.10: The computed harmonics as a function of current in the 80 mm aperture RHIC arc dipoles in the case when the yoke collaring keys are made of *non-magnetic stainless steel.*

I(kA)	B_o(T)	δTF(%)	b_2(ss)	b_4(ss)	b_6(ss)	b_8(ss)
0.0	0.00000	0.00000	0.000	0.000	0.000	0.000
1.0	0.70837	-0.02780	0.049	0.013	0.003	0.001
2.0	1.41669	-0.03190	0.009	0.020	0.006	0.001
3.0	2.12224	-0.16338	0.241	0.148	0.083	-0.005
4.0	2.79470	-1.39662	-0.369	1.037	0.603	-0.030
4.5	3.10599	-2.58986	-0.819	1.242	1.037	-0.037
5.0	3.39914	-4.05648	-2.600	0.778	1.303	-0.014
5.5	3.67461	-5.71010	-6.822	0.106	1.271	0.005
6.0	3.93935	-7.34050	-10.690	-0.235	1.125	0.013
7.0	4.44724	-10.33785	-13.925	-0.367	0.862	0.024

Table 3.2.11: The computed harmonics as a function of current in the 80 mm aperture RHIC arc dipoles in the case when the yoke collaring keys are made of *magnetic low carbon steel.*

I(kA)	B_o(T)	δTF(%)	b_2(mag)	b_4(mag)	b_6(mag)	b_8(mag)
0.0	0.000	0.000	0.000	0.000	0.000	0.000
1.0	0.70838	-0.02752	0.050	0.014	0.004	0.001
2.0	1.41670	-0.03119	0.019	0.021	0.006	0.001
3.0	2.12239	-0.15633	0.346	0.161	0.085	-0.005
4.0	2.79757	-1.29536	1.471	1.322	0.643	-0.026
4.5	3.11114	-2.42835	2.303	1.720	1.103	-0.031
5.0	3.40729	-3.82644	2.184	1.539	1.410	-0.002
5.5	3.68807	-5.36471	1.080	1.475	1.474	0.034
6.0	3.95648	-6.93758	-0.848	1.534	1.393	0.053
7.0	4.46426	-9.99470	-4.910	1.235	1.098	0.057

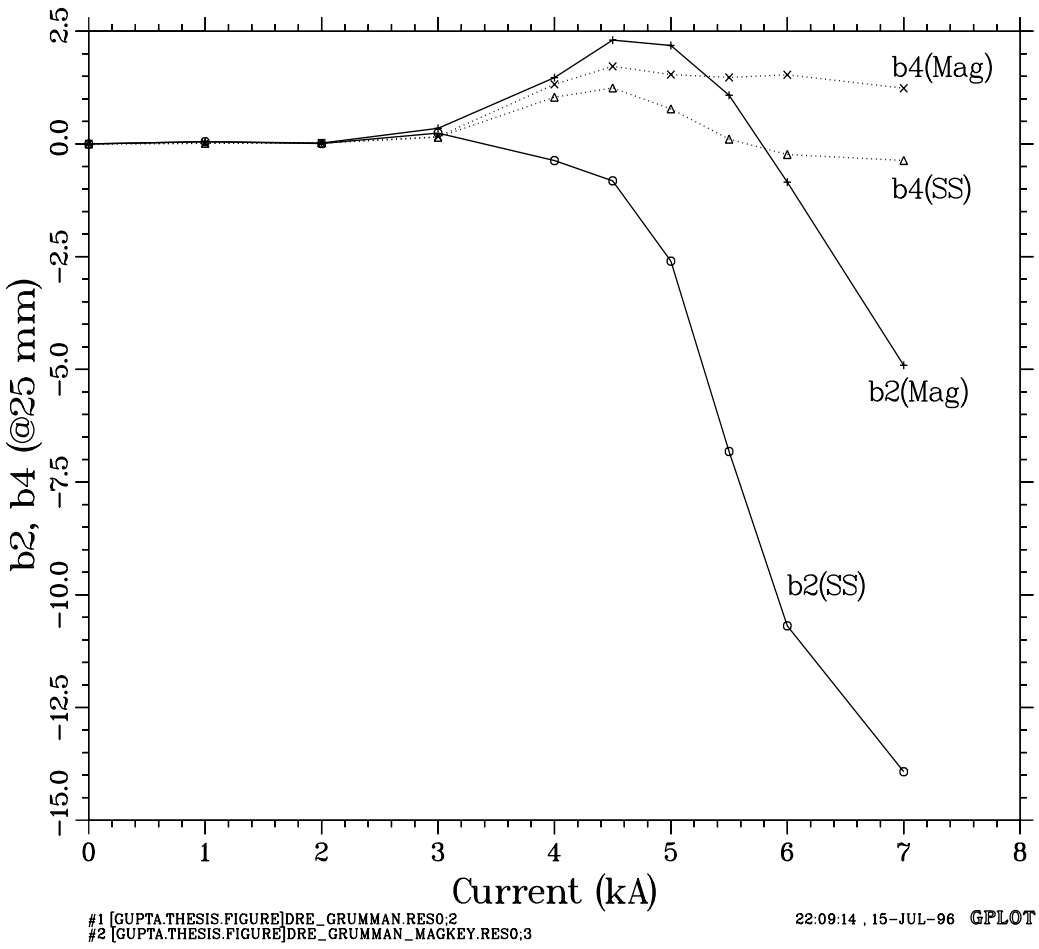

Figure 3.2.19: The computed saturation induced harmonics as a function of current in the RHIC arc dipoles when the material of the yoke collaring keys is either stainless steel (non-magnetic) or low carbon steel (magnetic). The material of the key has been used to reduce the saturation induced harmonics.

3.2.7. Tooth at the midplane of the yoke aperture

The center and orientation of the coil must be aligned to that of the yoke. The geometry of the coil in the magnet is controlled and defined by the structure between the yoke and the coil. In SSC magnets, it is a stainless steel collar whose function has been explained earlier. In RHIC magnets, it is a molded phenolic (brand name RX630) spacer, whose purpose, in addition to providing electrical isolation, is to fill the space such that the geometry of the coil is well defined with respect to the yoke. Both of these materials are non-magnetic.

The earlier designs of both SSC and RHIC magnets had a notch in the yoke inner diameter at the midplane for the purpose of alignment. This notch, however, can be put either at the midplane or at the pole. In both cases a part of the magnetic material (yoke) that is close to the magnetic center is removed. A midplane location for the notch is preferred over the pole location for magnetic reasons, since the magnetic field at the pole is a maximum and a notch there increases the pole saturation significantly. However, a pole location is preferred for mechanical reasons since that location gives better control in defining the coil location in the magnet. Since the pole saturation is compensated with other methods, in the final production design of RHIC magnets the pole location was used.

One can obtain the required mechanical alignment between the coil and yoke if the notch is put in the stainless steel collar or phenolic spacer instead of the yoke. In this case the iron has a tooth which protrudes inwards towards the coil. Although the notch and tooth provide a similar mechanical function, there is a significant difference in the magnetic properties of the two. In one case the iron is taken away from the midplane in the yoke aperture whereas in the other case, iron is added to the midplane. Because of this difference, the notch gives a negative b_2 and b_4 due to saturation, whereas the tooth gives a positive b_2 and b_4 due to saturation, as compared to the saturation in these harmonics when neither of the two is present.

A comparison of the effects of a tooth or a notch was seen in the measurements of RHIC long model magnets DRB005 and DRB006 having a notch at the midplane with that of short model magnet DRS003 having a tooth at the midplane. In the dipoles DRB005 and DRB006, the value of b_4 saturation was larger than desired. Calculations showed that if the midplane notch in the yoke were replaced by a tooth at the midplane, the b_4 saturation would be reduced from -5.8 unit to -3.1 unit. In Fig. 3.2.20, the saturation induced b_2 and b_4 harmonics are plotted in the presence of tooth or notch in magnets DRB005 and DRB006. The values are shown in Table 3.2.12 and in Table 3.2.13. A short magnet DRS003

was built to test these calculations and the measurements showed that the difference in saturation between this and magnets DRB005 and DRB006 was the same as predicted by the calculations. This feature was, however, not incorporated in the final RHIC arc dipole design because for mechanical reasons the preferred place for the notch or tooth is the pole instead of midplane. A tooth instead of notch would be undesirable at the pole location as that position would result in very large saturation harmonics. Hence, in the final design for the RHIC production magnets, a pole notch was used and the saturation induced harmonics created by it were compensated by the modifications in the yoke which are discussed in the other sections of this chapter.

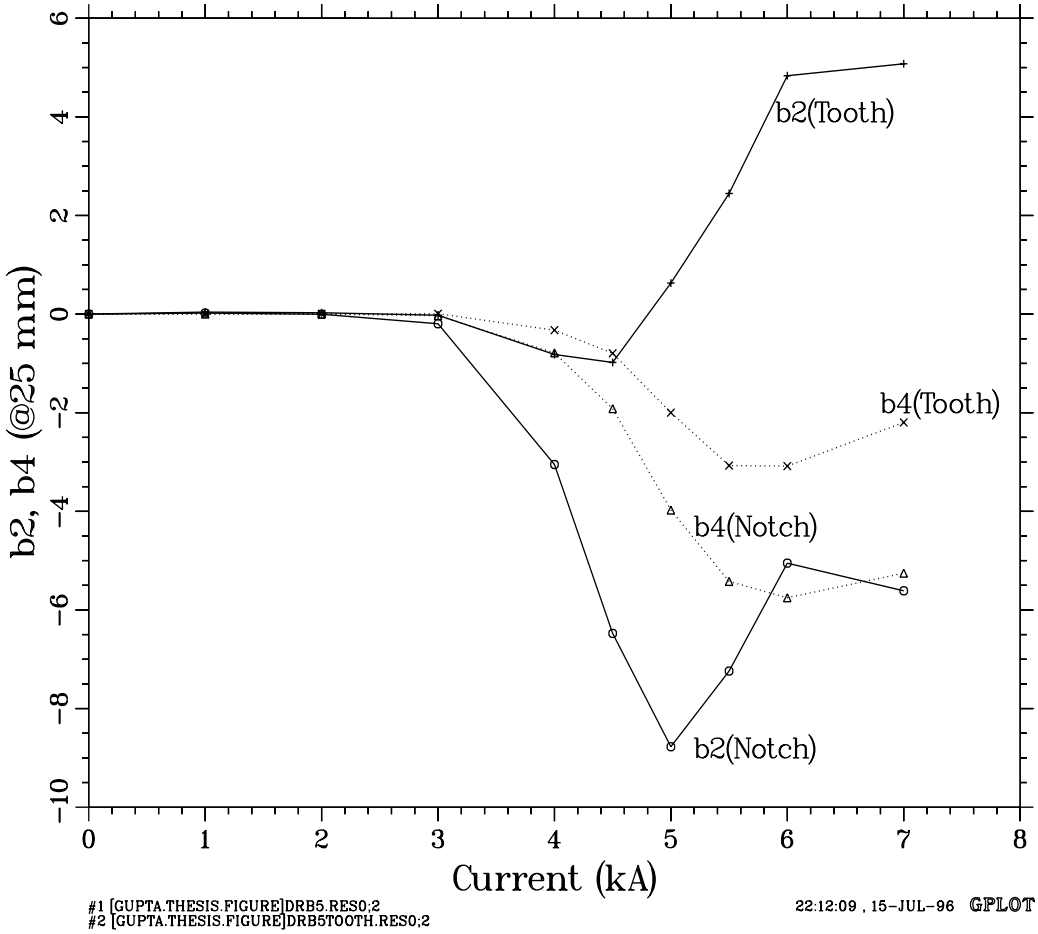

Figure 3.2.20: The computed variation in the b_2 and b_4 harmonics as a function of current when a notch is present at the midplane or when instead a tooth is present at the midplane. There is a significant improvement in the b_4 saturation when the notch is replaced by a tooth. There is also a significant change in the behavior of the b_2 saturation.

Table 3.2.12: The computed saturation induced harmonics in the RHIC arc dipoles DRB005 and DRB006 (as built per Drawing No. 22-398.05-5) which has notches in the yoke inner surface at the midplane.

I(kA)	B_o(T)	δTF(%)	b_2	b_4	b_6	b_8
0.0	0.00	0.00	0.000	0.000	0.000	0.000
1.0	0.70745	-0.02261	0.020	0.001	0.003	0.001
2.0	1.41485	-0.02600	-0.003	-0.002	0.001	0.001
3.0	2.12181	-0.04791	-0.196	-0.031	-0.003	-0.001
4.0	2.82004	-0.36729	-3.051	-0.787	-0.103	-0.019
4.5	3.15414	-0.94530	-6.476	-1.918	-0.208	-0.048
5.0	3.46817	-1.97496	-8.774	-3.974	-0.383	-0.082
5.5	3.76650	-3.22082	-7.239	-5.422	-0.599	-0.101
6.0	4.04390	-4.75201	-5.051	-5.753	-0.748	-0.121
7.0	4.54494	-8.24351	-5.612	-5.254	-0.791	-0.127

Table 3.2.13: The computed saturation induced harmonics when the midplane notches in the RHIC arc dipoles DRB005 and DRB006 are replaced by the tooths in magnet DRS003.

I(kA)	B_o(T)	δTF(%)	b_2	b_4	b_6	b_8
0.0	0.00	0.00	0.000	0.000	0.000	0.000
1.0	0.70752	-0.02219	0.040	0.006	0.004	0.001
2.0	1.41500	-0.02473	0.027	0.007	0.004	0.001
3.0	2.12216	-0.04074	-0.023	0.007	0.004	0.001
4.0	2.82350	-0.25435	-0.819	-0.326	-0.005	0.001
4.5	3.16289	-0.67977	-0.981	-0.795	0.031	0.000
5.0	3.48314	-1.56103	0.629	-1.999	0.046	0.010
5.5	3.78086	-2.86090	2.446	-3.072	-0.044	0.025
6.0	4.05747	-4.44131	4.834	-3.083	-0.087	0.033
7.0	4.55936	-7.96098	5.076	-2.197	-0.027	0.049

3.2.8. Cutout or Bump in the iron aperture

The saturation induced harmonics are significantly modified when a cutout or bump is introduced in the iron aperture. Coupland [30] has studied cutouts in the yoke aperture in superconducting magnets. The use of a cutout in the RHIC arc dipole magnets and a bump in the SSC collider dipole magnets is examined here. The bumps can also be visualized as shimming the yoke inner surface with some extra iron and the notch as trimming the yoke inner surface. A cutout and a bump are shown schematically in Fig. 3.2.21. The change in saturation in the RHIC arc dipoles due to a midplane notch or tooth was discussed in the last section. Those (located either at the midplane or pole) were special cases of a more general method of controlling saturation with the help of a cutout or bump at the yoke inner surface as discussed in this section.

The cutout and bump not only change the saturation induced harmonics, but also change the harmonics at all fields including those at low fields. A low field is defined as the field when the magnetization in the iron is far below its saturation magnetization. The coil cross section must be designed to remove the low field harmonics generated by a cutout or bump in the yoke aperture. Bumps and notches also change the transfer function, as shown in Fig. 3.2.22. At low field the change in transfer function is large due to a bump, particularly when it is near the pole. However, a bump like this saturates very rapidly and most of the increase is lost at high field.

The change in the value of an individual harmonic at saturation and the change in the value of that harmonic at low field depend on the size and the angular location of the cutout or bump. In Fig. 3.2.23, the low field b_2 harmonic and the saturation induced b_2 at 5000 amperes are plotted as a function of angle for a 5 mm $\times$5 mm bump or notch in the aperture of the RHIC arc dipoles. The saturation suppressor holes, which were mentioned in an earlier section, are not present in these computer models. In Fig. 3.2.24, the b_4 harmonic has been plotted for the same parameters and in Fig. 3.2.25 the b_6 harmonic.

It may be noted that the magnitude of the change in the saturation induced harmonic is quite large in this method. However, once the coil is designed, it can't be tuned to further optimize the saturation without iterating the coil cross section as well since it creates a rather large value of the low field harmonic as well.

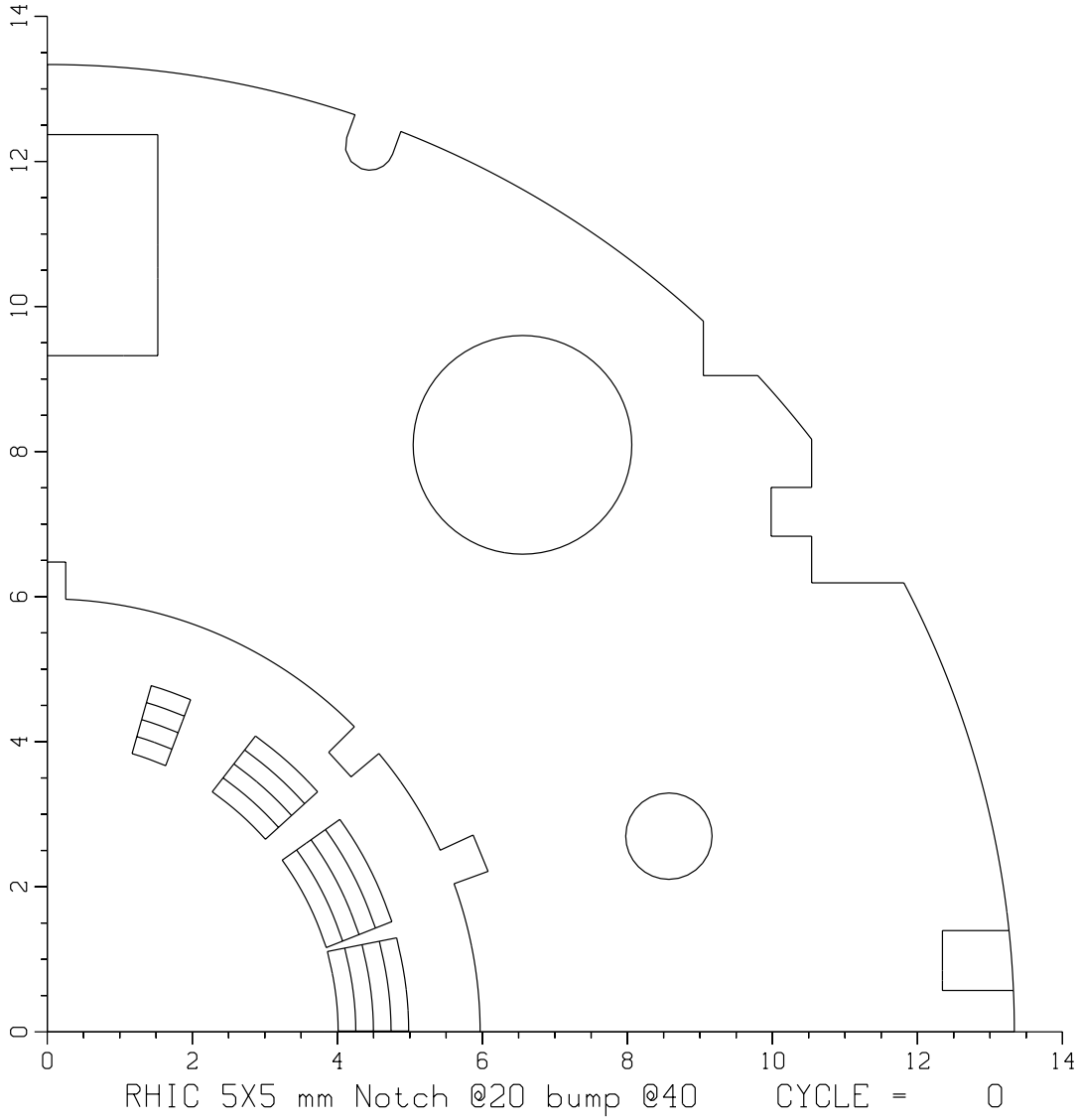

Figure 3.2.21: A computer model of a notch and a cutout in the iron aperture. The notch begins at $\theta = 20°$ and the bump at $\theta = 40°$. The notch cuts into the iron and the bump into the collar or spacer between the superconducting coil and the iron. Since the notch reduces the amount of iron it lowers the transfer function whereas the bump, because it adds iron, increases the transfer function. A 5 mm $\times$ 5 mm notch at the pole (90°) is part of the standard design.

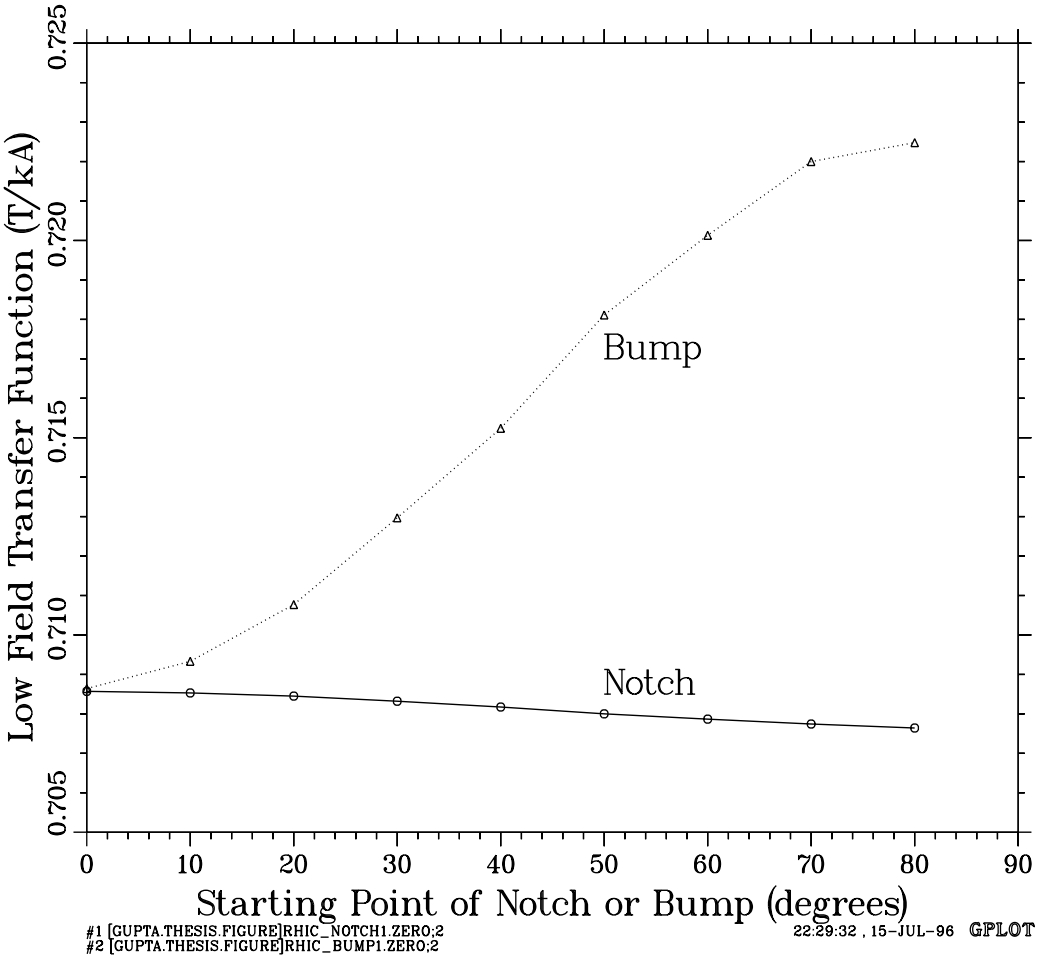

Figure 3.2.22: The transfer function at low field as a function of angle for a 5 mm $\times$5 mm bump or notch in the aperture of the RHIC arc dipoles. The notch (or bump) is in addition to a 5 mm $\times$ 5 mm notch at the pole (90°) which is part of the standard design.

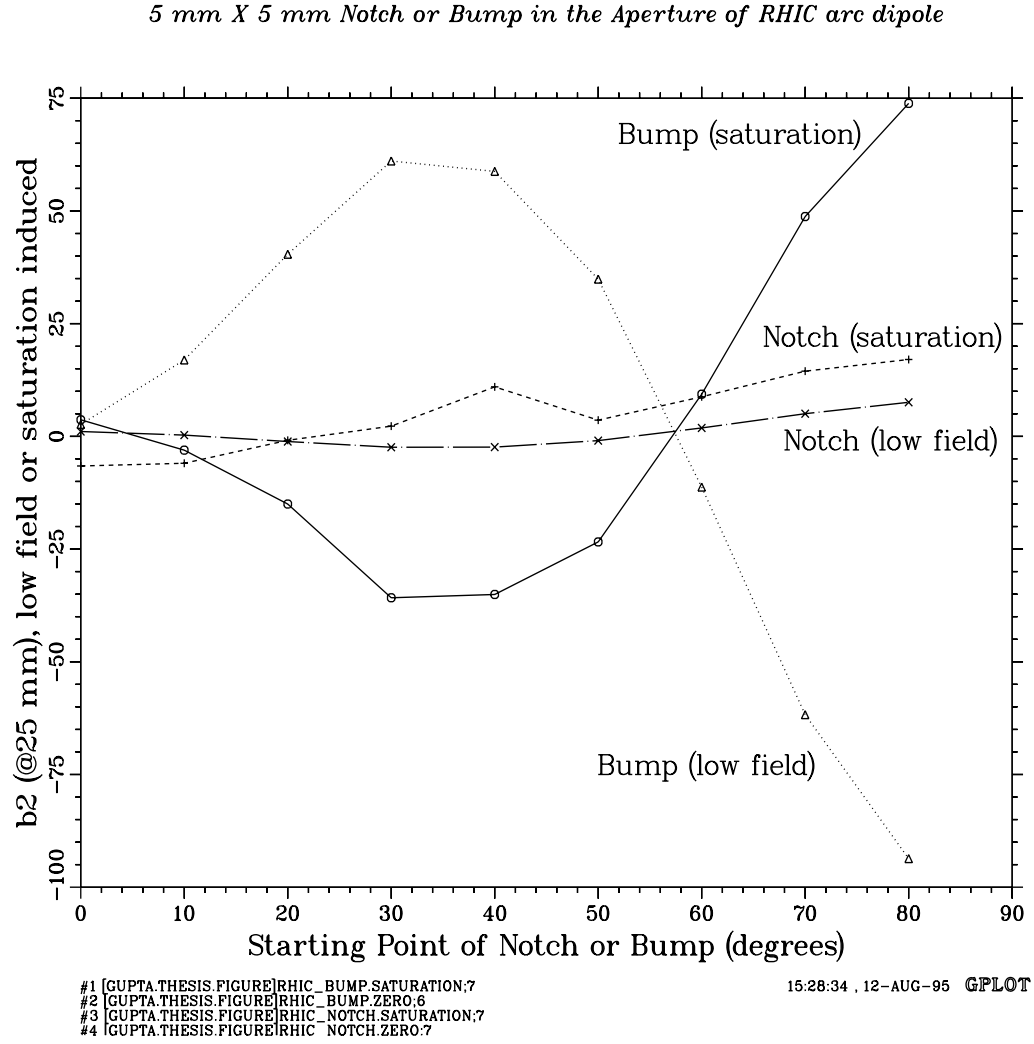

Figure 3.2.23: The low field and saturation induced b_2 harmonic at 5000 amperes as a function of angle for a 5 mm $\times$5 mm bump or notch in the aperture of the RHIC arc dipoles. The above notch (or bump) is in addition to a 5 mm $\times$ 5 mm notch at the pole (90°) which is part of the standard design.

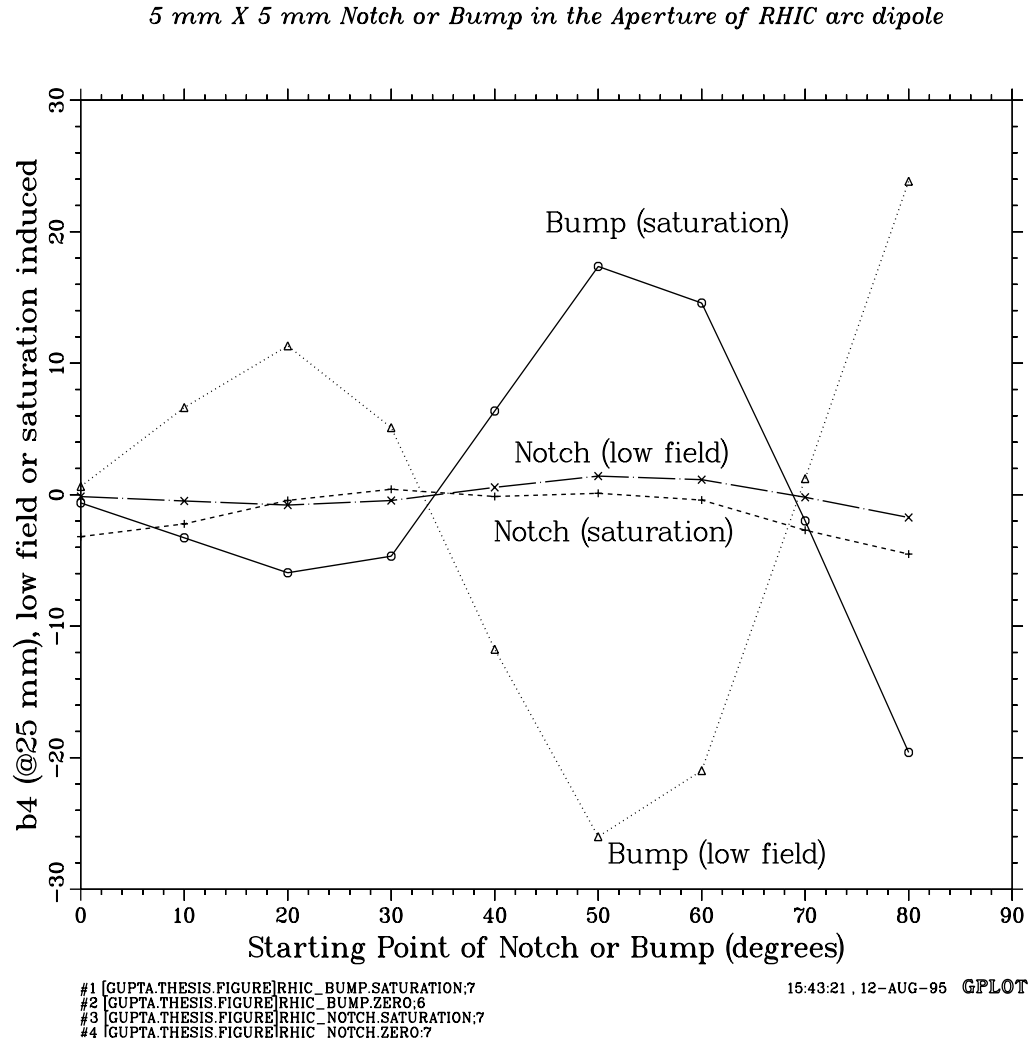

Figure 3.2.24: The low field and saturation induced b_4 harmonic at 5000 amperes as a function of angle for a 5 mm $\times$5 mm bump or notch in the aperture of the RHIC arc dipoles. The above notch (or bump) is in addition to a 5 mm $\times$ 5 mm notch at the pole (90°) which is part of the standard design.

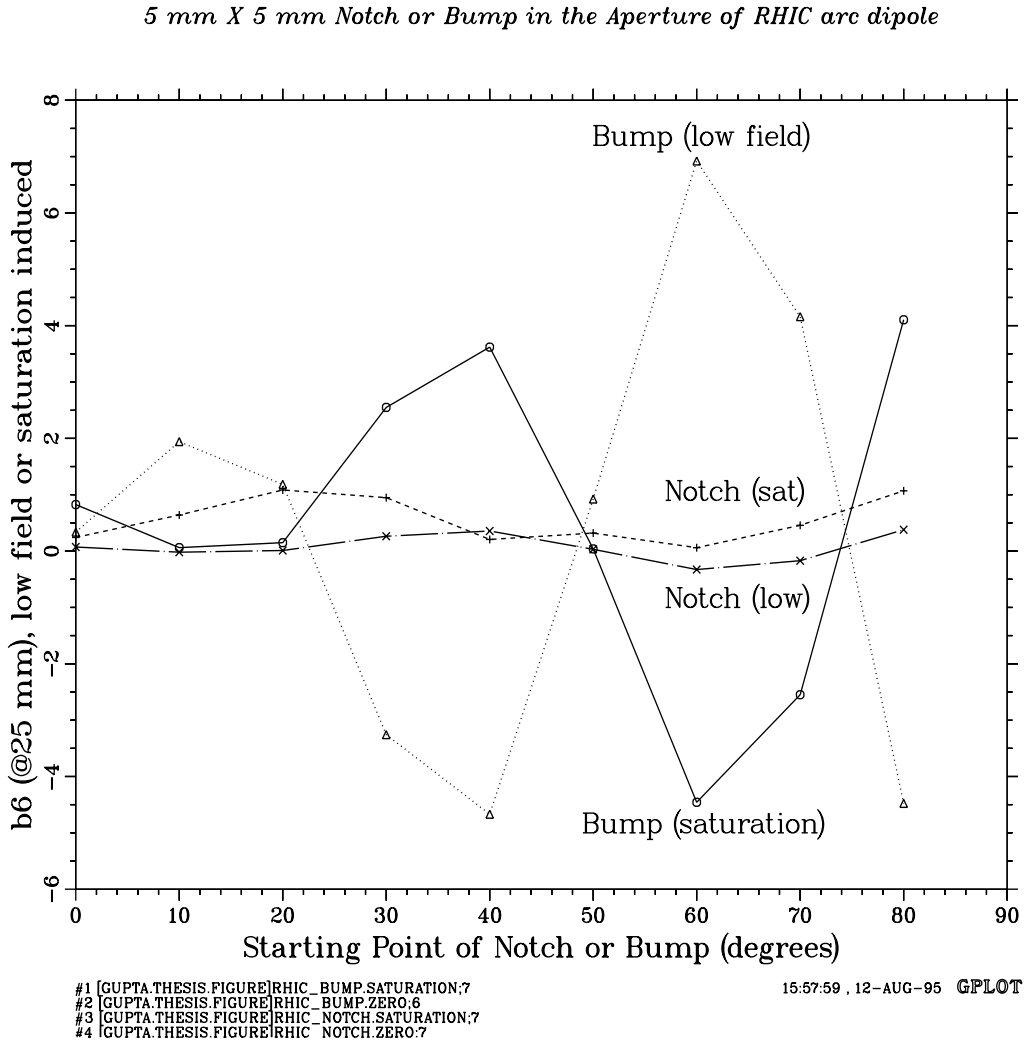

Figure 3.2.25: The low field and saturation induced b_6 harmonic at 5000 amperes as a function of angle for a 5 mm $\times$5 mm bump or notch in the aperture of the RHIC arc dipoles. The above notch (or bump) is in addition to a 5 mm $\times$ 5 mm notch at the pole (90°) which is part of the standard design.

3.2.9. Elliptical iron aperture

Morgan [118] has noted that the use of an elliptical iron aperture in the RHIC arc dipole can reduce the saturation induced harmonics. The way in which an elliptical aperture can reduce these saturation induced harmonics may be understood as follows: The iron is further away from the magnet center at the pole as compared to that at the midplane. Since the pole region is the first and by far the most to saturate, this effectively removes the saturating iron and therefore reduces the saturation induced harmonics. Though removing iron from the pole reduces the transfer function as compared to that in the circular aperture case, the reduction in saturation allows the iron to be brought closer to the coil elsewhere. This, in turn reduces the average yoke radius and hence increases the transfer function. The overall result is an increased transfer function with reduced saturation. The simple elliptical aperture mainly reduces the b_2 saturation. Morgan [118] has further investigated higher order deformations in the elliptical aperture to reduce the b_4, b_6 and other harmonics due to saturation.

These non-circular shapes change the values of low field harmonics by a significant amount. Therefore, the coil must be designed to cancel these harmonics. This method is examined here for an alternate design of the SSC 40 mm aperture dipole magnet. The shape of the aperture is shown in Fig. 3.2.26. The saturation induced harmonics are plotted in Fig. 3.2.27. The values are given in Table 3.2.14. As compared to the standard design, the increase in transfer function in this design was 6.6% at low field and 4.9% at the operating field together with a reduction in the values of saturation induced harmonics. This method was not adopted (or tested) in any SSC or RHIC magnet built at BNL due to mechanical complications. However, Dell'Orco, Caspi, et al. [41] at Lawrence Berkeley National Laboratory (LBNL) have designed, built and tested a magnet based on the basic elliptical aperture concept and thus the validity of the method has been verified.

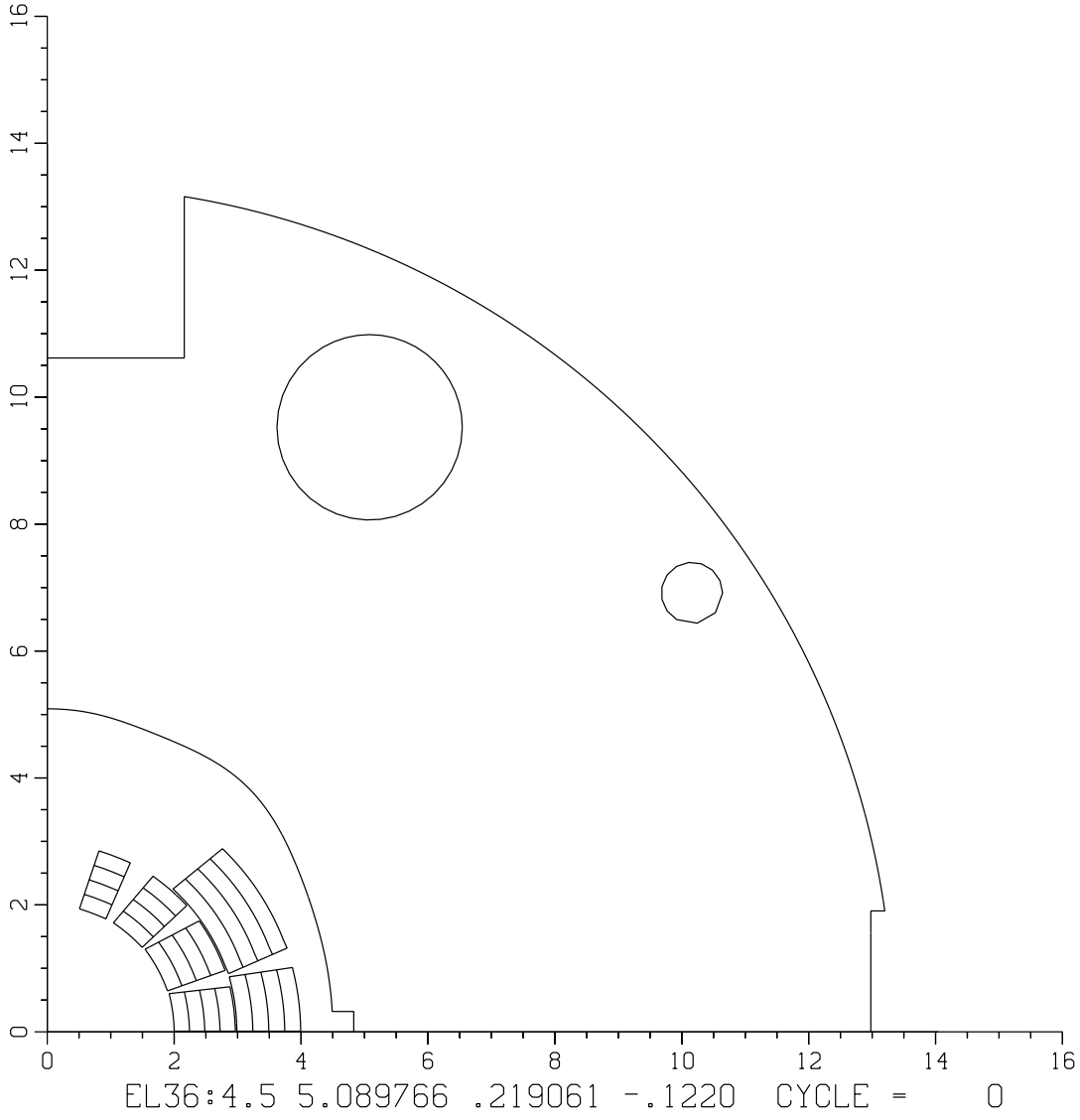

Figure 3.2.26: A computer model of an elliptical aperture dipole magnet. The shape of the aperture is optimized to increase the transfer function and reduce the field harmonics.

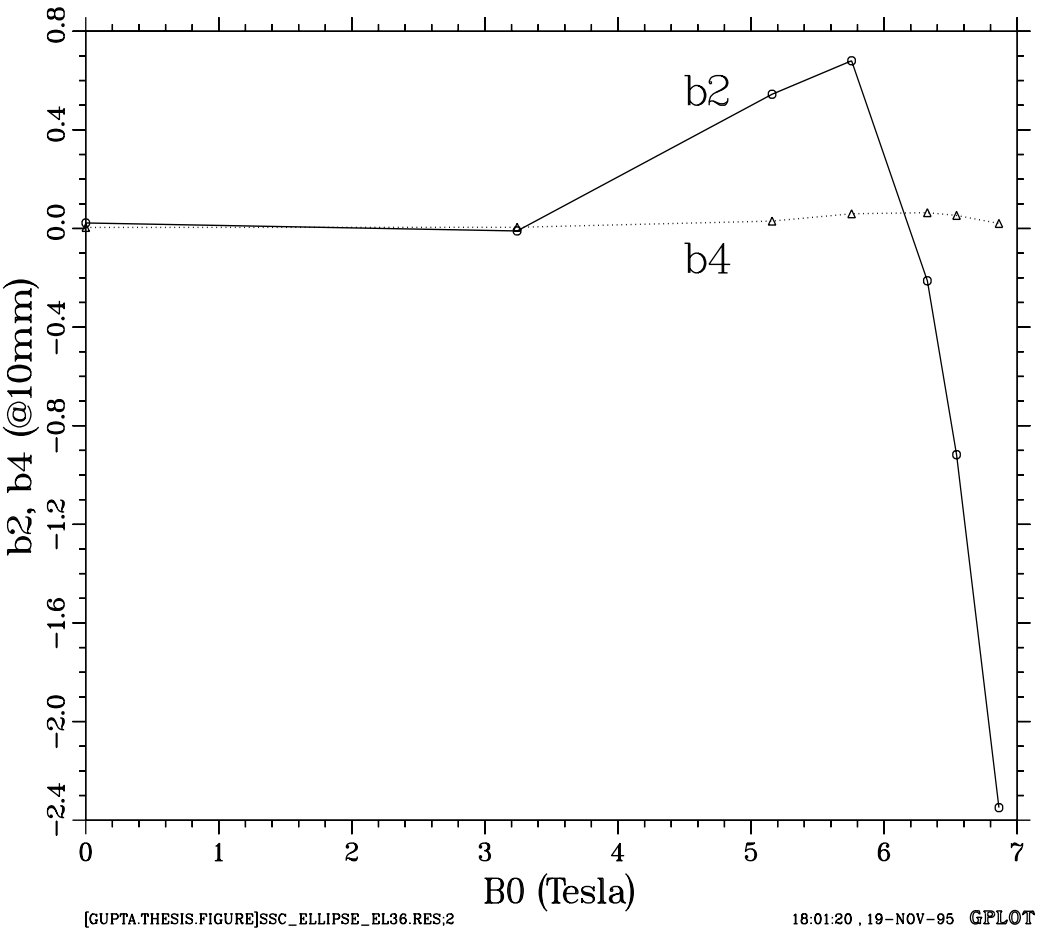

Figure 3.2.27: The variation in the sextupole (b_2) and decapole (b_4) harmonics as a function of current in the elliptical aperture design of the 40 mm coil inner diameter SSC dipole magnet.

Table 3.2.14: Saturation induced harmonics in the proposed SSC 40 mm Elliptical aperture dipole (EL36).

I(kA)	B_o(T)	δTF(%)	b_2	b_4	b_6	b_8
0.000	0.00000	1.105	0.02231	0.00423	0.02857	0.00963
2.950	3.24194	1.099	-0.01008	0.00474	0.02905	0.00985
4.720	5.15805	1.093	0.54434	0.02992	0.02635	0.01000
5.310	5.75570	1.084	0.68019	0.05964	0.02678	0.01008
5.900	6.32511	1.072	-0.21213	0.06409	0.02766	0.01042
6.136	6.54452	1.067	-0.91737	0.05291	0.02768	0.01057
6.490	6.86319	1.058	-2.34910	0.02028	0.02748	0.01077

3.2.10. Two radius aperture yoke

In superconducting magnets, the yoke aperture is usually circular. The saturation characteristics of the yoke can be drastically altered if the yoke aperture consists of circular arcs with two radii instead of one. It has been mentioned earlier that the field near the surface of the iron is maximum at the poles and minimum at the midplanes. The radius of the circular arc is made larger at the poles as compared to that at the midplanes.

The basic principle behind this method is explained here. Yoke saturation at the pole induces a change in the allowed harmonics at high fields with the sign of them changing alternatively with increasing harmonic number (i.e. $+\delta b_2$, $-\delta b_4$, $+\delta b_6$,, $-\delta b_8$,... in dipoles and $+\delta b_5$, $-\delta b_9$, $+\delta b_{13}$, $-\delta b_{17}$,... in quadrupoles) whereas yoke saturation at the midplane induces a negative change in all allowed harmonics. In a typical magnet design, the onset of iron saturation is observed by an increase (a positive change) in the first allowed harmonic as the level of excitation is raised. The harmonic referred to here is b_2 in dipoles and b_5 in quadrupoles. A larger yoke inner radius at the pole regions reduces a positive saturation in this harmonic and a smaller inner radius at the midplane further compensates it. This, however, increases the net (negative) saturation in the next allowed harmonic. The harmonic referred to here is b_4 in dipoles and b_9 in quadrupoles as the contribution is negative from both the midplane and pole saturation. Therefore, making the yoke inner radius smaller at the midplane and larger at the pole reduces the natural compensation and gives a larger negative saturation at high field in this harmonic. The third region which generates a significant change in the saturation induced allowed harmonics is the place where an abrupt transition from one radius to another radius takes place. This saturation can be used to further control the saturation induced allowed harmonics.

The two-radius method method has been successfully used in designing the 130 mm aperture quadrupole for the RHIC interaction region. The first allowed harmonic in the quadrupole is b_5 and by using this technique it was drastically reduced from 15 units to less than 1 unit. This two-radius method has been chosen over the elliptical aperture method in these magnets.

There are three parameters, in this method, which can be used to minimize the iron saturation. These are : (a) and (b) the values of the two radii and (c) the angle at which the radius of the aperture changes from one value to the other. The variation in the saturation induced b_5 and b_9 harmonics at a 40 mm reference radius at the maximum operating current of 5 kA and the percentage drop in transfer function relative to its low field value in the

Table 3.2.15: Values of the transfer function at 5 kA and percentage drop in transfer function relative to its low field value in the case of 130 mm aperture RHIC insertion quadrupoles as a function of the angle at which the yoke inner radius changes from 87 mm to 92 mm. The saturation induced allowed harmonics at 40 mm reference radius are also given.

Angle (degrees)	T.F. (T/m/kA)	δT.F. (%)	δb_5 (units)	δb_9 (units)	δb_{13} (units)
5	46.1625	-0.13002	0.638	-0.009	0.001
10	46.2516	-0.12849	0.501	-0.017	0.001
15	46.4231	-0.15174	-0.236	-0.026	0.003
20	46.6801	-0.23275	-1.394	0.062	0.010
25	47.0162	-0.38814	-1.768	0.273	0.006
30	47.4166	-0.61767	-0.132	0.425	-0.014
35	47.8620	-0.90488	3.808	0.289	-0.024
40	48.3406	-1.12132	8.224	-0.116	-0.004

case of the RHIC 130 mm aperture quadrupoles is given in Fig. 3.2.28 as a function of the angle at which the yoke inner radius changes. The yoke inner radius is always larger (92 mm) at the pole and smaller (87 mm) at the midplane and the two circular arcs are connected by a radial line. A larger value of this angle gives a larger transfer function which is desirable. The values of the transfer function at the maximum operating current (5 kA), the percentage drop in transfer function relative to its low value and the saturation induced allowed harmonics at a 40 mm reference radius as a function of angle at which the yoke inner radius changes are given in Table 3.2.15. The model used in this study is similar to the one shown in Fig. 3.2.29 except for the absence of the notch at the midplane and except that in this case the two radii are connected by a radial line.

In Fig. 3.2.29, a computer model of an octant of the 130 mm aperture RHIC insertion quadrupole is shown. The yoke inner radius is 87 mm at the midplane and 92 mm at the pole. The two radii are connected by a straight line (face) which is either parallel to the horizontal axis or to the vertical axis depending on the location. As shown in the figure, the two radii are connected by a vertical line in this octant. The change-over from one radius

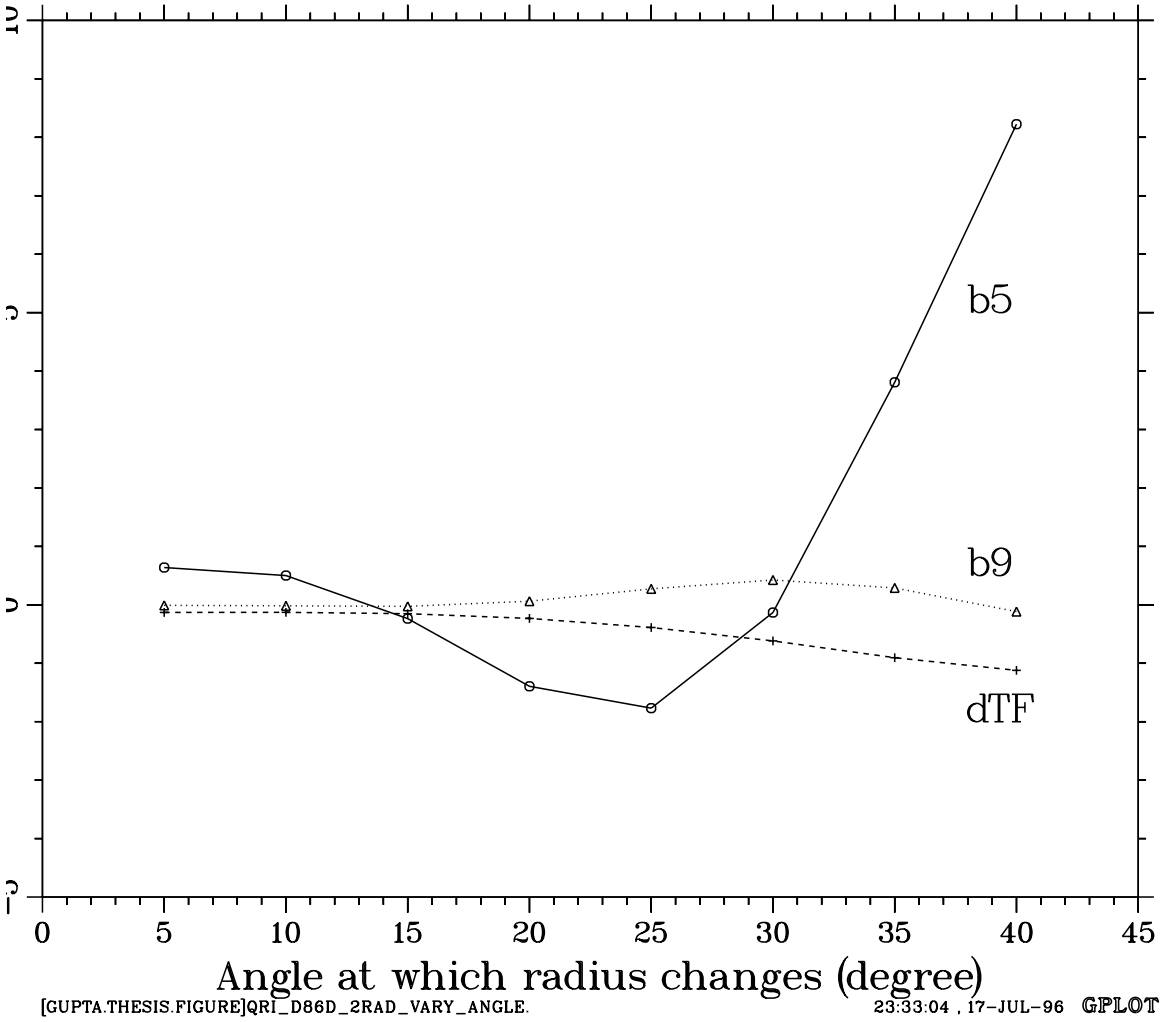

Figure 3.2.28: The variation in the saturation induced b_5 and b_9 harmonics at 5 kA at a reference radius of 40 mm as a function of angle at which the yoke inner radius changes from 87 mm to 92 mm in the case of the 130 mm aperture RHIC insertion quadrupole. The yoke inner radius is larger (92 mm) at the pole. The two circular are connected by a radial line.

to another radius takes place at an angle of about 30 degree in the first octant. The angles in the other octants are determined by quadrupole symmetry.

Fig. 3.2.30, Fig. 3.2.31 and Fig. 3.2.32 show the variation in the transfer function, b_5 and b_9 harmonics, respectively, as a function of current in the 130 mm aperture RHIC insertion quadrupoles. The three cases in each figure represent the aperture described (a) by one 87 mm radius for which the computed saturation induced harmonics are given in Table 3.2.16, (b) by one 92 mm radius (data in Table 3.2.17) and (c) by 87 mm at the midplane and by 92 mm radius at the pole (data in Table 3.2.18), with the change-over in the yoke inner radius taking place at $\theta = 30°$ in the first octant.

One can see from Fig. 3.2.31 that the saturation induced b_5 is smaller in the two radii case even as compared to the case when the radius was larger all over (inner radius = 92 mm). However, as shown in Fig. 3.2.32, the net b_9 saturation has increased now. This was expected from the explanation given earlier in this section. This increase is however too small to be of concern to RHIC operation. The transfer function (Fig. 3.2.30) is maximum when the radius is 87 mm. However, at high current in the two radius case, the transfer function approaches the transfer function of the 87 mm case. This is because in the lower yoke inner radius case, the pole is highly saturated and the permeability in the yoke is close to that of air, anyway.

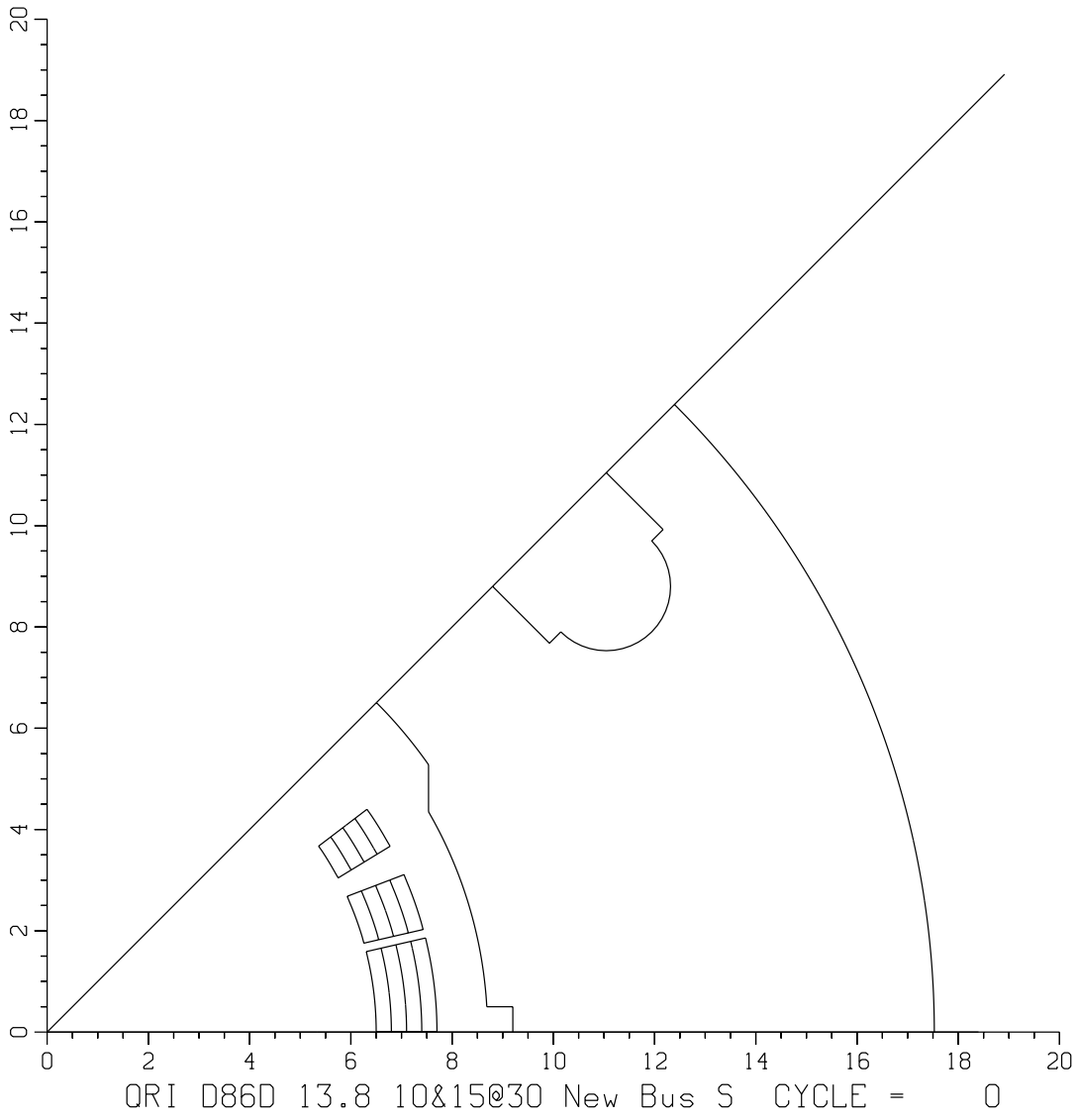

Figure 3.2.29: The computer model of the 130 mm aperture RHIC insertion dipole. The yoke inner surface is described by circular arcs having radii of 87 mm and 92 mm. The change over from 87 mm to 92 mm takes place around $\theta = 30°$. The method has been found to be very efficient in reducing the saturation induced harmonic in quadrupoles.

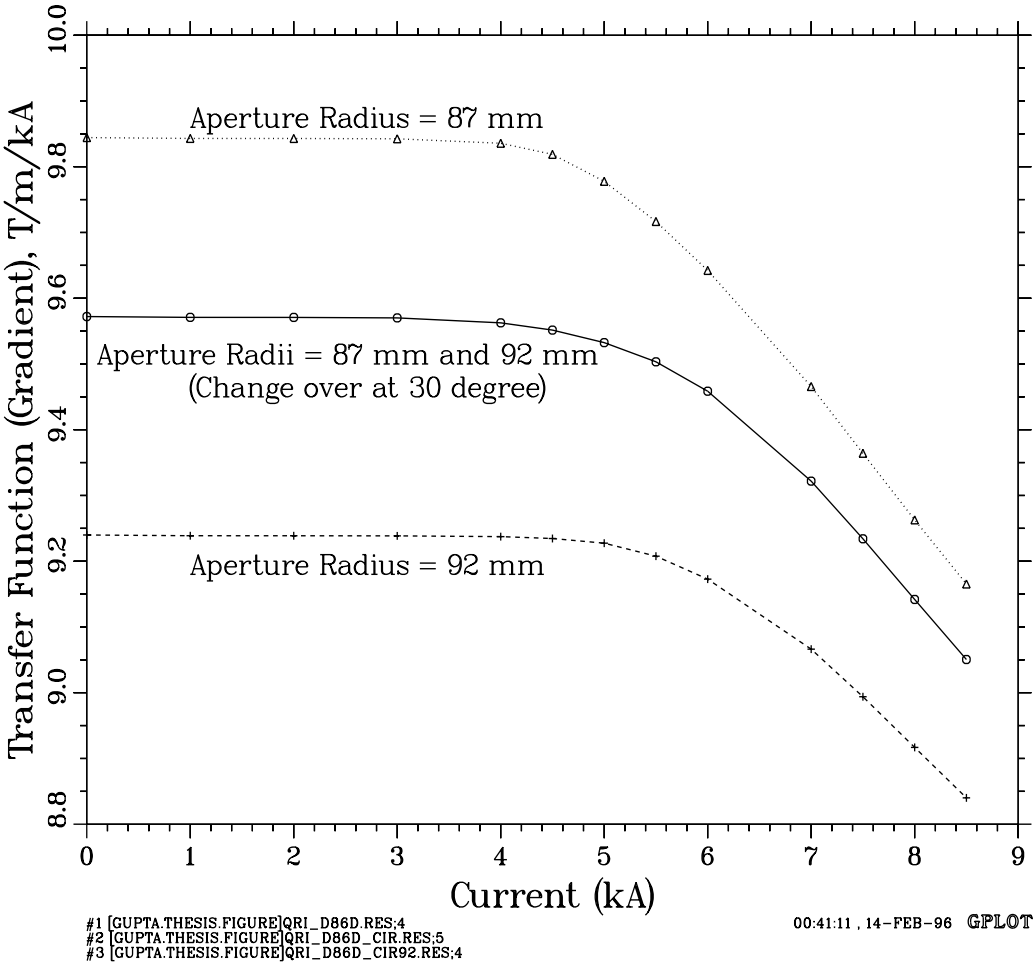

Figure 3.2.30: The variation in the transfer function as a function of current in the 130 mm aperture RHIC insertion quadrupole in the three cases of the yoke inner surface. The yoke inner surface is defined either by one single circle or by two circular arcs. The radii of these circles are indicated on the curves for the three cases.

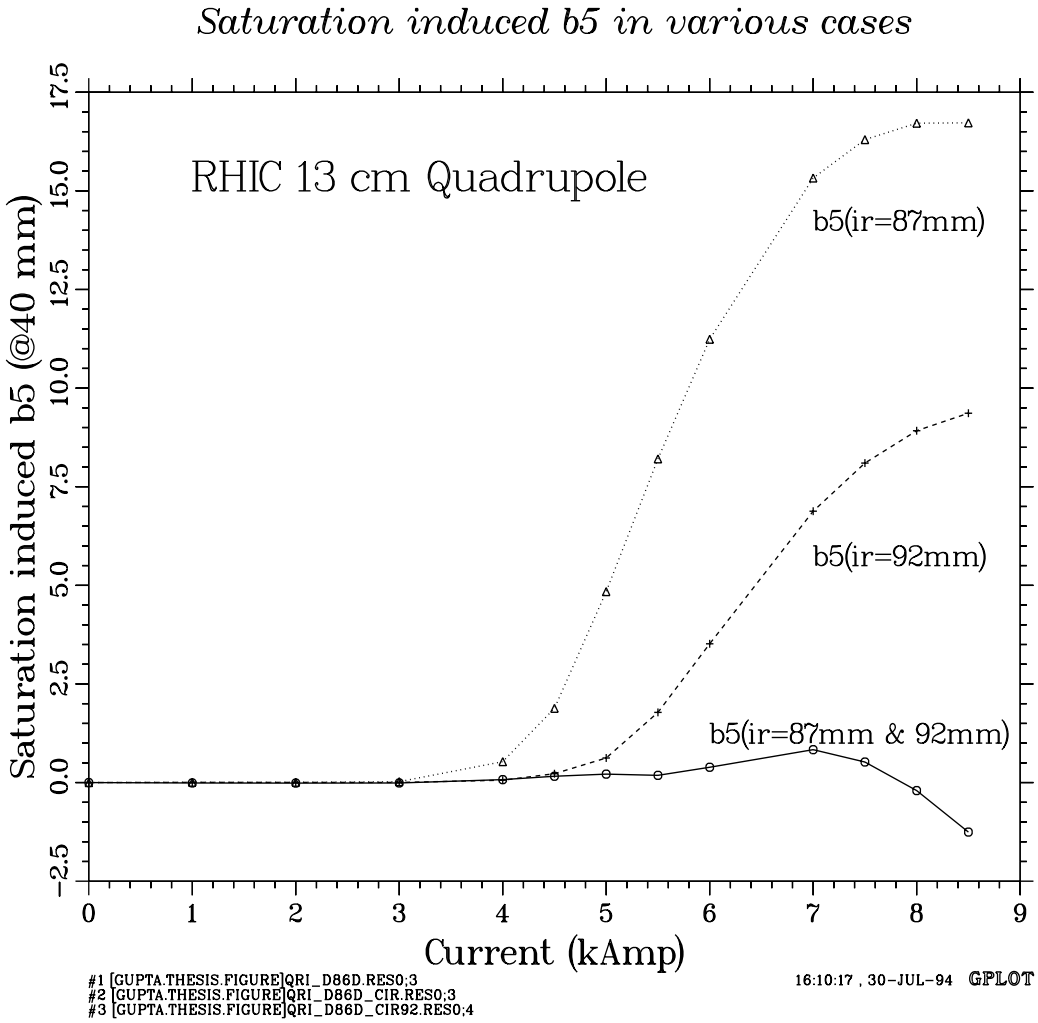

Figure 3.2.31: The variation in the dodecapole (b_5) harmonic as a function of current in the 130 mm aperture RHIC insertion quadrupole in the three cases of the yoke inner surface. The yoke inner surface is defined either by one single circle or by two circular arcs. The radii of these circles are indicated on the curves in various cases.

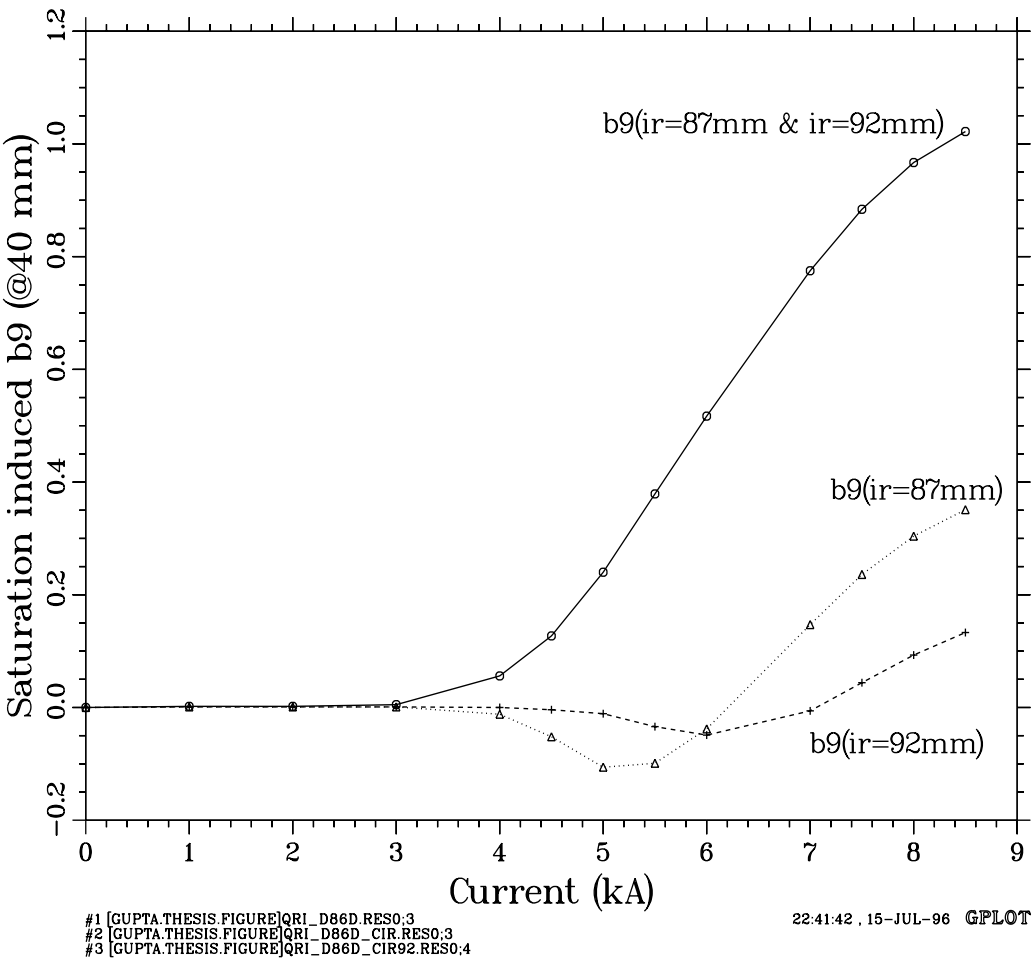

Figure 3.2.32: The variation in the b_9 harmonic as a function of current in the 130 mm aperture RHIC insertion quadrupole in the three cases of the yoke inner surface. The yoke inner surface is defined either by one single circle or by two circular arcs. The radii of these circles are indicated on the curves in various cases.

Table 3.2.16: Current dependence in field harmonics when the yoke aperture has a radius R = 87 mm.

I(kA)	Gradient(T/m)	δTF(%)	δb_5	δb_9	δb_{13}
0.0	0.00	0.00	0.0	0.0	0.0
1.0	9.84301	-0.01341	0.008	0.001	0.0
2.0	19.6859	-0.01402	0.007	0.001	0.0
3.0	29.5274	-0.01893	0.023	0.001	0.0
4.0	39.3427	-0.08791	0.530	-0.012	0.001
4.5	44.1844	-0.25979	1.882	-0.052	0.002
5.0	48.8889	-0.67602	4.840	-0.106	0.003
5.5	53.4417	-1.29676	8.205	-0.099	0.002
6.0	57.8534	-2.05292	11.238	-0.038	0.004
7.0	66.2596	-3.84661	15.325	0.147	0.012
7.5	70.2309	-4.87803	16.298	0.236	0.018
8.0	74.1027	-5.90688	16.715	0.304	0.024
8.5	77.9053	-6.89738	16.724	0.351	0.029

Table 3.2.17: Current dependence in field harmonics when the yoke aperture has a radius R = 92 mm.

I(kA)	Gradient(T/m)	δTF(%)	δb_5	δb_9	δb_{13}
0.0	0.00	0.00	0.0	0.0	0.0
1.0	9.23875	-0.01212	0.005	0.001	0.000
2.0	18.47740	-0.01266	0.004	0.001	0.000
3.0	27.71560	-0.01447	0.003	0.001	0.000
4.0	36.94950	-0.02700	0.060	0.000	0.000
4.5	41.55540	-0.05776	0.225	-0.004	0.000
5.0	46.13710	-0.13474	0.623	-0.011	0.001
5.5	50.64210	-0.34865	1.779	-0.034	0.002
6.0	55.03640	-0.72660	3.518	-0.049	0.003
7.0	63.46360	-1.87926	6.879	-0.006	0.006
7.5	67.45400	-2.66241	8.099	0.044	0.009
8.0	71.33440	-3.49648	8.919	0.093	0.012
8.5	75.14050	-4.32702	9.363	0.133	0.016

Table 3.2.18: Current dependence in field harmonics when the yoke aperture consists of arcs having two radii : R = 87 mm at the midplane and R = 92 mm at the pole. The radius changes at an angle of 30° in the first quadrant.

I(kA)	Gradient(T/m)	δTF(%)	δb_5	δb_9	δb_{13}
0.0000	0.00000	0.00000	0.000	0.000	0.000
1.0000	9.57088	-0.01264	-0.010	0.002	0.000
2.0000	19.14160	-0.01348	-0.013	0.002	0.000
3.0000	28.71020	-0.02114	-0.010	0.005	0.000
4.0000	38.25020	-0.09967	0.075	0.056	-0.003
4.5000	42.98180	-0.21499	0.160	0.127	-0.006
5.0000	47.66230	-0.41402	0.214	0.240	-0.009
5.5000	52.26810	-0.71875	0.183	0.379	-0.011
6.0000	56.75130	-1.18615	0.388	0.517	-0.010
7.0000	65.25230	-2.61525	0.834	0.775	-0.004
7.5000	69.25570	-3.53106	0.521	0.884	0.001
8.0000	73.13450	-4.49513	-0.203	0.967	0.006
8.5000	76.92910	-5.44925	-1.255	1.022	0.010

3.3. Saturation Induced Allowed Harmonics in RHIC Arc Dipoles

In this section the saturation induced allowed harmonics are reviewed in various full length RHIC arc dipoles. This includes the earlier designs for the R&D phase of the program through the final production design [72] used by industry (the Northrop Grumman Corporation) in building the machine magnets. The cross section of the production design is shown in Fig. 3.3.1. The original yoke and magnetic design of this magnet was carried out by Thompson [156] and most of the research work described in this section has been performed in collaboration with him. With several iterations using the techniques described in the earlier sections, the saturation induced sextupole (b_2) and decapole (b_4) harmonics in the present design are reduced by over an order of magnitude as compared to that in the initial design. A comparison of the calculations and measurements in the various yoke designs will be made.

The measured current dependence in the harmonics comes not only from the non-linear properties of iron (saturation induced) but also from (a) the persistent currents in the superconductor (whose fractional contribution is more at low current) and (b) deformation of the superconducting coils due to Lorentz forces on them. In a typical measurement of the current dependence, the harmonics are measured during the up ramp (when the current is increased) and also during the down ramp (when it is decreased). The sign of the harmonics created by the persistent currents is opposite in the up and down ramps. Moreover, it has been found that in the RHIC operating range, the magnitude of the persistent current harmonics is about the same during up and down ramp. Therefore, the persistent current effects can be mostly removed from the data by taking the average of the measurements during the up and down ramp. However, there is no easy method of removing the harmonics produced by the coil deformation due to Lorentz forces and therefore when comparing calculations and measurements, this effect contributes to the differences between the two. However, in a RHIC dipole magnet built to specifications, this effect is rather small.

During the R&D phase of the program, usually two magnets were built with the same yoke design. It has been found (both in RHIC and SSC magnets) that the variation in the magnet-to-magnet current dependence of the saturation induced harmonics, in magnets built with the same yoke design, is rather small. Therefore, for clarity, the measurements from only one magnet per design will be included in the tables and plots which show the current dependence of the field harmonics. In Fig. 3.3.2, Fig. 3.3.3 and Fig. 3.3.4 the measured current dependence in the sextupole (b_2), decapole (b_4) and 14-pole (b_6)

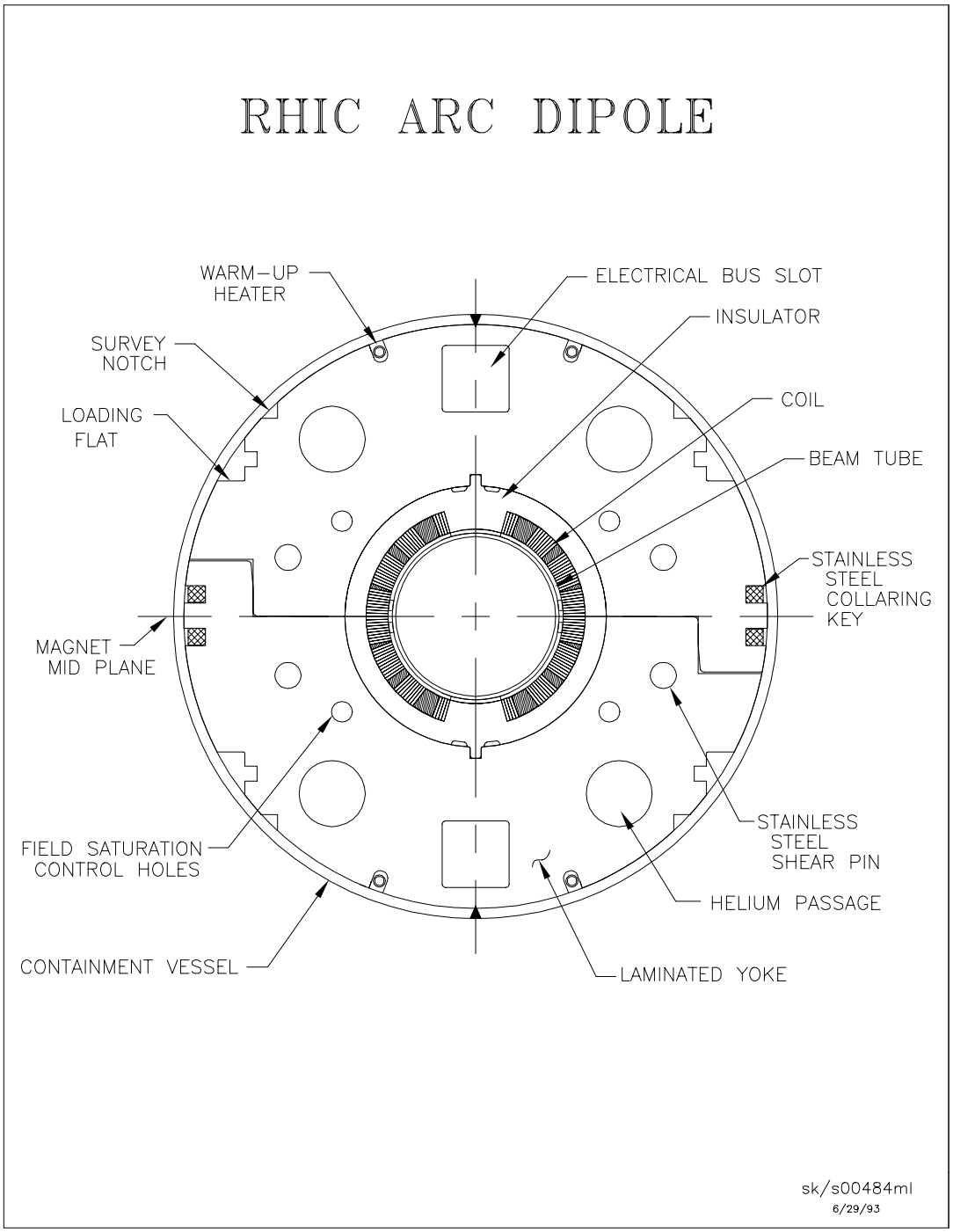

Figure 3.3.1: The cross section of the production series of the cold mass of the 80 mm aperture RHIC arc dipoles. This cold mass is put inside a cryostat (not shown here).

harmonics, respectively, is shown. The magnet nomenclature used here (for example in DRE011) is such that "D" is for dipole, "R" for RHIC, "E" for design series and "011" for the magnet number. The first digit was 0 in R&D magnets and is non-zero in production magnets. As mentioned earlier, the measured current dependence is the average of the up and down ramps. Moreover, in order to make an easy comparison in the relative current dependence, a proper offset is added so that each curve starts from zero at 2 kA.

One can see from Fig. 3.3.2 and Fig. 3.3.3, that the current dependence over the design range (up to ~5KA) in the sextupole harmonic (b_2) and decapole (b_4) harmonic is reduced by over an order of magnitude between the first *DRA* design and the present *DRG* design. Two production series magnets (DRG) have been tested up to 7 kA and they show that the current dependence remains small up to that current. In the first long (~9.5 meter) magnet, DRA001, the maximum variation in the b_2 harmonic between 2 kA and 5 kA was over 42 units and in DRG101 magnet this variation is reduced to about 2 units. Similarly, one can see from Fig. 3.3.3 that the b_4 variation has also been reduced by over an order of magnitude. In DRA001, the maximum variation in the b_4 harmonic between the 2 kA and 5 kA current was over 8 units and in DRG101 this variation is reduced to 0.6 unit. However, as shown in Fig. 3.3.4, the variation in the b_6 harmonic in DRG101 has become more than in some intermediate prototype magnets though its magnitude is still about the same as it was in DRA101. This harmonic was not minimized as it does not adversely affect RHIC performance. In the recent yoke design of the 10 cm aperture insertion dipole D0, this harmonic was included in the optimization and it was also made small using similar techniques. Very little current dependence (<0.3 unit) has been observed in b_8 and higher order harmonics in all magnets.

The series of yoke iterations done to achieve the above mentioned improvements will now be described. The discussion will be restricted to only those features in yoke design which influence the saturation characteristics of the cross section.

DRA001, DRA002 and DRA003 dipoles were constructed with a small (5mm) radial gap between coil outer diameter and yoke together with pole notches in the yoke aperture. Both of these features give a large iron saturation and over 42 units of b_2 saturation and -8 units of b_4 saturation were observed. These are the maximum values of saturation induced harmonics between 2 kA and 5 kA. Magnet DRA004 was built with the same basic features except for some changes near the outer surface of the iron which reduced b_2 saturation from 42 units to 35 units and b_4 saturation from -8.5 units to -5.7 units.

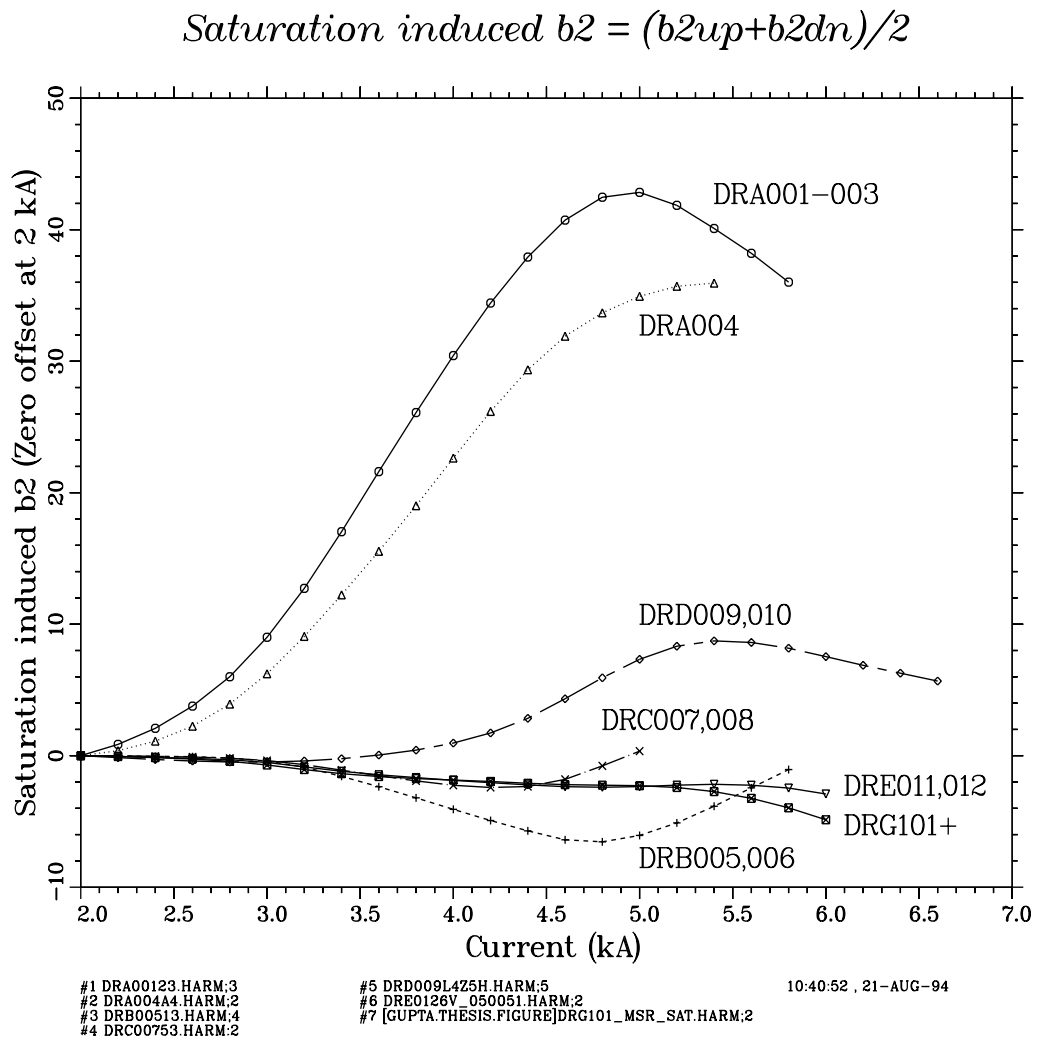

Figure 3.3.2: Measured saturation induced sextupole harmonic (b_2) as a function of current. The b_2 harmonic shown here is the average of b_2 measured during an up and down ramp. This removes the persistent current b_2 to first order in the operating range. Moreover, in order to make an easy relative comparison between various designs, the value of b_2 in each magnet is biased so that each curve starts from a zero value at 2 kA.

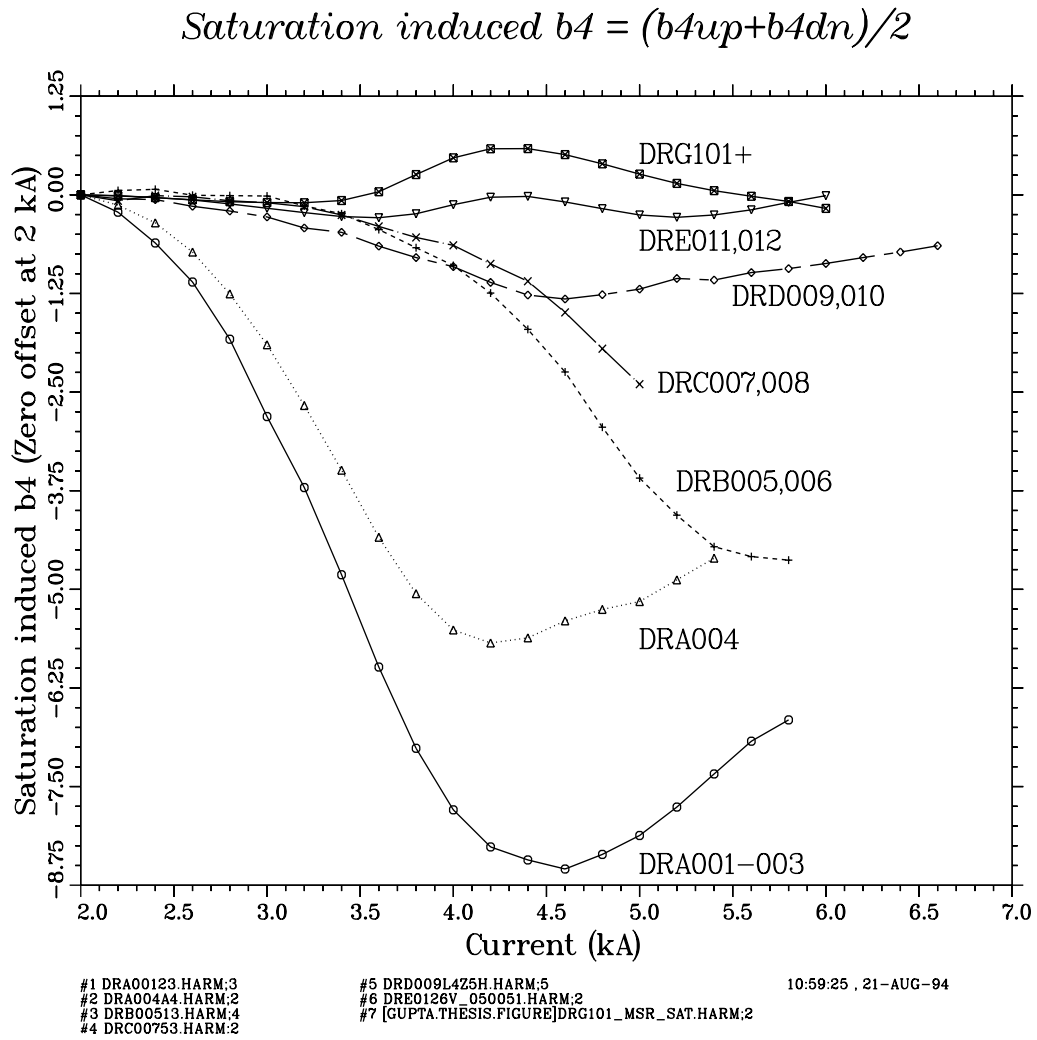

Figure 3.3.3: Measured saturation induced decapole harmonic (b_4) as a function of current. The b_4 harmonic shown here is the average of b_4 measured during an up and down ramp. This removes the persistent current b_4 to first order in the operating range. Moreover, in order to make an easy relative comparison between various designs, the value of b_4 in each magnet is biased so that each curve starts from a zero value at 2 kA.

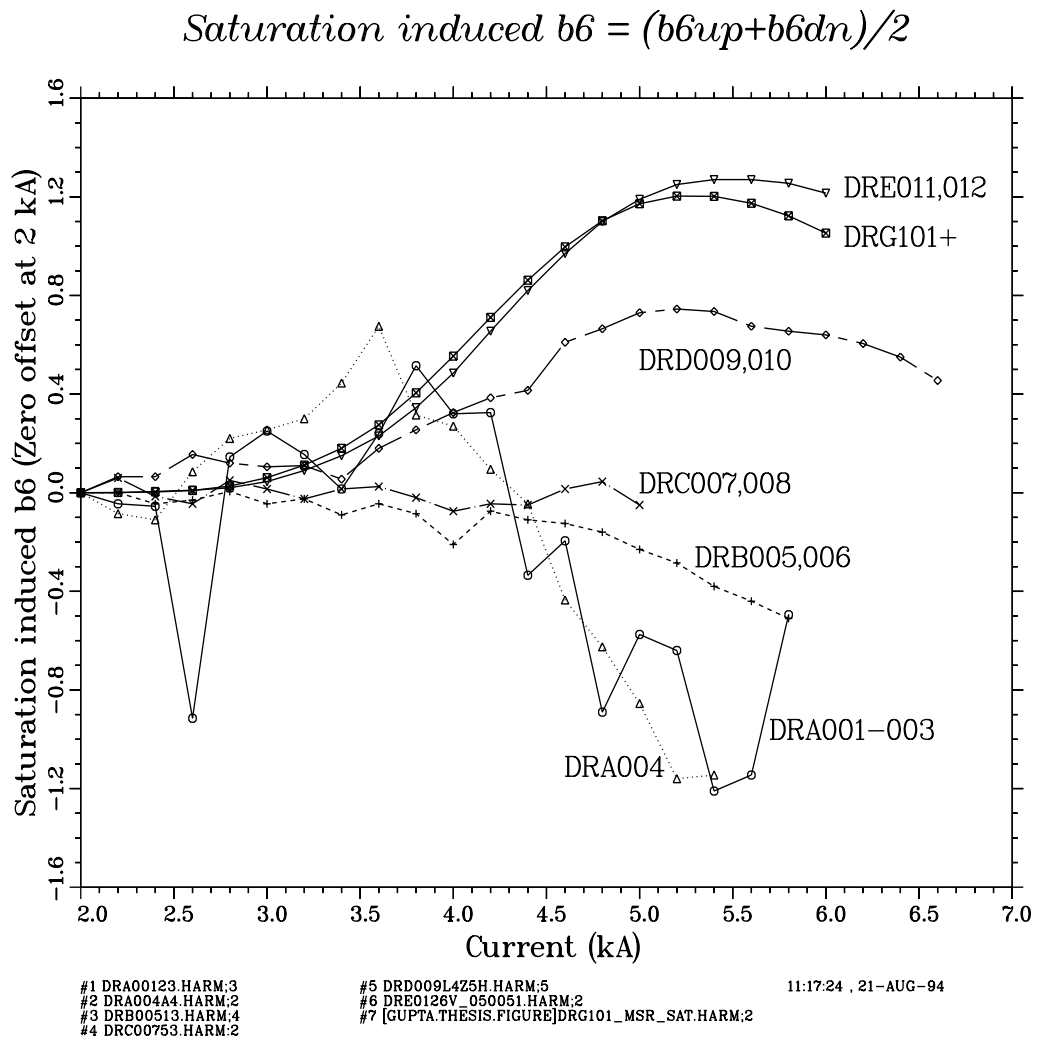

Figure 3.3.4: Measured saturation induced b_6 harmonic as a function of current. The b_6 harmonic shown here is the average of b_6 measured during an up and down ramp. This removes the persistent current b_6 to first order in the operating range. Moreover, in order to make an easy relative comparison between various designs, the value of b_6 in each magnet is biased so that each curve starts from a zero value at 2 kA.

To make a significant reduction in the saturation, the radial gap between the coil and yoke was increased from 5 mm to 10 mm and the coil-yoke locating notch was moved from the pole to the midplane in magnets DRB005 and DRB006. This brought b_2 saturation down from +35 units to -6 units and b_4 saturation from -5.7 units to -3.6 units. These *DRB* magnets were built with non-magnetic stainless steel yoke midplane keys. In magnets DRC007 and DRC008, the material of this key was changed from non-magnetic stainless steel to low carbon magnetic steel. This increased the effective magnetic thickness of the yoke at the midplane and therefore modified the saturation induced harmonics. This change reduced b_2 saturation from -8.5 units to -2.5 units and b_4 saturation from -3.6 units to -2.4 units.

Though the midplane notch (along with magnetic keys) gave the best saturation performance thus far, these features were not desired in the production magnets. It has been believed that a pole locating notch would be better able to define the pole location of the coil and hence would give less variation in the harmonics produced by coil geometry. These harmonics are commonly referred to as the geometric multipoles. Moreover, the goal at that time was to reduce b_4 saturation to less than 2 units. As mentioned earlier, a pole notch is bad magnetically. That made the above observed b_4 saturation of -2.4 units even worse. Therefore, a detailed study was undertaken to modify the cross section to significantly change the magnetic properties of the yoke, while retaining the desired mechanical properties. After examining a large number of options in the yoke design, it was found that simply a relocation of the helium bypass hole was very effective in controlling saturation induced harmonics. This, despite the presence of the pole notch, significantly reduced the saturation in b_4 harmonic. Magnets DRD009 and DRD010 were built on this cross section. They were built with stainless steel keys and as in all previous magnets, the shear pins (two 9.52 mm diameter rivets which are used to hold each pair of yoke laminations together) were made with low carbon magnetic steel. The crucial b_4 saturation in this "DRD" series magnets now became -1.3 units (an improvement from the previous value of -2.4 units in "DRC" series magnets). This improvement came however at the cost of b_2 saturation which now increased to +7.3 units (the value of b_2 saturation in the "DRC" series was 0.4 unit with a maximum change of -2.4 units at an intermediate current).

Finally, saturation suppressor holes were added in magnets DRE011 and DRE012. The size and location of the holes were optimized to reduce b_2 and b_4 saturation to values that can be tolerated in the machine (i.e. b_2 saturation about 2 units and b_4 saturation about $\frac{1}{2}$

unit). The optimized azimuthal location of a 9.52 mm diameter hole in the first quadrant was 33° when located at a radial distance of 75 mm from the magnet center. In addition to this change the material of the shear pins was changed from magnetic low carbon steel to non-magnetic stainless steel for mechanical reasons. To deal with this change, the material of the yoke keys was changed to magnetic low carbon steel. This inter-change of material produced little change in the saturation induced harmonics. The goal of minimizing b_2 and b_4 due to saturation at this level requires a careful analysis and inclusion of those small effects that were previously ignored (because of their relatively minor contributions) was necessary. The calculations and measurements and their differences, are given in Table 3.3.1.

Table 3.3.1: The saturation induced values of b_2 and b_4 harmonics at 5 kA in RHIC long dipoles. The model used in these calculations did not include the cryostat, which induces a change in b_2 of $\sim$+1.5 units and b_4 of $\sim$-0.1 unit at 5 kA. Since very little variation has been observed in the saturation induced harmonics in multiple magnets built with the same yoke cross section, only one from each series is listed here.

Magnet Name	b_2 Measured	b_2 Computed	Difference Meas-Comp	b_4 Measured	b_4 Computed	Difference Meas-Comp
DRA001	42.8	36.0	+6.8	-8.1	-7.0	-1.1
DRA004	34.5	35.5	-1.1	-5.2	-5.8	+0.6
DRB005	-6.1	-8.8	+2.7	-3.6	-4.0	+0.4
DRC007	0.4	0.8	-0.4	-2.4	-2.4	0.0
DRD009	7.3	9.4	-2.1	-1.2	-0.4	-0.8
DRE012	-2.4	0.1	-2.5	-0.3	0.7	-1.0
DRG101	-2.3	-2.6	+0.3	0.3	0.8	-0.5

Some possible sources of the differences between the calculations and the measurements are :

(a) The calculations did not include the effect of the cryostat around the yoke. The inclusion of the cryostat in a computer model means that a larger geometry is included in the model which requires lowering the mesh density in the yoke region. This is in conflict with the requirement that, to

obtain a high accuracy in the change in harmonics due to yoke saturation, the model in the yoke region should have sufficient mesh density. However, based on a typical calculation, the change in the saturation induced b_2 and b_4 due to the cryostat at 5 kA is respectively $\sim$+1.5 units and $\sim$-0.1 unit.

(b) The calculations ignore a small wedge-shaped gap at the mating plane of the top and bottom yoke halves. The average width of this gap is about 0.0254 mm with a maximum value at the yoke outer radius. This small gap is difficult to include in a reliable finite element computer model. This gap, when included in the model, results in a mesh in which two angles of the triangles defining the mesh in the gap are very small and the third is very large. Such triangles give large errors in this region and therefore the results of the computations are not very reliable. However, some model calculations suggest that this wedge-shaped gap may give as much as 2 units of b_2 and 0.2 unit of b_4 at 5 kA.

(c) As mentioned earlier, calculations are done here only for the saturation induced harmonics. Harmonics due to coil deformation as a result of the Lorentz force on the coil are not included. The deformation is radially outward at the horizontal midplane (which could be significant above a medium current of $\sim$3 kA) and azimuthally from pole to midplane (which could be significant above a high current of $\sim$4.5 kA, after the compression from the Lorentz forces has overcome the initial pole pre-compression). In order to compute these effects, the coil deformation must be known to 0.0254 mm level. Mechanical modelling based on finite element codes is perhaps not reliable to this accuracy. However, the estimated current dependence caused by these Lorentz forces is about 2 units in b_2 and 0.2 unit in b_4 in the design operating current range of RHIC arc dipoles. This deformation is not separable in the measured harmonics from the change in harmonics due to iron saturation, unless the coil deformation is very large. This was found to be the cause of a much larger than expected current dependence in b_2 harmonic in some SSC magnets [64]. The source was traced to a radial gap of about 100 μm between the stainless steel collar and yoke which allowed an extra deflection of the collared coil at the yoke midplane.

(d) The differences shown in Table 3.3.1 are the differences between the measured and computed values at 5 kA. The ideal goal would be to minimize the peak rather than the value at 5 kA. In general the calculations and measurements do not peak at the same current and sometimes the two peaks are separated by a few hundred amperes of current. The difference between the two in the operating range may be as much as 2 units for b_2 and about 0.3 unit for b_4. This may give a small error when the differences between the calculations and measurements are being empirically removed.

Therefore, when the goal is to optimize b_2 saturation to within a few units and b_4 saturation to within a few tenths of a unit, the uncertainties in the current dependence in the harmonics due to computer modelling and magnet manufacturing are appreciable. In order to overcome these limitations, first the differences between the calculations and measurements in each harmonic, $\delta b_n = b_n(computed) - b_n(measured)$, are obtained. These differences are then empirically removed while optimizing the location of the saturation suppressor holes by making the target to be -δb_n instead of zero. It is important to note that in order for this scheme to work as desired, no other significant change should be simultaneously made in the magnet. This approach is validated by the small measured values of b_2 and b_4 due to saturation as shown in Fig. 3.3.2 and Fig. 3.3.3. in magnets DRE011 and DRE012.

In the final design of the production series magnet (the *DRG* series), it was decided to change back the material of the collaring keys to non-magnetic stainless steel (see Fig. 3.3.1). This change was made to match the thermal contraction (during cool down) of the stainless steel shell with the thermal contraction of the collaring keys in the axial direction. Therefore, in this design both the keys and the shear pins are made of non-magnetic material. This made a significant impact on the saturation characteristic of the magnet. In order to maintain small values of b_2 and b_4 due to saturation, the saturation suppressor hole was moved from 33° to 35.5°. Moreover the value of the small yoke gap (described in item *(b)* above) was also changed. This change was not included in the computer modelling. The final *DRG* design for the production magnets gave a measured b_2 saturation of $\sim$2 units and b_4 saturation of $\sim$0.6 unit in the entire range of operation.

3.4. Reduction in the Saturation-induced Non-allowed Harmonics

In superconducting accelerator magnets, the radial thickness of the yoke is seldom adequate to contain all the magnetic return flux exterior to the coil at the maximum design field. Therefore the presence of magnetic material outside the yoke may influence the field uniformity in the aperture of the magnet. These effects are seen only after a certain threshold field which is usually close to the maximum operating field. The harmonics created are the reflection of the relative geometry of the yoke and the outside magnetic material.

In the RHIC and SSC dipole magnets, these effects can be separated in to two major classes. The first is the presence of another magnet in a colliding beam accelerator. This is more important in the interaction region magnets, where the separation between the inner and outer ring is a minimum. The left-right symmetry in RHIC dipoles is broken, introducing a current dependence in the odd normal harmonics (b_1, b_3, b_5, etc.) at high field.

The second class is the influence of the cylindrical vacuum tank containing the yoke which also serves as the cryostat wall. In the RHIC and SSC dipole designs the center of the cryostat does not coincide with the center of the yoke or cold mass. The cold mass refers to the part of the magnet mass that is at low temperature (4.5 kelvin in RHIC) and it includes the assembly of superconducting coils, yoke, etc. The center of the cold mass is located above the horizontal midplane of the cryostat to allow a maximum space for the support post. This reduces the heat load on the cryo-system at the expense of breaking the top-bottom symmetry. An absence of top-bottom symmetry (but the presence of left-right symmetry) introduces the odd skew harmonics (a_1, a_3, a_5, etc.). This effect is seen only at high field levels where the yoke is not able to contain the field lines. Moreover, in RHIC dipoles the left-right symmetry is also broken to some extent. This is because the cryostat is straight but the cold mass is curved to follow the beam, which is bent significantly by the dipole field. This generates a small but noticeable current dependence in the b_1 harmonic as a function of axial position since the yoke center does not always coincide with the cryostat.

In addition, a current dependence in the non-allowed harmonics may also be generated by a difference in the weight of the two yoke halves and by the influence of the currents in the bus (see Fig. 3.3.1) when the yoke at high field does not provide sufficient magnetic shielding. These and other sources will be discussed in this section.

3.4.1. b_1 saturation — Cross talk

In colliding beam accelerators, the magnets guiding the counter-rotating beams in the two rings are near each other. The magnets are usually closest to each other near the interaction regions where the two beam are brought together to collide. At high field, when the permeability of the iron yoke is too low to provide adequate magnetic shielding, the field in the aperture of one gets influenced by the field of the other. This condition is commonly referred to as "cross talk". If the two magnets lie on the same horizontal plane it generates odd normal harmonics like b_1 and if they lie on the same vertical plane it generates odd skew harmonics like a_1. In RHIC, the magnets lie on the same horizontal plane and thus the cross talk generates b_1, b_3, b_5, ... The b_1 generated would be much larger in "2-in-1" superconducting magnets where the coils of the two magnets are contained in a common yoke. In these "2-in-1" designs the separation between the two apertures and hence the thickness of the yoke providing the magnetic shielding between the two is generally small. In this case the field of one dipole could affect the field in the aperture of the other dipole at high field. This is also referred to as cross talk and it may generate a significant amount of b_1 and other odd normal harmonics at high fields.

The amount of cross talk induced b_1 depends on *(a)* the center-to-center distance between the two magnets, *(b)* the field in the aperture of the magnet, *(c)* the yoke thickness and *(d)* the coil aperture. The cross talk problem is examined here in the RHIC 100 mm aperture insertion dipole *D0*. A cross section of the cold mass of *D0* is shown in Fig. 3.4.1. Two such magnets are placed in a common cryostat. The center-to-center distance between the two cold masses is determined by the machine layout. The distance between the t-wo varies axially and it is smallest (and hence the magnetic coupling between the two is largest) on the end that is towards the beam crossing. The direction of the field in the two *D0* dipoles is the same since the two counter-rotating beams have the same sign of charge.

In Fig. 3.4.2, b_1 is plotted as a function of field for 100 mm, 105 mm and 110 mm coil apertures when the magnitude of the field in the two dipoles is the same. In Fig. 3.4.3, b_1 is plotted as a function of field when the ratio of the field in the two dipoles is 2.5:1, which is the maximum difference in this ratio. For a constant separation between the centers of two magnets, a smaller aperture allows a thicker yoke shielding between the two and hence reduces the cross talk induced harmonics at high field. The final choice of 100 mm aperture was made to keep cross-talk induced harmonics to a reasonable value at the design field of 3.5 Tesla.

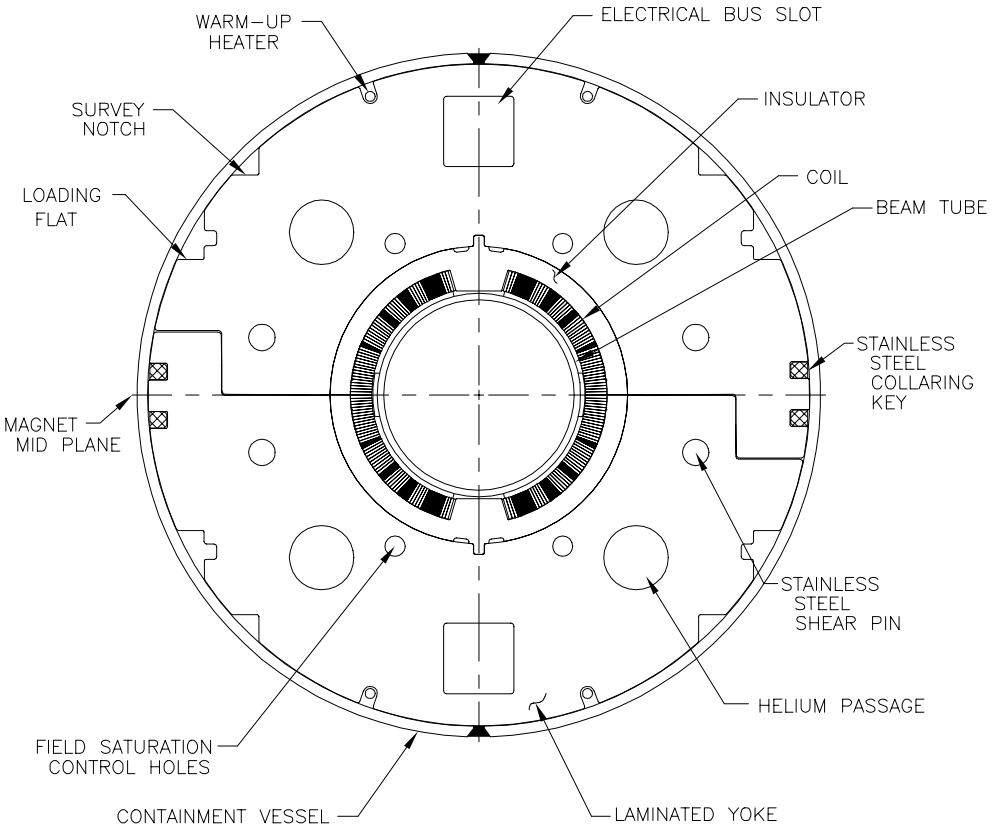

Figure 3.4.1: A cross section of the 100 mm aperture RHIC insertion dipole *D0* cold mass. Two such cold masses will be inside a common cryostat (not shown here).

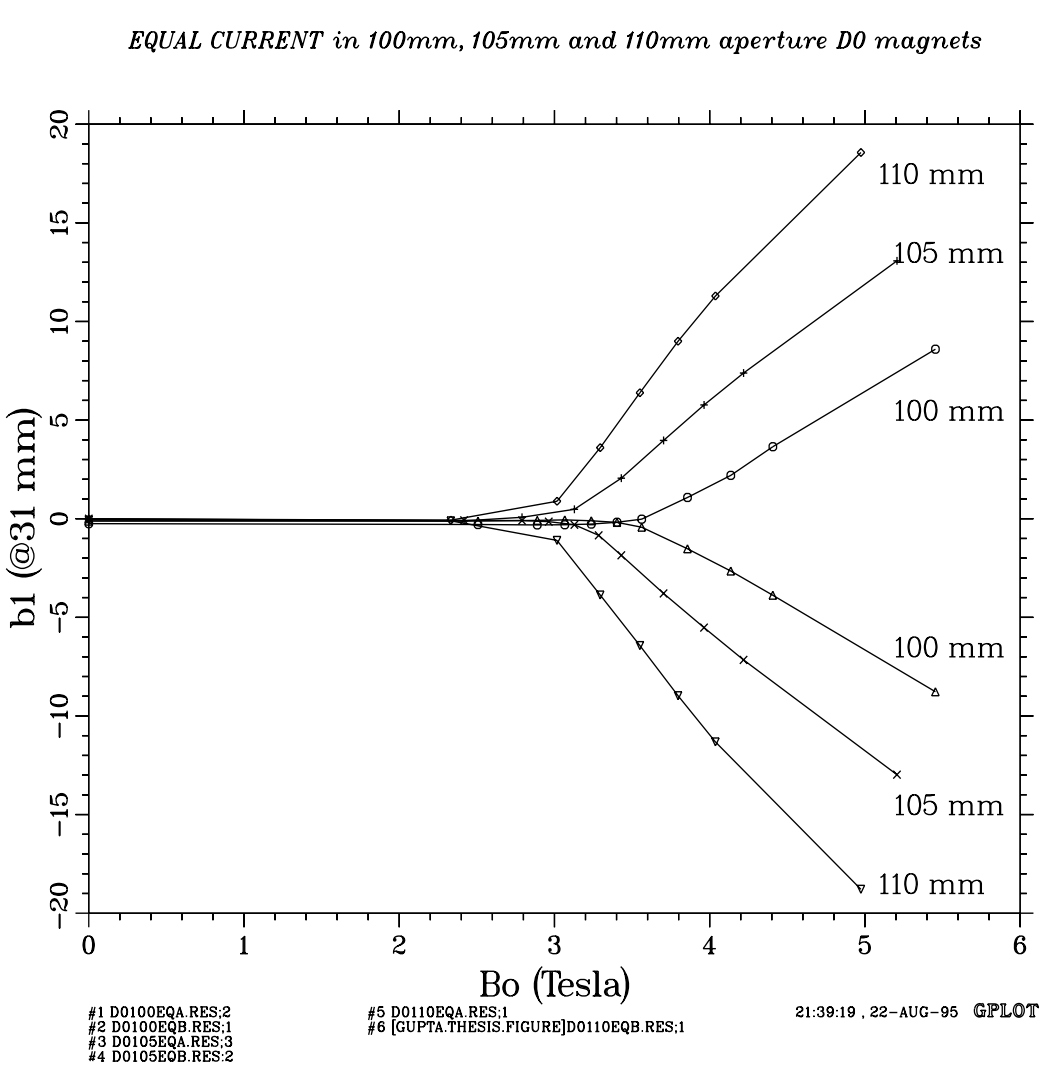

Figure 3.4.2: b_1 as a function of field in the 100 mm, 105 mm and 110 mm aperture designs of the *D0* magnets. This is the cross talk induced harmonic in the two apertures when both the magnitude and direction of the field in the two dipoles is the same. The sign of b_1 is positive in the magnet on the right hand side and negative on the left hand side.

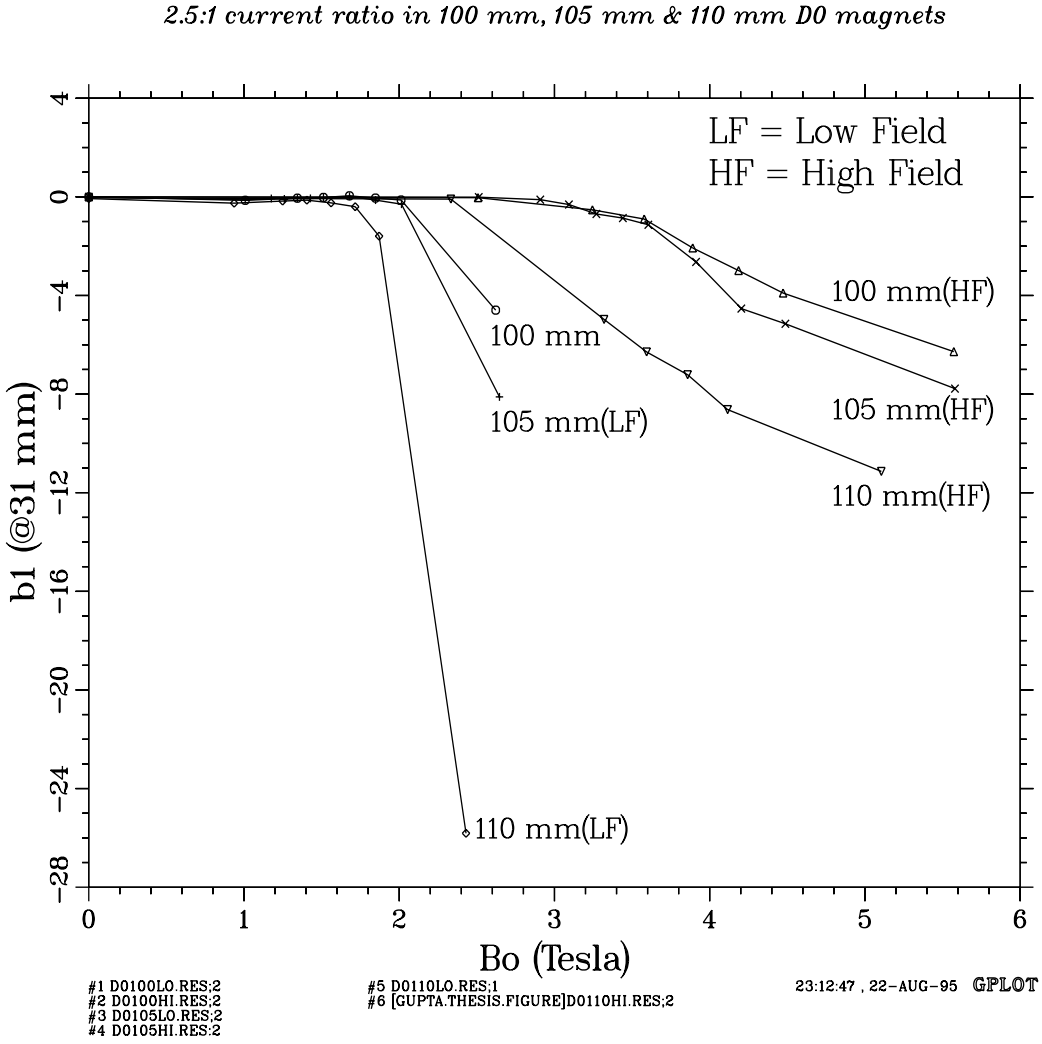

Figure 3.4.3: b_1 as a function of field in the 100 mm, 105 mm and 110 mm aperture designs of the *D0* magnets. This is the cross talk induced harmonic in the two magnets when the direction of the field in the two is the same and the current is in the ratio of 2.5:1. The maximum high field in operation is 3.5 tesla.

In Fig. 3.4.4 a POISSON model and field lines are shown for a 40 mm aperture SSC 2-in-1 magnet. The field lines are shown when the field in both aperture is equal to the design field of 6.6 tesla. A quadrupole harmonic (b_1) is created at this field since the field in the iron and hence iron saturation is not left-right symmetric about the vertical axis of either aperture. A left-right asymmetry in the field lines across the vertical axis of the two apertures (y-axis) can be seen in Fig. 3.4.4.

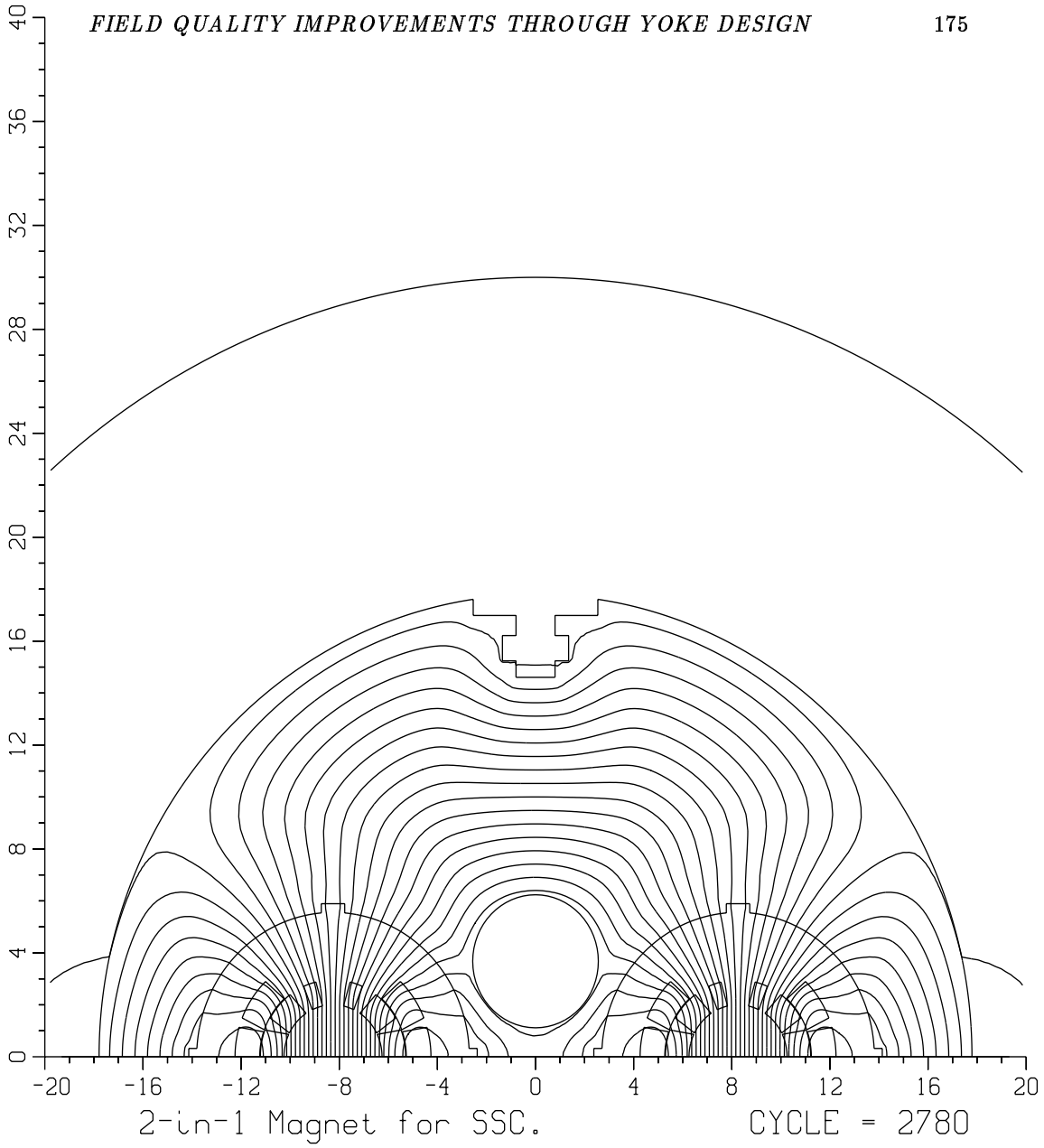

Figure 3.4.4: POISSON model and field lines in the upper half of the 40 mm aperture SSC 2-in-1 magnet. The field lines are shown when the field in both apertures is equal to the design field of 6.6 tesla.

3.4.2. a_1 saturation — Cryostat and other sources

A large current dependence in the skew quadrupole harmonic (a_1) has been observed in both SSC and RHIC dipole magnets. The variation of a_1 with current at high field is commonly referred to as "a_1 saturation" even though a number of sources other than the off-centered cryostat (discussed earlier) are responsible for it. The effects and their magnitude in SSC magnets will be discussed in detail. The change in a_1 at the design current (6600 A for SSC magnets and 5000 A for RHIC magnets) with respect to its geometric value at low current (2000 A for SSC magnets and 1450 A for RHIC magnets) will be evaluated by the following quantity :

$$SSC \rightarrow \qquad \delta a_1 = \left[a_1\left(@6600A\right) - a_1\left(@2000A\right)\right],$$

$$RHIC \rightarrow \qquad \delta a_1 = \left[a_1\left(@5000A\right) - a_1\left(@1450A\right)\right].$$

The low current value for the geometric harmonic is chosen so that it is below where iron saturation sets in and yet high enough that a_1 induced by the persistent currents has been significantly reduced.

The current dependence measured [70] with a 1 meter-long measuring coil in several 15 meter long BNL-built SSC magnets is shown in Fig. 3.4.5. To facilitate comparison, the curves are offset along the y-axis such that the value of a_1 is zero at 2 kA for all the magnets.

In the rest of this section the sources responsible for the variation in the current dependence of a_1 are discussed. For each of these sources, an estimate of δa_1 in SSC magnets is also given.

(a) **Off-centered cryostat :** At high current when the flux lines are not contained in the iron cross section, they leak outside the yoke. The magnetic iron in the cryostat (vacuum vessel) provides an additional magnetic path to return the flux lines. However, since the center of the cryostat is below the center of the yoke, an up-down asymmetry is introduced. Calculations for the SSC magnets show a noticeable a_1 current dependence beyond 6.0 tesla and the computed δa_1 is $\sim$ –0.2 unit. A computer model for the code POISSON with the field lines at the maximum design current for this problem is shown in Fig. 3.4.6. Calculations and measurements

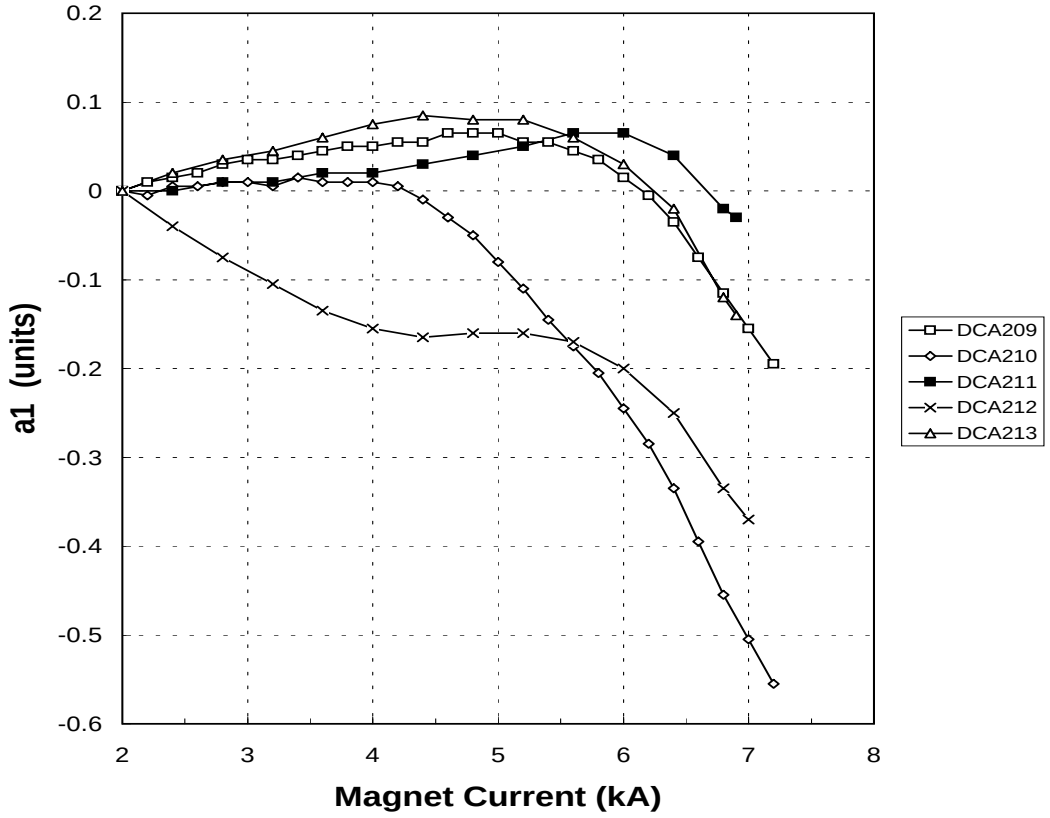

Figure 3.4.5: Current dependence of the skew quadrupole (a_1) harmonic in the SSC 50 mm aperture prototype dipoles DCA209 to DCA213. The curves are offset such that a_1 at 2 kA is zero for all magnets.

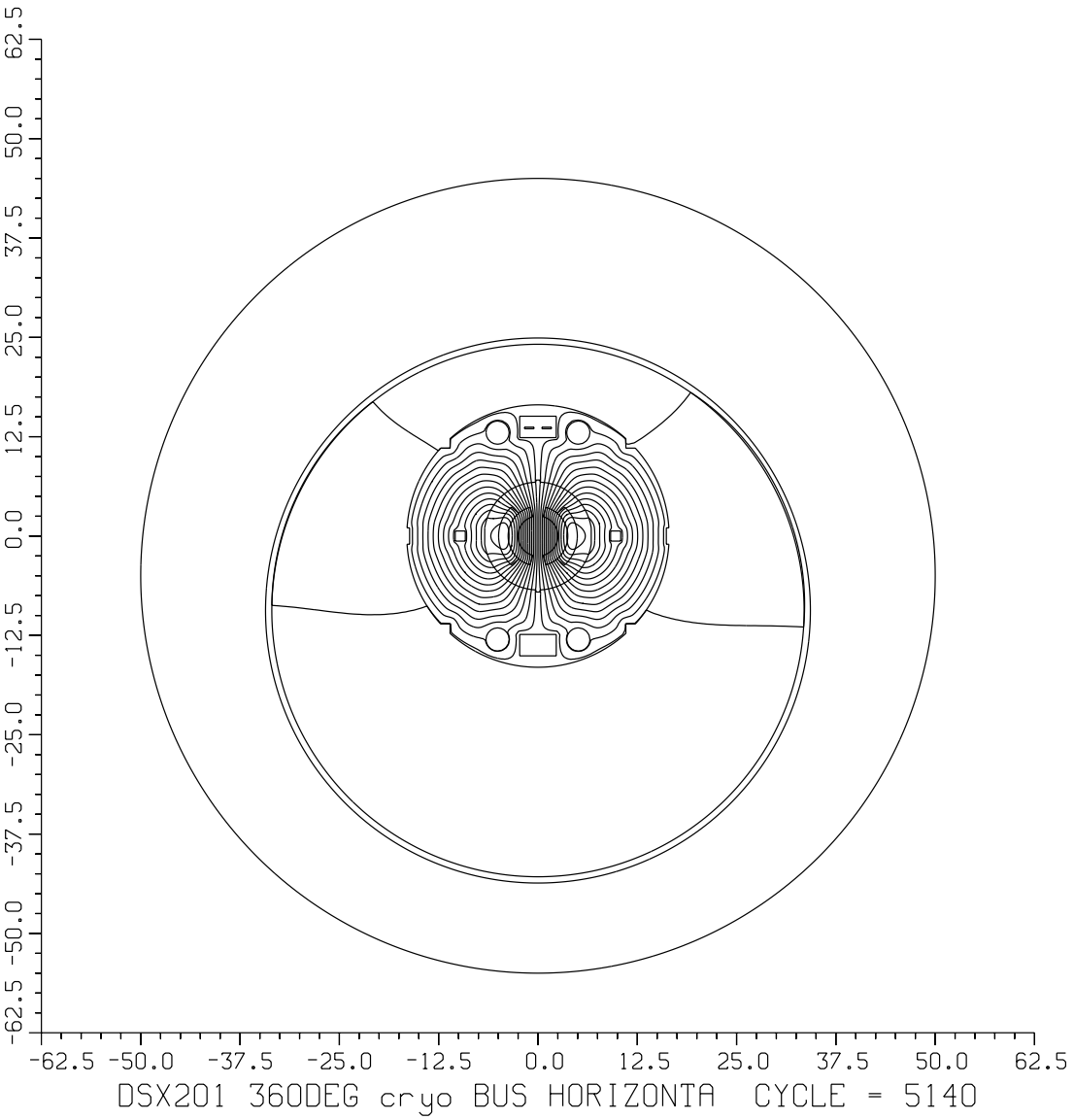

Figure 3.4.6: A computer model of the SSC 50 mm aperture dipole coldmass in the cryostat. The field lines are shown at the maximum design current of 6600 A. The center of the coldmass is located above the center of the cryostat and at high field when the yoke can not contain the field lines (one line per quadrant in the above diagram), this asymmetry creates a current dependence in the value of the skew quadrupole harmonic. The upper bus slot (between two helium holes near the perimeter of yoke) contains lead and return current cables. A proper placement of them can partly compensate the above asymmetry.

for the RHIC arc dipole magnets also show an a_1 saturation of ~-2.0 units at the design field of 3.45 tesla. This will be discussed in more detail later.

(b) **Difference in the packing factor between the upper and lower yoke halves :** The packing factor is defined here as the ratio between the volume occupied by the iron to the theoretical maximum in the given cross section (i.e. the holes, etc. are not included in the volume calculations). The relative variation in it can be evaluated by comparing the yoke weight per unit length in various lamination packs. Though the overall difference in the packing factor between the top and bottom yoke halves is well controlled, there may be some local variations along the length of the magnet as these have not been controlled. In the BNL-built SSC magnets, the iron weight of each 76.2 mm long block (a riveted pack containing 12 laminations) used in the top and bottom yoke halves has been measured. Since the length of the measuring coil is one meter, a top bottom weight difference in the yoke in a 1 meter region (the region of field measurements) may be seen in the field harmonics. The 2-d calculations for SSC magnets show that a 0.1% higher packing factor in the upper yoke half would give $\sim$ –0.1 unit of δa_1. This is the net change at 6600 A but the effect begins to appear at 3000 A. In RHIC magnets the calculations show that a 0.1% higher packing factor in the upper yoke half would give $\sim$ -0.3 unit of a_1 at the design field. The 2-d calculations, however, may be over-estimating this effect because in reality the field lines would not only move from bottom to top (as reflected in the calculations) but they may also move in the axial direction (if the iron density in the neighbouring pack is different) giving a lesser δa_1. This will be discussed in more detail later in this section.

(c) **Off-centered coil in the yoke :** If the coil center is above or below the yoke center, an additional δa_1 will be seen. This will also give a geometric a_1. Calculations for the SSC magnets show that for a $25\mu m$ off-centered coil above the midplane there would be an additional $\delta a_1 \sim +0.1$ unit and the geometric a_1 would be $\sim$ –0.12 unit.

(d) **Difference in the top-bottom coil sizes :** A difference between the top and bottom coil sizes gives a geometric a_1. Calculations for the SSC

magnets show that if the upper coil half is $25\mu m$ larger in size (which means that the midplane is shifted down by half of this amount), the geometric a_1 would be $\sim +0.7$ unit. It also gives a small additional contribution to the saturation induced δa_1, which is about 1% of the geometric a_1.

There is a second effect of coil size differences. An asymmetric coil package (midplane shifted downward or upward) produces an asymmetric Lorentz force (which is basically I^2 dependent). As a result, the asymmetry would be enhanced at high field by Lorentz forces. Mechanical calculations to compute the amount of displacement have not been done but it may be pointed out that merely a 2.5 μm additional displacement in the coil center would give a contribution of about 0.14 unit to the observed δa_1.

(e) **Special purpose holes in some yoke packs :** At about 5 meter from the lead end, strain gauges were installed in the SSC prototype magnets built at BNL. In order to bring the wiring out, two ~10 mm diameter holes were drilled in one yoke pack from the iron inner radius to the two *He* bypass holes. This was done only in the bottom half of the magnet. This gave a large local a_1 saturation, which has been measured. As mentioned earlier the measuring coil is one 1 meter long and the estimated value of this effect is an additional δa_1 of $\sim$ -0.15 in SSC magnets.

(f) **Persistent Currents :** Persistent currents in the superconductor of a magnet change when the current in the coils is changed. An up-down asymmetry either in the geometry of the coil (which also gives geometric a_1) or in the properties of the superconducting cables used in the top and bottom coils may generate an a_1 due to persistent currents. Since the magnitude of persistent current induced a_1 decreases at higher field, the difference between 5000 A and 2000 A values would contribute to the observed δa_1. The calculation of this effect is beyond the scope of this work. However, measurements show that δa_1 from this source is relatively small (under 0.05 unit) in SSC magnets.

(g) **Electrical Bus near the perimeter of the yoke :** A large number of magnets in the accelerator are connected in series so that a common power

supply and control can be used for all. The current from one magnet to the next is carried by a bus that is placed in a rectangular cutout near the perimeter of the yoke (see Fig. 3.4.6). The cutout also contains a bus for the return current, which depending on its configuration with the lead (supply) bus, may nearly cancel the lead bus contribution. A saturated iron yoke at high field does not provide adequate magnetic shielding at the center of the magnet against the field lines produced by the two currents in the bus. In the SSC and RHIC dipole magnets the bus is placed at the top of the yoke. This breaks an up-down symmetry and produces a current dependent a_1 at high field. The amount of δa_1 depends on the exact configuration of the two conductors in the bus; a significant δa_1 may be produced if the conductors in the bus are separated. The position of this bus and the configuration of the two conductors is chosen such that it has a minimum influence on the field at the center of the magnet and produces a small δa_1.

3.5. a_1 Saturation in SSC Dipole Magnets

In this section the variations in δa_1 are examined in SSC magnets (both within a magnet and magnet to magnet). Several methods for compensating a large systematic δa_1 due to an off-centered cryostat are proposed.

3.5.1. δa_1 variation with axial position within a magnet

Axial scans of the field harmonics have been made, using a one meter long measuring coil [70], in the prototype SSC magnets DCA209 through DCA213 at 2000A and 6600A current. The difference between these two values at each position gives δa_1 (a_1 saturation). It has been found that δa_1 varies significantly along the length of a magnet. This is shown in Fig. 3.5.1. Amongst the various mechanisms discussed in the previous section, the off-centered yoke in the cryostat (a) and electrical bus (g) give a constant δa_1 and thus can't account for the variation with position. The magnitude of the persistent current effects (f) is rather small. Of the remaining mechanisms, a difference in the packing factor (b) between the upper and lower yoke halves can be examined from the data on individual yoke block weights. As pointed out earlier, a difference in upper and lower yokes could affect δa_1.

The local asymmetry in the top and bottom yoke block weights is defined as :

$$\text{asymmetry} = \frac{\text{Weight of bottom block} - \text{Weight of top block}}{\text{Average of top and bottom weights.}} \times 100\%$$

The yoke weight in each block and the location of each block was carefully recorded [122] by BNL engineers. Fig. 3.5.2 shows the local asymmetry in the top and bottom yoke block weights averaged over the length of the measuring coil (one meter), as a function of block number (position along the magnet) in magnet DCA213. As can be seen from the figure, although the average asymmetry for the magnet is nearly zero, there can be a local asymmetry of up to $\pm 0.2\%$, when average values over one meter length are considered. The asymmetry is most prominent when the measuring coil center is located around block numbers 3, 60 and 90. Fig. 3.5.2 also shows the variation of δa_1 with position. A good correlation between the yoke asymmetry and δa_1 is seen. A similar correlation has been seen in other SSC prototype magnets. This leads to the conclusion that a major cause of δa_1 variation along the length of the magnet is a local top-bottom asymmetry in the iron weight (packing factor). A similar variation in the vertically split prototype magnets [133]

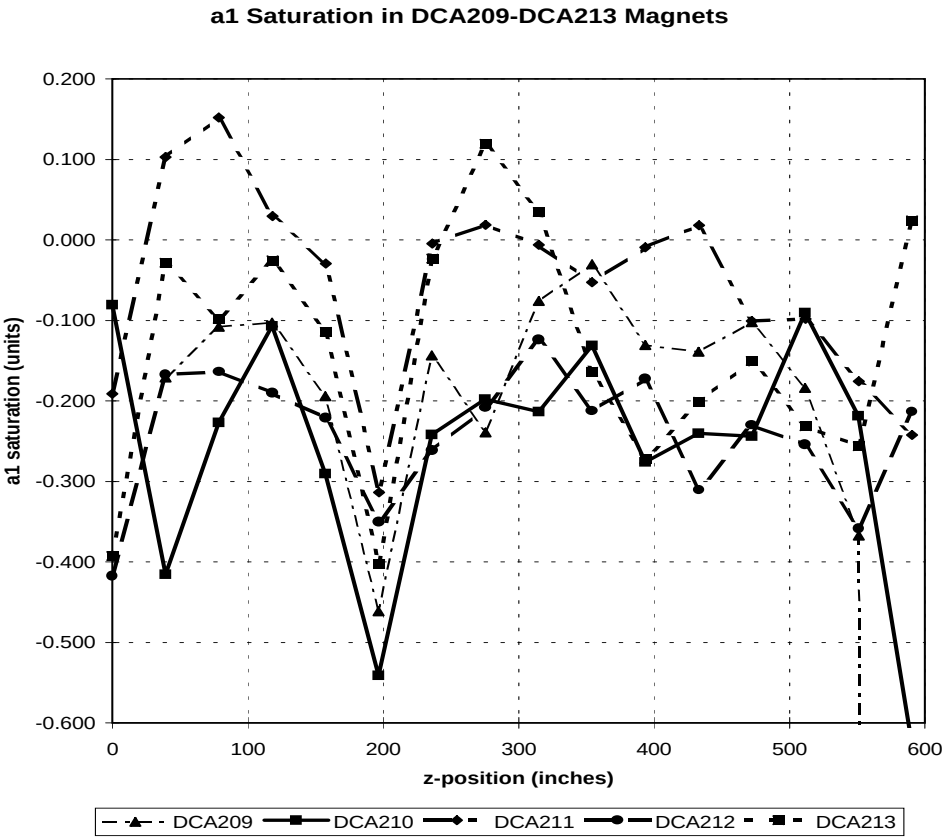

Figure 3.5.1: Variation in a_1 saturation along the length of the five, 15 meter long, SSC 50 mm aperture prototype dipole magnets DCA209-DCA213.

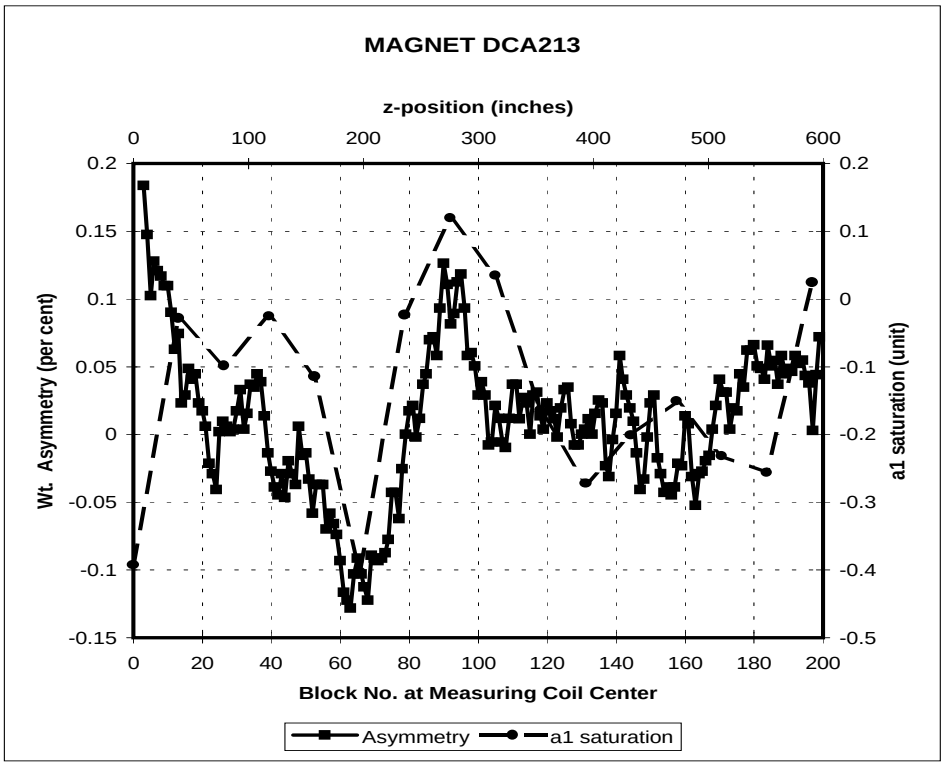

Figure 3.5.2: Variation of top-bottom weight asymmetry and a_1 saturation (δa_1) along the length of the SSC prototype magnet DCA213.

built at Fermilab, has been observed in b_1 saturation, which could be associated with a left-right asymmetry in the packing factor.

An examination of the a_1 saturation profiles for all the magnets (Fig. 3.5.1) shows a large δa_1 at about 5 meter (200 inches) in all the magnets. This can be linked to item (d) described in the previous section, which refers to the presence of a $\sim$10 mm diameter radial hole in the lower yoke block at this location. All SSC 50 mm aperture prototype magnets built at BNL had this hole to route the wiring for the strain gauges. Though the effect of this hole on the weight when averaged over 1 meter is negligible, the local perturbation on the field harmonics is much larger due to its geometry. Therefore, based on the computed estimates and measured systematic value of δa_1, it is correlated with the radial hole, rather than the weight asymmetry alone. It may be pointed out that the hole would not have been a part of the design of production magnets.

3.5.2. Magnet to magnet variations in the integral δa_1

Since the total yoke weight in the top and bottom halves is well controlled, one would not expect a magnet to magnet variation in δa_1 integrated over the entire length of the magnet. Table 3.5.1 lists the average values and RMS variations in a_1(@2000A), a_1(@6600A) and δa_1 in the straight sections of the SSC magnets DCA209-213 measured with the one meter long measuring coil.

Table 3.5.1 shows that the integral δa_1 does have a significant magnet to magnet variations. Thus, the observed δa_1 averaged over a magnet depends on factors other than the total yoke weight alone. A strong correlation is seen between the geometric a_1 [a_1(2000A)] and the integral δa_1. Please see Table 3.5.1 and Fig. 3.5.3 which shows the integral δa_1 as a function of geometric a_1 in magnets DCA209-213. A linear dependence of δa_1 on a_1 is observed and it is parameterized as [70]

$$\delta a_1 = -0.209 \; + \; 0.104 \times \; a_1\,(2000\mathrm{A})$$

The constant term agrees with the value of an -0.2 unit calculated for the effect of the off-centered yoke in the cryostat in the absence of any other asymmetry. The second term gives the dependence on the geometric a_1. A coefficient of 0.104 implies that there is a $\sim$10% enhancement in coil asymmetry (and hence in a_1) at 6600 A. The enhancement may have been caused by (a) asymmetric Lorentz forces due to asymmetry in the coil geometry,

Table 3.5.1: Integral Skew Quadrupole in DCA209-213

Magnet Magnet	$< a_1 > \pm \sigma(a_1)$ (2000A)	$< a_1 > \pm \sigma(a_1)$ (6600A)	$< \delta a_1 > \pm \sigma(\delta a_1)$ (6600A-2000A)	δa_1 (max-min)
DCA209	0.261 ± 0.408	0.086 ± 0.420	-0.175 ± 0.115	0.43
DCA210	-0.229 ± 0.227	-0.474 ± 0.211	-0.245 ± 0.118	0.45
DCA211	1.758 ± 0.623	1.724 ± 0.706	-0.034 ± 0.115	0.46
DCA212	-0.187 ± 0.200	-0.417 ± 0.220	-0.230 ± 0.070	0.24
DCA213	0.607 ± 0.335	0.477 ± 0.351	-0.130 ± 0.139	0.52
Average	$0.442 \pm 0.812^{**}$	$0.279 \pm 0.897^{**}$	$-0.163 \pm 0.085^{**}$	0.42 ± 0.11

** Sigma refers to magnet to magnet variation.

(b) saturation due to asymmetric placement of the coil in the yoke and (c) contribution of the persistent current induced a_1 in the coil. Using the above equation, one can predict the saturation δa_1 for any BNL built, horizontally split, 50mm SSC dipole magnet.

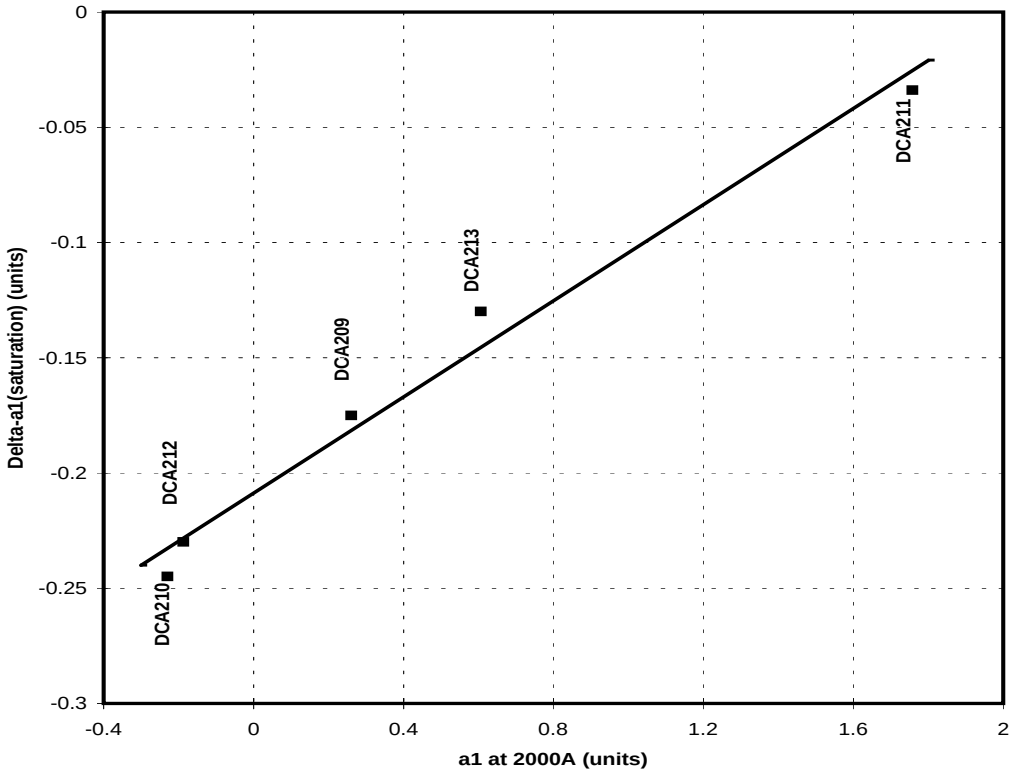

Figure 3.5.3: Correlation between geometric a_1 (a_1 at 2000 Amp) and a_1 saturation (δa_1).

3.5.3. Compensation of the saturation induced a_1 in SSC magnets

As discussed in the previous sections, both the calculations and measurements show a significant variation in a_1 (skew quadrupole) as a function of current beyond 6 tesla central field in SSC dipoles. In this section the discussion is restricted to the a_1 caused by the saturating iron in the yoke, the center of which is located asymmetrically 93.7 mm above the horizontal axis of the magnetic cryostat vessel. The effect on a_1 is several times the specification, a maximum of 0.04 unit for the systematic a_1. In the SSC 50 mm dipole the computed a_1 saturation is 0.2 unit at 6600 A. A few methods are discussed here which reduce this systematic change in a_1 and bring it within the specification.

(a) **Placing the conductors in a computed location in the bus slot:** It has been mentioned earlier that a saturated iron yoke does not provide adequate magnetic shielding against the field lines produced by currents in the bus conduit (item (g) in the previous section). Since the two conductors in the bus slot (see Fig. 3.4.6) carry currents in opposite directions, a dipole field is created by them. However, the direction and the magnitude of the field produced at the magnet center depends on their orientation, the separation between them and on the saturation of the yoke between the bus slot and magnet aperture. At high field, a δa_1 may be created, which then may be used to partly compensate the δa_1 produced by the cryostat. A maximum δa_1 is generated in the configuration when the conductors in the bus slot are oriented in such a way that they produce a vertical field (side-by-side configuration) and a minimum when they produce a horizontal field (up-down configuration). POISSON calculations show that in the side-by-side configuration if the spacing between the midpoint of the two conductors is 10 mm, the net δa_1 in the magnet stays within the specified tolerance of 0.04 unit. In the given configuration, the relative direction of the current in the bus conductors should be opposite to that of the direction of the current in the main magnet coil in the aperture of the magnet.

(b) **Iron weight difference between the upper and lower yoke halves:** In the BNL-built SSC dipole magnets the yoke is split in two halves at the horizontal plane. If the number of magnetic laminations or their weight

is different between the top and bottom halves of the magnet, δa_1 is created (see item (b) in previous section). This could be used to significantly compensate the δa_1 produced by the cryostat. One practical way to implement this scheme in a magnet could be that some of the low carbon steel (magnetic) laminations are replaced by stainless steel (non-magnetic) laminations in the upper yoke-half. If the number of non-magnetic laminations is a small fraction of the magnetic laminations, the situation can be simulated in a computer program by using a difference in packing factor between the top and bottom halves of the yoke. POISSON calculations show that $\sim 0.1\%$ difference in packing factor is adequate to bring the net a_1 within the specified tolerance of 0.04 unit.

(c) **Placing extra magnetic steel at the bottom of yoke:** Since the saturation a_1 is caused by the proximity of the iron cryostat wall at the top half of the magnet, a natural solution to this problem would be to put some extra iron on the opposite side of it. Several configurations have been examined to put (or attach) this extra iron at the bottom half of the magnet. POISSON calculations show that a 1 mm thick iron strip from 180 degree to 360 degree on the yoke outer radius (just outside the stainless steel shell) would be adequate to produce the required compensation. If the strip is put from 225 degree to 315 degree (width = 90 degree) the thickness required would be 10 mm.

General Dynamics has examined [76] placing this extra iron inside the magnet coldmass and have found that would also generate an adequate compensation.

3.6. a_1 Saturation in RHIC Dipole Magnets

In the RHIC arc dipoles, as in the case of the SSC dipoles discussed above, the center of the cold mass lies above the center of the cryostat (see Fig. 3.6.1). This introduces a systematic top-bottom asymmetry leading to a skew quadrupole (a_1) harmonic at high fields [97]. The magnitude of this a_1 depends on the current (field). Moreover, like the SSC dipoles built at BNL, the RHIC dipoles also have a horizontally split yoke design and the weight of the top and bottom yoke is not always the same. This may create an additional current dependence in the skew quadrupole harmonics. These two effects are studied here. An attempt is made to compensate the a_1 created by the cryostat with an a_1 created by a deliberate asymmetry between the top and bottom yoke weights. The results of this attempt will be discussed.

3.6.1. Magnet to magnet variation in a_1 saturation

The field quality in all the RHIC dipoles is measured at room temperature using a one meter long rotating coil system. [155] The integral harmonics are determined from an axial scan of the magnet in one meter steps. The first 30 dipoles were also measured cold with the rotating coil system. Subsequently, only about 8% of the dipoles are tested cold. The field measurements in cold magnets consist of axial scans at 660A (near injection), 1450A (near transition) and 5000A (near storage). In addition, the complete current dependence from 50A to 6000A is studied at one location in the center of the magnet. The dependence of the skew quadrupole term on current, measured in the axial center of two of the RHIC dipoles, is shown in Fig. 3.6.2. In order to facilitate comparison between the two magnets, the geometric skew quadrupole term is removed by subtracting the value at 1450A. The possible sources leading to variation of a_1 with current in the SSC have been discussed earlier and those sources play a similar role in RHIC magnets.

The major systematic source of the current dependence is the same as in SSC magnets, which is the cryostat. The major source of magnet to magnet variation could be the differences in persistent currents in the cable used in the upper and lower coils and the differences in yoke weights between the upper and lower halves. The skew quadrupole contribution at 1450A due to superconducting cable magnetization is less than 0.1 unit in the magnets measured so far.

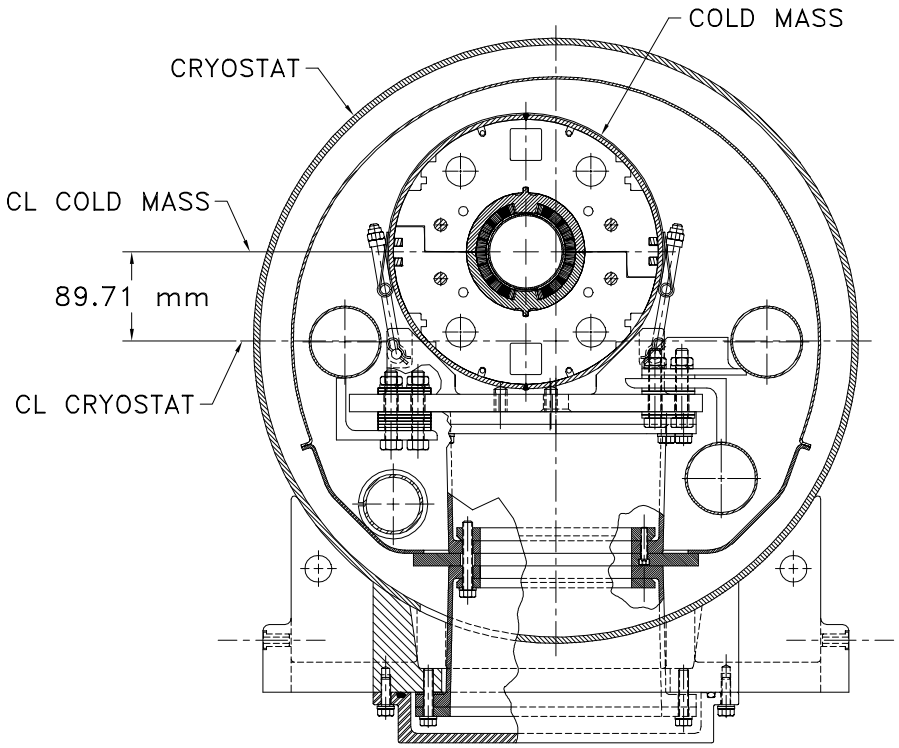

Figure 3.6.1: A cross section of the RHIC arc dipole showing the asymmetrically located cold mass in the cryostat. The top-bottom asymmetry generates a skew quadrupole harmonic (a_1) at high fields. The left-right asymmetry generates a normal quadrupole harmonic (b_1) at high fields. The latter asymmetry, which varies along the axis, is generated because the cold mass is curved to match the beam curvature and the cryostat is not. The cross section shown above is at the axial center.

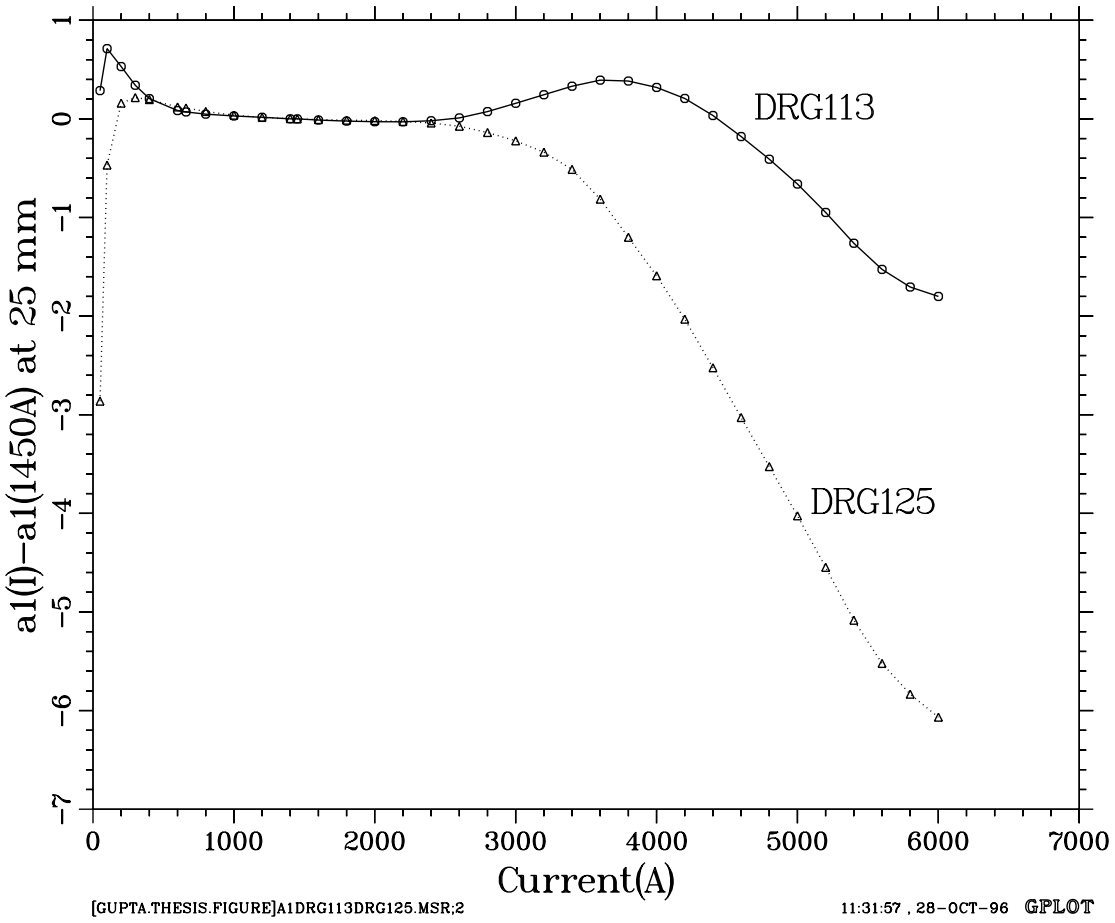

Figure 3.6.2: Dependence of the skew quadrupole term on current in the dipoles DRG113 and DRG125. The magnitude of change between low currents and 5000A is larger in DRG125 and is smaller in DRG113.

The two magnets for which data are shown in Fig. 3.6.2 exhibit the largest (DRG125, filled boxes) and among the smallest (DRG113, solid line) skew quadrupole due to saturation. In SSC dipole prototypes, a good correlation was found between the top-bottom yoke weight asymmetry and the a_1 saturation. In RHIC dipoles, the upper and the lower iron yoke weights are available in three different axial sections. The values of the skew harmonic terms are integrated over each of these three sections in a magnet by appropriately summing the values measured in axial scans. Using axial scans at 1450A and 5000A, the a_1 saturation in each of the three sections is computed.

Fig. 3.6.3 shows the correlation between the yoke weight asymmetry and a_1 saturation in RHIC dipoles. The yoke weight asymmetry is defined here as [97]

$$\text{asymmetry} = \frac{\text{Weight of Top block} - \text{Weight of Bottom block}}{\text{Average of top and bottom weights}} \qquad (3.6.1)$$

There are a total of 38 magnets in the plot shown in Fig. 3.6.3, for a total of 114 (=3x38) points in the plot. A good correlation is seen between the yoke weight asymmetry and the saturation in skew quadrupole, as expected. The solid line shows a linear fit to the data points. A few of the data points are seen to lie away from the line. This lack of correlation in certain sections of a few magnets could be due to incorrect recording of the yoke weight. The linear fit shown excludes such data points (seven points in all, belonging to six different magnets). The linear fit gives an a_1 saturation of -1.9 units for zero asymmetry in yoke weight, in good agreement with the computed value of -2.0 units. Furthermore, the slope of the line gives a change of -2.8 units in a_1 saturation for a 1% asymmetry in the iron yoke weight. This is also close to the computed value. The calculated current dependence of the skew quadrupole term is shown in Fig. 3.6.4 for various values of top-bottom weight asymmetry. The calculated curves are similar to the measured current dependences shown in Fig. 3.6.2.

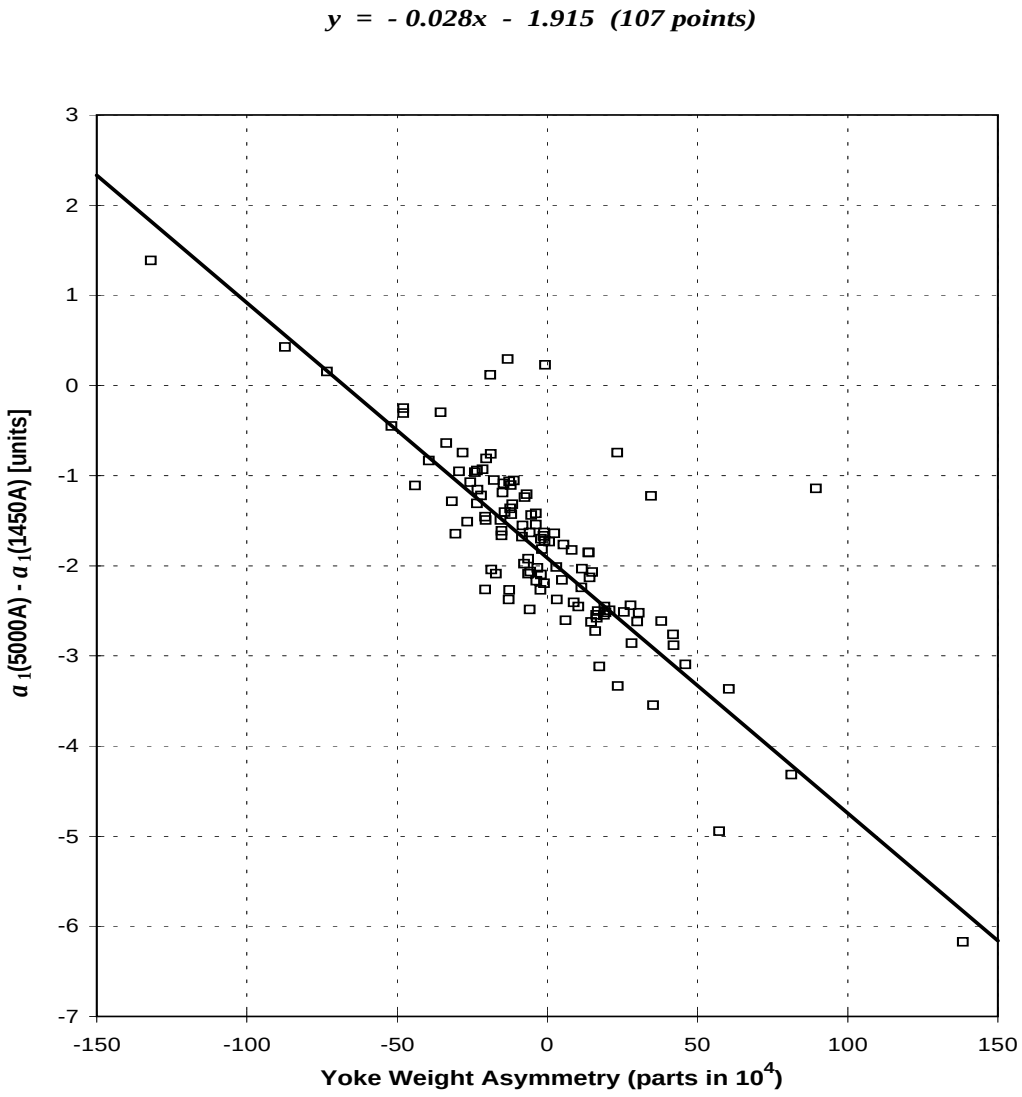

Figure 3.6.3: Correlation between the RHIC dipole yoke weight asymmetry and the saturation in the skew quadrupole term. There are three data points for each magnet corresponding to the three sections of the yoke blocks for which the weights are known. The equation on the top of the figure is obtained by a least square fit with x representing the yoke weight asymmetry and y the change in a_1 (@2.5 cm) between 5000 A and 1450 A. (Courtesy A. Jain).

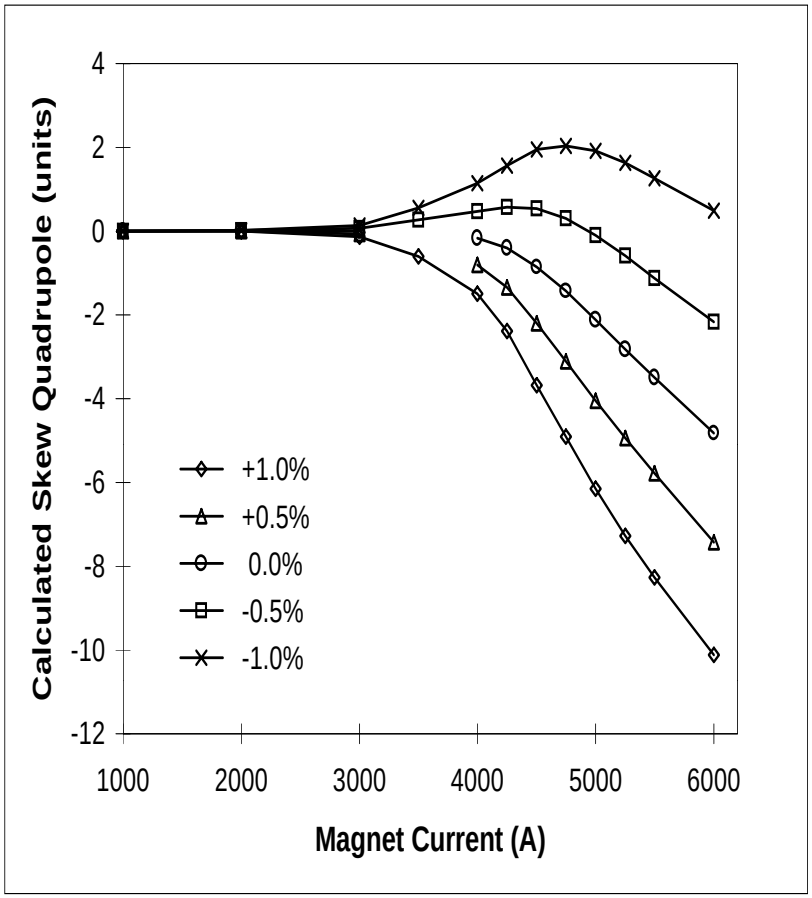

Figure 3.6.4: The calculated current dependence of the skew quadrupole term for various values of the asymmetry between the top and the bottom halves of the yoke.

3.6.2. Reduction in a_1 saturation in RHIC dipoles

As seen from Fig. 3.6.3, there is considerable magnet to magnet variation in a_1 saturation. This variation is a result of asymmetry in the top and bottom yoke weights. The production specifications for the RHIC dipoles specify that the total weight of the yoke be held constant within ± 2 kg. The total yoke weight is approximately 2764kg. Ideally, the weights of the yoke halves should be controlled with little magnet to magnet variation. However, such a requirement is difficult to fulfill in practice. Since the yoke laminations are 6.35 mm thick with a tolerance of 0.25 mm, the weights of the yoke packs are expected to differ somewhat. The systematic value of the skew quadrupole measured at low fields in the RHIC production dipoles is close to zero. If the upper and the lower yoke blocks are exactly matched in weight, this would imply a systematic a_1 of -1.9 units at 5000A due to the cryostat. It is possible to reduce this systematic a_1 at high fields by counteracting the asymmetry of the cryostat by some other means. Various possible means to achieve this have been discussed above.

The control of a_1 saturation essentially requires that additional iron be available in the bottom half of the yoke compared to the top half. A study of yoke weight data in the first $\sim$50 RHIC dipole magnets showed that there was a significant variation in the weights of yoke blocks. This natural variation in the yoke weights has been utilized to create a deliberate top-bottom asymmetry to compensate the asymmetry created by the off-centered cryostat. In practical terms, this reduces the net a_1 saturation without incurring any additional cost in the production. In the dipoles now under production at the Northrop Grumman Corporation, the yoke blocks are assigned in such a way that the heavier blocks are used for the bottom half and the lighter ones for the top half. A top-bottom weight difference of 0.5% of the total (top + bottom) yoke weight (or an asymmetry of 0.01 as defined in Eqs. (3.6.1)) is targeted to counteract the -1.9 units of systematic a_1 saturation.

Fig. 3.6.5 shows the asymmetry in the total upper and the lower yoke weights in all the dipoles delivered so far. The current scheme of yoke block assignment was implemented starting with dipole sequence number 63. For dipoles 1 through 62, no attempt was made to control the upper and the lower yoke weights separately. As can be seen in Fig. 3.6.5, most magnets in this group had a positive asymmetry, which only added to the effect from the cryostat. For dipoles numbered 63 onwards, the lower half of the yoke was made heavier than the top half as much as allowed by the actual weights of the yoke block in each magnet up to a limit of 0.01 in asymmetry. This is reflected in the negative values of asymmetry

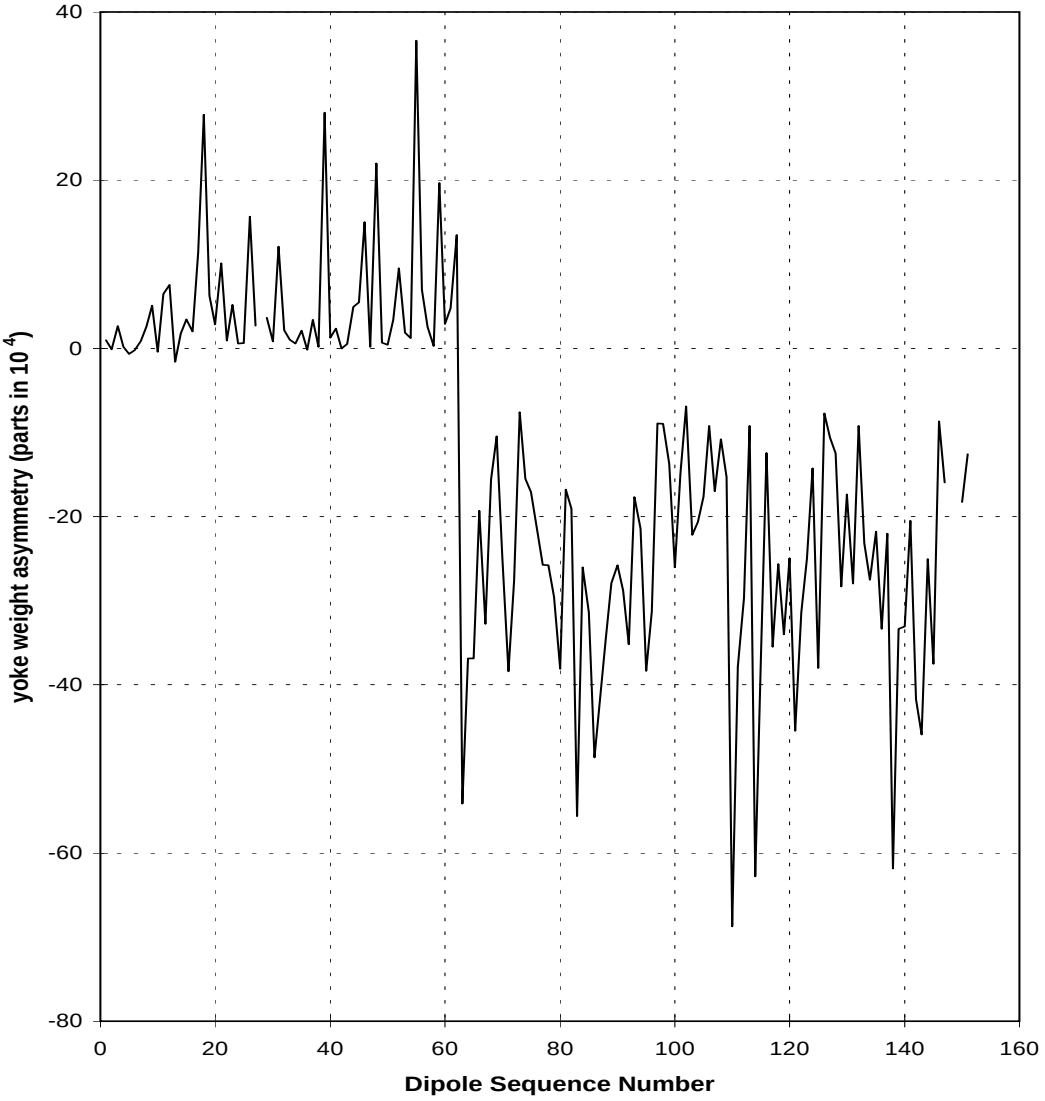

Figure 3.6.5: The asymmetry in the weights of the upper and the lower yoke halves in the RHIC arc dipoles. Starting with magnet sequence number 63, the lower yoke half was made heavier than the top half. (Courtesy A. Jain).

in Fig. 3.6.5 for sequence number 63 and higher. The additional iron on the bottom is expected to counteract the effect of the cryostat proximity on the top.

The integral values of a_1 in the magnets were obtained by summing the fields measured in the axial scans. The integral values of a_1 saturation were calculated using the integral values from the axial scans at 1450A and 5000A. The correlation between the integral a_1 saturation and the asymmetry in the total upper and the lower weights is shown in Fig. 3.6.6 for both the intial magnets (open boxes), and the current production (filled boxes). Once again, the correlation with iron weights can be seen to hold for most of the magnets. The solid line shows a linear fit to the data. Some of the points do not fall close to the line. It should be noted that most of these points belong to the same magnets that did not show a good correlation in Fig. 3.6.3.

It is clear from Fig. 3.6.5 that the magnets in the new scheme (production sequence 63 and higher) have a negative top-bottom asymmetry in yoke weight on an average. This has resulted in a correspondingly lower a_1 saturation (see Fig. 3.6.6). The average a_1 saturation in the magnets 1 through 62 (cold data in 33 magnets) is -1.95 units, whereas the corresponding average for the magnets 63 onwards (cold data in 7 magnets) is only -0.83 units. Thus, on the average a reduction of about 1.1 unit in a_1 saturation has been achieved. In principle, the average a_1 saturation could have been made zero by applying a proper yoke weight asymmetry. In RHIC magnets, since it was not critical to the machine performance, the extra complication and effort did not justify reaching this goal. It may be mentioned again that the above reduction in a_1 saturation is obtained without incurring an extra cost or excessive complications during the magnet production; only the scheme of assigning the location of the eight yoke blocks in each magnet has been modified.

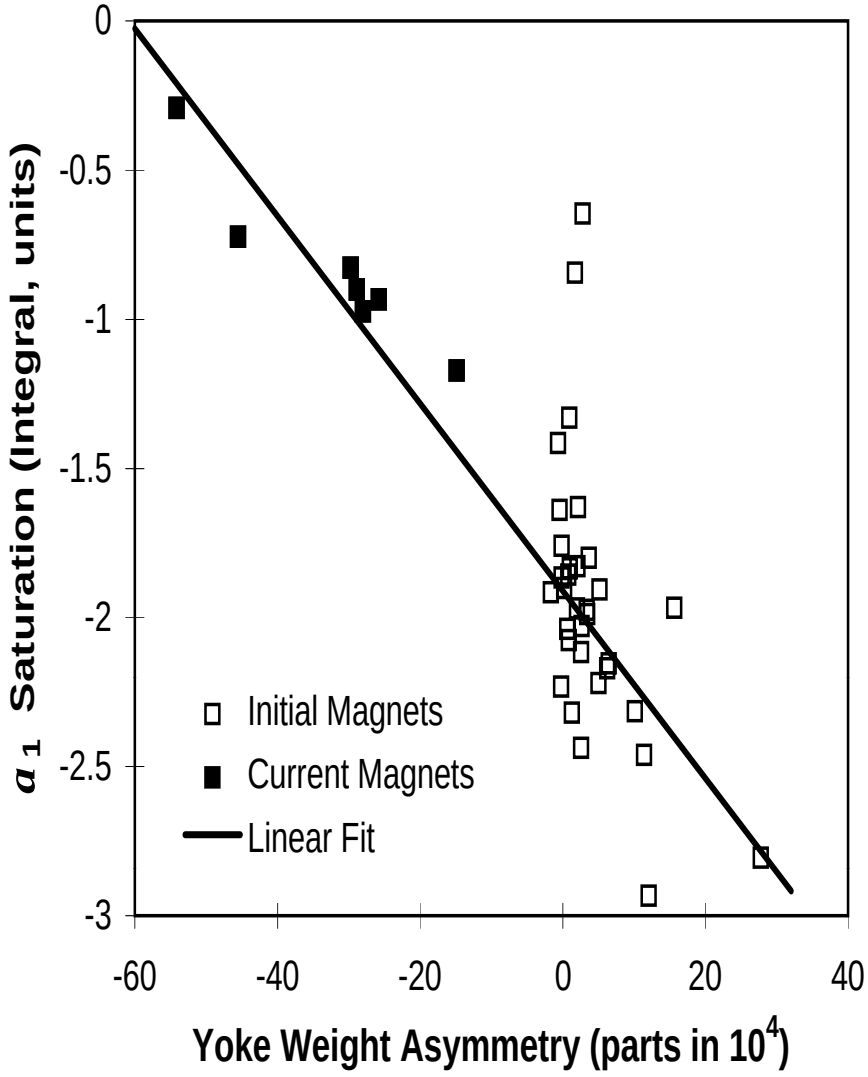

Figure 3.6.6: Correlation between the integral a_1 saturation and the asymmetry in the total weights of the upper and the lower yoke halves. (Courtesy A. Jain).

3.7. Conclusions on the Field Quality Improvements through Yoke Design

The magnetic field (or current) dependence in harmonics due to iron saturation could be a major problem particularly in the magnets such as those for RHIC where the iron contributes a significant fraction of the total field. Several methods have been examined and developed here to minimize this current dependence to a level where it is of little concern to the beam dynamics in the entire operating range of the machine. It has been demonstrated here that by a proper yoke design one can eliminate the need for external corrector magnets which may otherwise be needed to compensate for the harmonics generated by iron saturation.

The methods examined here can be put in three major categories : (a) optimization of the yoke radial thickness at the midplane by choosing the yoke inner and outer radius, (b) optimization of the yoke inner surface geometry such as by the use of a 2-radius aperture design or an elliptical aperture design and selecting an average gap between the coil and iron and (c) the optimization (and addition) of the size and location of a number of holes and cutouts in the yoke geometry to control the yoke saturation. The efficiency of a particular approach depends on the design details.

These approaches have significantly (about an order of magnitude) reduced the current dependence of the b_2 and b_4 harmonics in the 80 mm aperture RHIC arc dipole magnets as shown in Fig. 3.3.2 and Fig. 3.3.3. The field dependence of the average (mean) values of allowed harmonics in the production dipole magnets built by Northrop Grumman Corporation for the RHIC machine is given in Fig. 3.7.1. Since not all magnets are tested cold, the current dependence is obtained from a one meter long section in the body (straight section) of the magnet *DRG107* and it is superimposed over the measured mean of the warm measurements in all magnets based on a warm-cold correlation. The harmonics are given at 25 mm reference radius. The current dependence in the two ends of the magnet is somewhat different from that observed in the body and it gives a small positive contribution to the integral b_2 harmonic at fields higher than 2.5 tesla. The current dependence in b_2 (see Fig. 3.7.1) at lower fields (below 1.6 tesla) is due to persistent currents. The current dependence above 1.6 tesla is primarily due to the saturation of the yoke iron and also due to the coil deformation as a result of Lorentz forces. Only a high field saturation induced current dependence is minimized here. As a result, one can see that the field harmonics remain small even beyond the operating field of 3.46 tesla. The geometric b_2 in the magnet is optimized so that b_2 is small at 3.46 T (5 kA). The actual variation in the mean value of

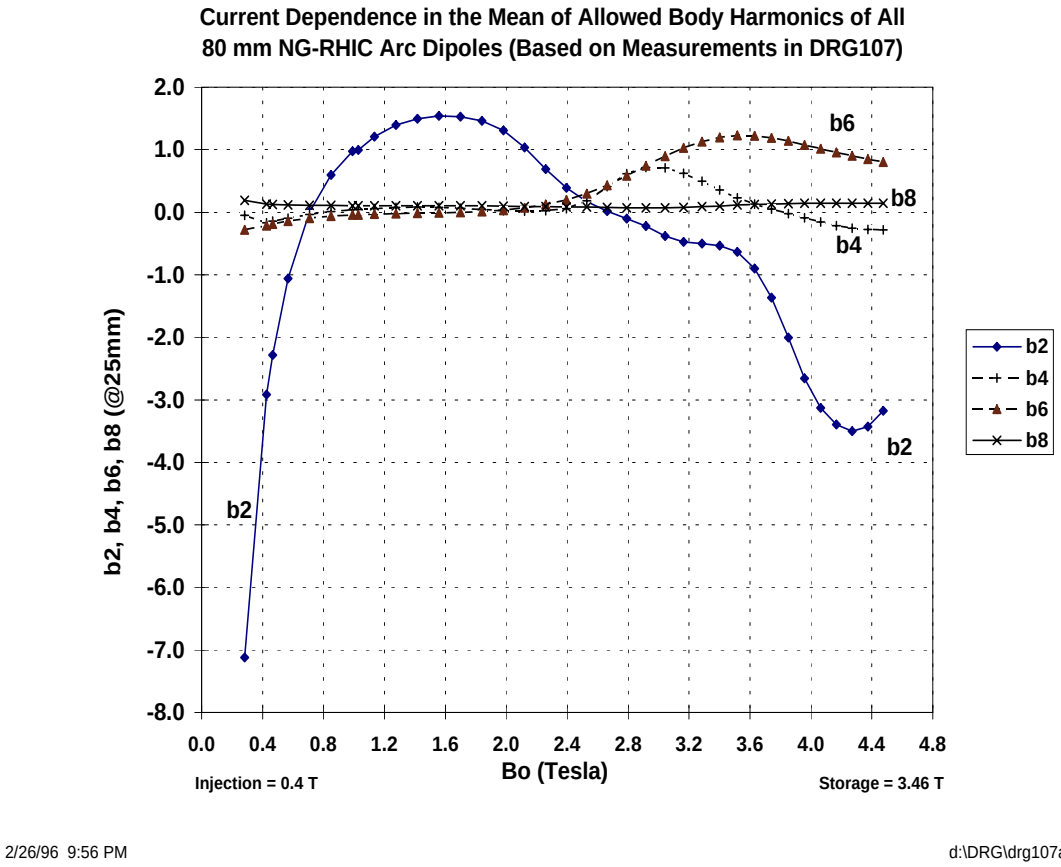

Figure 3.7.1: The current dependence of the average values of the allowed field harmonics in the Northrop Grumman built RHIC 80 mm aperture arc dipole magnets based on the measured current dependence in DRG107. A Warm-cold correlation is used here to shift the measurements in DRG107 to the average values of the allowed harmonics in all magnets.

the integral b_2 (Fig. 3.7.1 shows only that for the body of the magnet) in the entire series of RHIC dipole production magnets remains within ± 3 unit from injection (0.4 T or 570 A) to quench ($\sim$4.5 T or $\sim$7.2 kA which is $\sim$40% over the maximum design operating current of 5.1 kA). Most accelerator magnets have a large saturation in sextupole harmonics beyond their operating current. This unusually small current dependence beyond operating current is attributed to the methods used in optimizing the yoke design of RHIC magnets.

To minimize the saturation induced harmonics at high fields one should minimize the variation of iron magnetization or $|B|$ at the yoke inner surface. Although in RHIC magnets the variation in the current dependence of field harmonics was minimized, a more direct approach could have been to minimize the azimuthal variation of $\frac{\mu-1}{\mu+1}$. The function $(\frac{\mu-1}{\mu+1})$ lies in the range of 0 to 1 and it reflects the iron contribution to the total field. The function is 1 when μ is large (μ is a few thousand at low fields when the iron is not saturated) and is 0 when μ is one (at high fields when the iron is completely saturated). The importance of this function is clear from Eqs. (1.5.60) which gives the harmonics b_n and a_n due to a conductor in a cylindrical iron aperture. In Fig. 3.7.2, the variation in the magnitude of the field ($|B|$) is shown in the RHIC 80 mm aperture dipole in the case of (a) the circular aperture yoke without any holes or cutouts and (b) the yoke having holes and cutouts used in the present optimized design. These figures are given at 7 kA current (or 4.5 T field), which is significantly above the 5.1 kA ($\sim$3.46 T) operating current. As mentioned earlier, the saturation remains small even at these high fields. A high field is chosen here to enhance the contrast between the two cases. In Fig. 3.7.3, the variation in the function $\frac{\mu-1}{\mu+1}$ is shown for the same two cases. The computer model shown in Fig. 3.7.2 and in Fig. 3.7.3 was made by P. Thompson and the design work for the RHIC arc dipole magnets has been carried out in collaboration with him. A significant reduction in the azimuthal variation of $|B|$ and in $\frac{\mu-1}{\mu+1}$ can be seen, particularly in the iron near the yoke inner surface . This reduction is made possible by optimizing the location and size of various holes and cutouts and by putting additional holes dedicated to controlling the iron saturation.

The design of the 130 mm RHIC insertion quadrupole is based on the two radius method for controlling iron saturation in the yoke. This method has resulted in reducing b_5 by an order of magnitude (see Fig. 3.2.31). In quadrupoles, the 2-radius saturation control method has been found to be more efficient than the hole method used effectively in dipoles. The primarily reason for this is that the amount of flux per pole in quadrupoles is half of that in dipoles and therefore manipulating that smaller amount of flux to force saturation at the

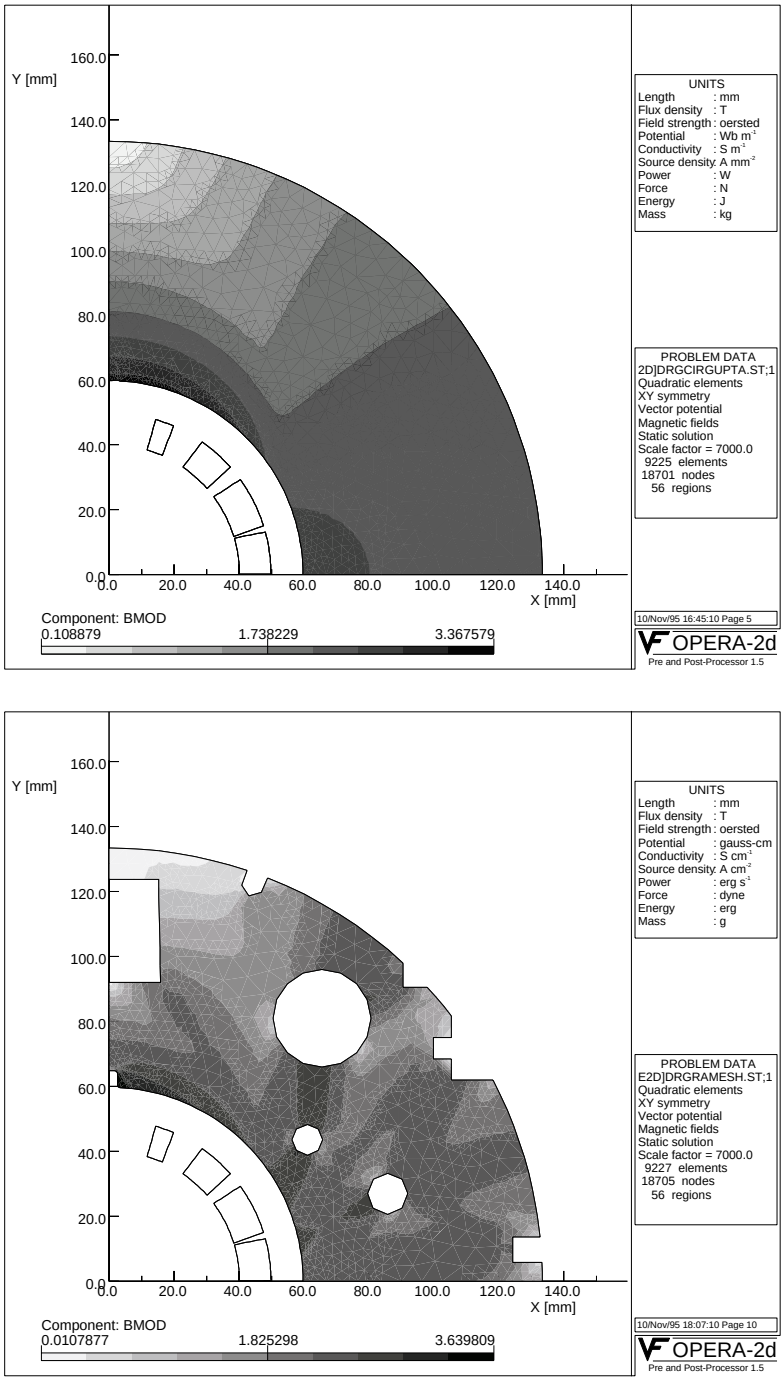

Figure 3.7.2: The magnitude of the field in the iron yoke of the RHIC 80 mm aperture arc dipole magnet at 7.0 kA in (a) circular aperture case (upper figure) with no holes, etc. and in (b) the optimized design (lower figure) with all holes and other structures. A reduction in the variation, particularly at the yoke inner surfaces may be seen. The design operating current in these magnets is $\sim$5.1 kA.

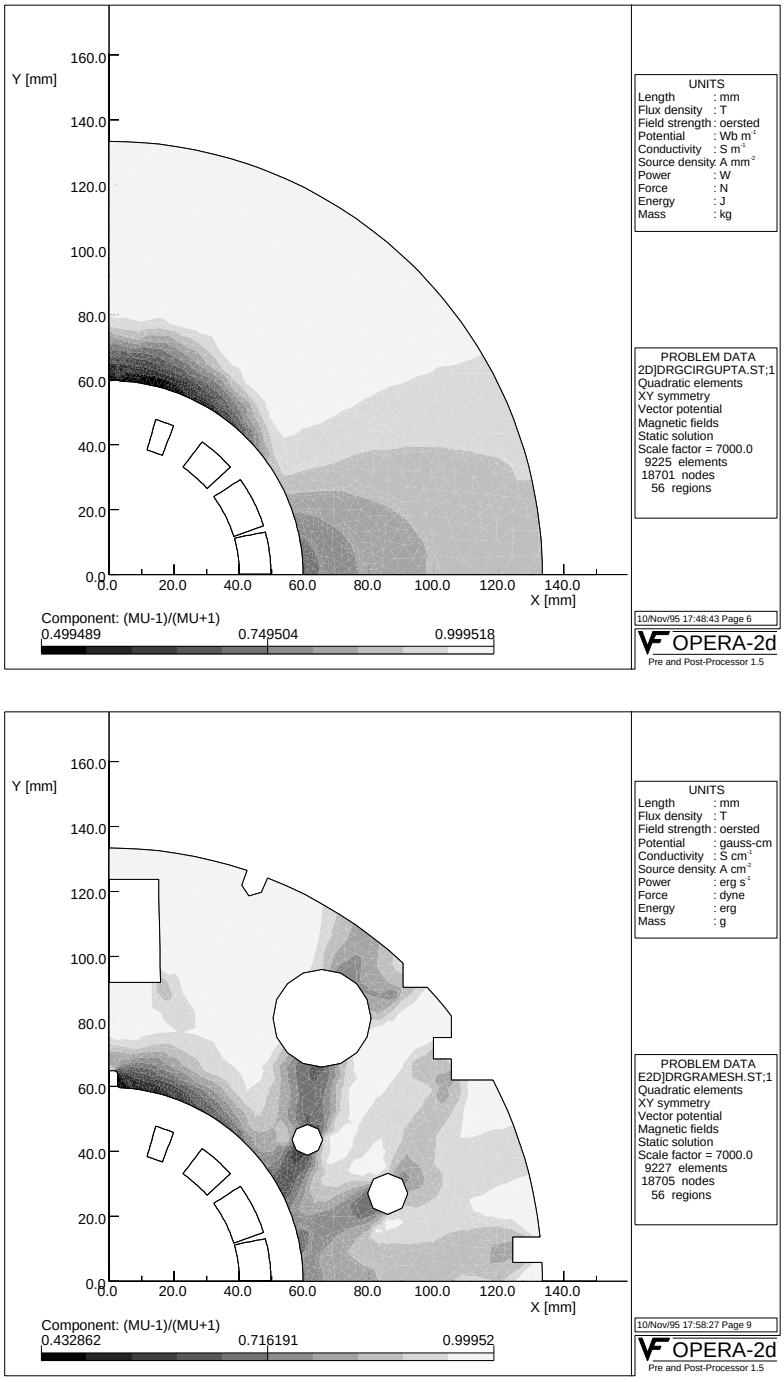

Figure 3.7.3: $\frac{\mu-1}{\mu+1}$ in the iron yoke of the RHIC 80 mm aperture arc dipole magnet at 7.0 kA in (a) circular aperture case (upper figure) with no holes, etc. and in (b) the optimized design (lower figure) with all holes and other structures. $\frac{\mu-1}{\mu+1}$ is related to the "yoke-air" boundary condition. A reduction in the variation of this function, particularly at the yoke inner surface, reduces the saturation induced harmonics.

yoke inner surface is not as efficient unless the yoke outer radius is reduced by an excessive amount.

An asymmetric placement of the cold mass in the cryostat results in the introduction of a large a_1 at high field when the field lines are not contained in the iron yoke. This has been found in both the SSC and the RHIC dipoles. Moreover, if there is a difference in the yoke weights between the top and bottom halves, an additional current dependence in saturation a_1 is also generated. In the RHIC arc dipoles, the effect of an off-centered cryostat on the saturation a_1 has been compensated by deliberately making the lower yoke half heavier than the upper. This has resulted in reducing the average saturation induced a_1 at the design current by about a factor of 2 (from about -2 units to within -1 unit).